Fredi Jovani Soares Brigham
BSc in Biochemistry

Insights into the structure, kinetics and aggregation of α-synuclein by charged metabolites

Dissertação para obtenção do Grau de Mestre em
Bioquímica para a Saúde

Orientador: Doutor Aldino Viegas, Investigador, NOVA School of Science and Technology
Co-orientador: Professor Eurico Cabrita, Professor, NOVA School of Science and Technology

[Março 2023]

Fredi Jovani Soares Brigham
BSc in Biochemistry

Insights into the structure, kinetics and aggregation of α-synuclein by charged metabolites

Dissertação para obtenção do Grau de Mestre em
Bioquímica para a Saúde

Orientador: Doutor Aldino Viegas, Investigador, NOVA School of Science and Technology
Co-orientador: Professor Eurico Cabrita, Professor, NOVA School of Science and Technology

Júri:

Presidente: Prof. Doutora Maria Teresa Nunes Mangas Catarino
Arguente: Prof. Doutora Maria Leonor Carvalho Morgado
Vogal: Prof. Doutor Aldino José Martins Viegas

NOVA School of Science and Technology

[Março 2023]

To my Families.

ACKNOWLEDGMENTS

First and foremost, I would like to express my gratitude towards my supervisors Professor Eurico Cabrita and Dr. Aldino Viegas, who entrusted me with this project and offered me unconditional support.

I would like to give a special thanks to **Ana Ferreira** whose contributions were **essential** for completing my master's thesis. I cannot overstate this enough, in the final weeks of the project when I was struggling considerably. Ana instinctively and selflessly provided me with much-needed support (in several areas of the thesis). I would like to thank all the members of Laboratory 302 for their good mood and support as well as Professors Helena Vieira and Mario Diniz for their kindness and contribution to the experimental phase of the project.

E em português, quero agradecer a minha família que me apoiou desde sempre, e que **sempre** será a minha prioridade. Quero também mencionar o grande apoio da minha família longe de casa, os Bombeiros Voluntários de Agualva-Cacém (**1138**), que contribuíram para me formar como pessoa e mostrar aquilo que realmente é importante na vida.

“What we do for ourselves dies with us. What we do for others and the world remains and is immortal.” (Albert Pine)

ABSTRACT

Alpha-Synuclein (αS) is a small intrinsically disordered protein (IDP) abundantly expressed in presynaptic terminals of neurons that displays a highly amyloidogenic nature. Pathological conditions can trigger the transition of soluble αS monomers into fibrils in a cooperative and nucleation-dependent manner. The accumulation of αS in the brain has been linked to the development of Parkinson's disease (PD).

Amino terminally acetylated αS (Ac-αS) is the physiologically relevant form of the protein in humans. The crowded pre-synaptic milieu is home to several charged metabolites that can reach concentrations at the molar scale *in vivo* and display remarkable protein-stabilizing properties. High concentrations of charged metabolites are a vital prerequisite for the formation of biocompatible ionic liquids (ILs), hinting at the possibility of the formation of endogenous ILs.

The aim of the current study was to assess the effect of a putative naturally occurring IL, choline glutamate ([Ch][Glu]), on the stability of Ac-αS. Fibrillation assays identified [Ch][Glu] and NaCl as destabilizing ionic compounds that interact with αS variants in a concentration-dependent fashion.

Nuclear magnetic resonance spectroscopy (NMR) revealed an unexpected contrasting behavior of acetylated and non-acetylated αS when interacting with [Ch][Glu]. These differences are consistent with a more effective destabilization of Ac-αS which might be related to a of the early onset disruption of N-terminal long-range stabilizing interactions.

This relatively straightforward *in vitro* model can be used to elucidate on protein stability and hence fibrillation propensity as a function of osmolyte fluctuations.

Keywords: Parkinson's Disease, Acetylated Alpha-Synuclein, Ionic Liquids, Choline Glutamate

RESUMO

A alfa-sinucleína (αS) é uma pequena proteína intrinsecamente desordenada (IDP) e amiloidogénica abundantemente expressa em terminais pré-sinápticos de neurónios. As condições patológicas podem levar à transição dos monómeros solúveis αS para fibrilas de um modo cooperativo e dependente da nucleação. A acumulação de αS no cérebro tem sido ligada ao desenvolvimento da doença de Parkinson (PD).

Nos Humanos, a forma fisiologicamente relevante da αS é acetilada (Ac-αS). O meio pré-sináptico apresenta metabolitos carregados que podem atingir concentrações na ordem dos molares com notáveis qualidades estabilizadoras de proteínas. Concentrações elevadas de metabolitos carregados é um pré-requisito essencial para a formação de líquidos iónicos biocompatíveis (ILs), sugerindo a possibilidade da formação endógena de ILs.

O objetivo deste estudo foi avaliar a estabilidade da Ac-αS na presença de glutamato de colina ([Ch][Glu]), como um possível IL natural. Os ensaios de fibrilação permitiram identificar o [Ch][Glu] e o NaCl como sendo desestabilizadores αS e que mecanismo de agregação é dependente da concentração de composto iónico.

Os estudos de ressonância magnética nuclear (RMN) verificaram que a Ac-αS apresenta uma desestabilização mais efetiva que pode estar ligada á disrupção das interações de longo alcance do N-terminal.

Este é um modelo *in vitro* simples que possibilita o estudo de proteínas amilodogénicas em função das variações de osmólitos.

Palavras chave: Doença de Parkinson, Alfa-Sinucleína acetilada, Líquidos Iónicos, Colina Glutamato

CONTENTS

LIST OF FIGURES

ACRONYMS

(Ac-)αS	Acetylated and Non-Acetylated Alpha Synuclein
[Ch][Glu]	Choline Glutamate Ionic Liquid
[Ch+]	Choline Ion
[Glu-]	Glutamate Ion
Ac-αS	Acetylated Form of Alpha Synuclein
Amp	Ampicillin
BD	Bi-distilled
BMRB	Biological Magnetic Resonance Bank
Chl	Chloramphenicol
CSP	Chemical Shift Perturbation
CSPα	Cysteine String Protein Alpha
DSS	Sodium 3-(trimethylsilyl)propane-1-sulfonate
HSQC	Heteronuclear Single Quantum Coherence
IDP	Intrinsically Disordered Protein
IEC	Ion Exchange Chromatography
IL	Ionic Liquid
IPTG	Isopropyl β-D-1-Thiogalactopyranoside
LA	Luria (Bertani) Agar
LB	Luria (Bertani) Broth
LBD	Lewy Body Dementia
LBs	Lewy Bodies
LNs	Lewy Neurites
LyB	Lysis Solution
M9	M9 Minimal Medium

MEM	Minimum Essencial Medium
MQ	Mili-Q grade
MSA	Multiple Systems Atrophy
NAC	Non-Amyloid-β Component
NMR	Nuclear Magnetic Resonance
NSF	N-Ethylmaleimide-Sensitive Factor
OD	Optical Density
PAF	Pure Autonomic Failure
PD	Parkinson's Disease
pI	Isoelectric Point
pNatB	Plasmid Encoding For The NatB Complex
PTM	Post Translational Modification
SNARE	Soluble NSF Attachment Receptor
SNc	Substantia Nigra Pars Compacta
SSP	Secondary Structure Propensity
SUV	Small Unilamellar Vesicle
TH	Tyrosine Hydroxylase
ThT	Thioflavin-T
Tris	Tris(Hydroxymethyl)Aminomethane
VMAT2	Vesicular Monoamine Transporter 2
WT	Wild Type Strain
αS	Alpha-Synuclein

1 INTRODUCTION

1.1 Overview

1.1.1 α-Synuclein

General Features

Alpha synuclein (αS) is a highly soluble, intrinsically disordered protein **(Figure 1)** found in vertebrates. Human αS is a relatively small protein (14.460 kDa) composed of 140 amino acids which can be functionally organized into 3 domains **(Figure 2)**: **(i)** the N-terminal domain, a highly conserved amphipathic region with α-helical propensity involved in membrane binding; **(ii)** the non-Amyloid *β* component, which corresponds to the highly amyloidogenic hydrophobic core of the protein; and **(iii)** the C-terminal domain, a highly flexible portion of the protein that mediates protein-protein interactions **[see subsection 1.2.2]**. A total of 7 imperfect repeats are distributed throughout the protein (XKTKEGVXXXX).

Akin to most intrinsically disordered proteins, αS is an efficient mediator of protein interactions, with at least 50 reported protein interactions.[1] αS displays no native conformation in solution but is often termed "protein chameleon" due to the wealth of adopted conformations in the presence of specific environmental factors, proteins, and ligands.[2] Yet, under physiological conditions, αS may assume two major conformations: **(i)** the preferred unfolded random coil structure, when in solution, and **(ii)** an α-helix rich "horseshoe" conformation upon membrane binding. Additionally, αS may also assume pathological forms: **(i)** highly organized αS fibrils (also known as amyloids), common to Parkinson's disease, or **(ii)** amorphous aggregates, common in other α-synucleinopathies **[see subsection 1.2.4]**.

Physiology and Pathology

The physiologic role of αS has yet to be completely elucidated. Still, the highly promiscuous nature of αS suggests that this protein plays several physiological roles. For instance, prominent theories link αS to vesicle trafficking and recycling, dopamine synthesis and transport, among others.[3] Moreover, human αS is subject to several post translational modifications (PTMs) that modulate its activity and stability. The most well reported PTM is phosphorylation, as αS is constitutively phosphorylated at S87, with the phospho-αS presenting a reduced aggregation tendency.[4] In mammals, αS is also constitutively acetylated in the N-terminal (Met1). This modification has been shown to increase membrane affinity and aggregation resistance **[see subsection 1.2.3]**.[5,6]

αS is prone to misfolding[7,8], a nucleation-dependent process that begins with the coalescence of multiple hydrophobic cores which grow exponentially and mature into large insoluble aggregates. These oligomers have been shown to disrupt neuronal homeostasis and are linked to various cellular disorders (*e.g.,* microtubule impairment, synaptic and mitochondrial dysfunctions, and oxidative stress).[9] Several missense mutations in the SNCA gene promote the amyloid state of αS **(Figure 2)**. It is important to note that most point mutations that are linked to PD can be associated with the NAC region[10], highlighting its importance **[see subsection 1.2.4.]**.

1.1.2 Ionic Liquids

General Features of ILs

Over the last few decades, Ionic Liquids (ILs) have delivered on many promises in both the academic and industrial scales[11] which is reflected in the exponential growth of related publications. ILs are an assorted class of compounds, which subvert the conventional description of molecular solvents as they exhibit a unique set of physicochemical features (*e.g.*, low melting temperatures, negligible volatilities, and high thermal stability), which can contribute not only to greater safety in the processes to which they are applied but also have enhancing their recyclability addressing the safety, health and environmental concerns raised by traditional organic solvent systems.[12,13] These compounds are classically defined as molten salts with melting points below 100 °C hosting bulky asymmetrical organic cations. ILs are appropriately referred to as designer solvents, in connection to their tailorable properties that may be adjusted by varying anion-cations combinations (*e.g.,* dielectric constant, conductivity,

biological activity, hydrophobicity, acid-base character, and polarity).[13,14] This tunable character makes the potential number ILs to be projected to be 10^{18}[11], compared to the less than 1000 organic solvents, which have led to their exploitation in diverse applications, e.g. in synthesis, catalysis, and electrochemistry to name a few examples **[See section 1.3].**

Bioinspired Ionic Liquids

Toxicity is one of the major setbacks of this remarkable class of compounds. Conventional ionic liquids are regarded as toxic and minimally biodegradable which could have an extremely negative impact on the environment.[11] To tackle this, bioinspired ILs have been recently developed and used in pharmaceutical and biological applications. These bio-ILs share characteristic features (*e.g.,* renewable, biocompatible, biodegradable, and minimally toxic towards the environment) that can be further adjusted in terms of biological activity by permuting building blocks (*e.g.,* osmolytes, amino acids, and sugars).[11,15]

Osmolytes, for instance, are of extreme interest to the field of protein stabilization, as some of these compounds display osmoprotectant properties towards proteins.[16–18] These candidate ions play important roles *in vivo* where they may reach molar concentrations.[19] Naturally, there is a great interest in combining these compounds into biocompatible ILs that display minimal toxicity towards cells. The interest in charged metabolites was further strengthened by the first reports of naturally occurring IL with physiological significance.[20]

One of such osmolyte is cholinium (Cho). Cholinium-based ILs are reported to have a stabilizing effect on proteins. Some studies report on the ability of cholinium-based ILs to suppress the formation of fibrils and even dissolve mature fibrils.[21]

Dicarboxylic acid-based ILs (DAILs) are also of interest due to their stabilizing properties. Glutamate analogues such as bitartrate and α-ketoglutarate have shown stabilizing properties towards proteins **[see subsection 1.3.4.]**.[22]

Cabrita's group combined the two moieties of cholinium and glutamate to form the cholinum glutamate ionic liquid, [Cho][Glu]. Using GB1 protein, they have shown that this IL can display both stabilizing and destabilizing properties depending on the concentration. In diluted media, [Cho][Glu] has been shown to stabilize proteins, while crowded conditions, favor ion pairing, which has the opposite effect.[23,24]

1.1.3 Significance Statement

Human αS is abundantly expressed in the brain where it may undergo the pathologic transformation into amyloid fibrils.[25] A growing body of evidence directly links these αS aggregates to the development of Parkinson's disease [26], the second most frequent neurodegenerative disorder.[27] Currently αS is regarded as a major therapeutic target by the scientific community, which is reflected by the wealth of αS related publications. Yet **disease-modifying therapies** remain a major unmet need for Parkinson's disease and related pathologies.

The IL choline glutamate ([Cho][Glu]) is a prime candidate for the stabilization of monomeric αS, as it inherits many of the protein stabilization traits of cholinium and dicarboxylic acid-based ILs. In fact, this ionic liquid has been shown to successfully stabilize several model proteins.[24,28] Individually, the cholinium and glutamate ions share a set of important key features that can be linked to αS: **(i)** these charged metabolites represent some of the most abundant charged metabolites of neuronal cells, **(ii)** they are essential to neuronal physiology, displaying possible links to αS's functioning. **(iii)** These components are found in high concentrations near the presynaptic terminals where αS is abundantly expressed.

1.2 Alpha Synuclein

1.2.1 General Features

Alpha-synuclein (αS) is regarded as the most popular member of the synuclein family, a highly conserved group of proteins (62% and 55% of sequence identity to *β*- and *γ*-synuclein, respectively).[29] αS is a small and highly soluble neuronal protein with a characteristic acidic nature (14,460 kDa, pI of 4,67).[30] In humans, αS is encoded by the SNCA gene (also known as PARK1 gene) and is abundantly expressed in the brain, particularly in the axon terminals of presynaptic neurons of the frontal cortex, hippocampus, striatum, and olfactory bulb[31,32], where it makes up as much as 1% of cytosolic proteins. Smaller amounts can also be found in other tissues (*e.g.,* heart and muscles).[31]

Besides its monomeric form, αS can also be found in a wide range of high molecular weight assemblies (*e.g.,* dimers, tetramers, multimers, aggregates, and fibrils) [30]. These findings suggest the existence of a dynamic equilibrium set between monomeric (major protein fraction) and several multimeric forms of αS, which are assumed to be stabilized when binding to other proteins, lipids and small molecules.[33]It should be noted that multimeric variants only represent a small proportion of αS conformations (precise conformer distribution is not known)

but may have a great influence on the physiological and cytotoxic effects of αS as a whole and should therefore not be underestimated.

αS is often termed "protein chameleon" due to the abundance of adopted conformations in the presence of specific environmental factors, proteins, metals, and ligands. When in solution, αS behaves like an intrinsically disordered protein (IDP), presenting a mostly unfolded random coil structure.[8] Another major physiological conformation of αS is the α-helical variant, created upon membrane binding **(Figure 1A and B)**.[34,35] Recent studies suggest that the α-helical "horseshoe" variant may assemble into higher-order multimers.[36] Other possibly relevant physiologically relevant forms of αS include dimers, trimers, tetramers, and other higher order multimers.[5] Additionally, αS may assume two major pathological conformations: **(i)** αS fibrils (also known as amyloids) **(Figure 1C)**, which promote the degeneration of the dopaminergic system in PD, and **(ii)** amorphous aggregates which can be found in other α-synucleinopathies (*i.e.,* Lewy body dementia).[37]

αS is an efficient mediator of protein interactions. This ability stems from the conformational plasticity of the protein which allows for the creation of strong specific interactions with a multitude of protein partners.[1] In fact, αS is reported to have more than 50 different interactions with other proteins (*e.g.*, SNARE, CSPα, phospholipase D2, Rab Small GTPases).[38] It is important to note that the conformational plasticity of αS is strongly dependent on environmental factors such as pH, temperature, or the presence of ligands (*e.g.,* dopamine, lipids, metals and ions) which may preferentially stabilize a given conformation.[39,40]

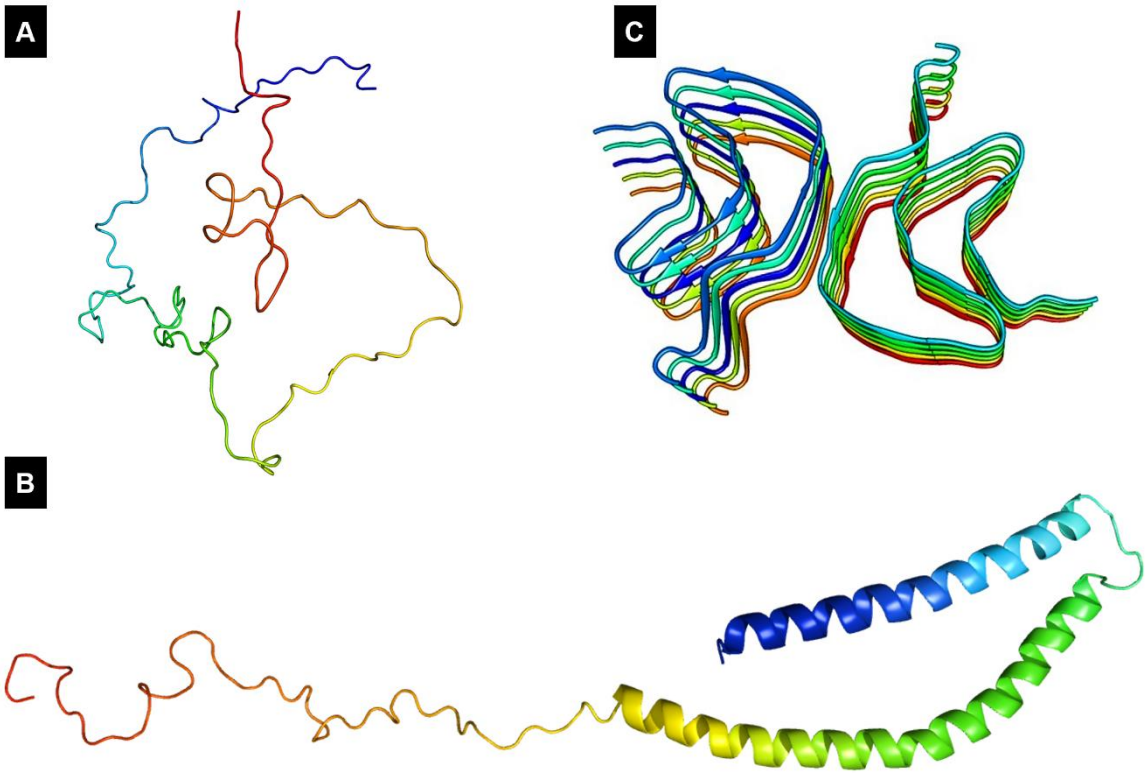

Figure 1 – Relevant Forms of αS

A) αS as an intrinsically disordered protein in solution. **B)** The α-helix enriched conformation of αS upon membrane binding (PDB code 1XQ8). **C)** The typical fibril structure of αS (PDB code 1MU4).

1.2.2 Primary Sequence and Domains

Primary sequence

Human αS is composed of 140 amino acids **(Figure 2B)**. Noticeably the primary sequence does not contain any cysteine or tryptophan residues, with the absence of the later hindering "normal" protein quantification via intrinsic tryptophan fluorescence. A single histidine residue (H50) can be found, as well as 5 proline residues. A total of 7 imperfect repeats are distributed throughout the protein, following the consensus sequence XKTKEGVXXXX (characteristic of the synuclein family). This motif shares similarities to lipid binding motifs found in other proteins (*i.e.,* apolipoproteins).[41]

Functionally, αS can be organized into 3 domains **(Figure 2C)**: **(i)** the N-terminal domain (residues 1 to 60), responsible for lipid binding and acetylation in mammals, **(ii)** the hydrophobic and highly amyloidogenic core of the protein (residues 61 to 95), also known as non-

amyloid β component (NAC), and **(iii)** the highly flexible and acidic C-terminal domain (residues 96 to 140), directly involved in protein interactions and solubility.

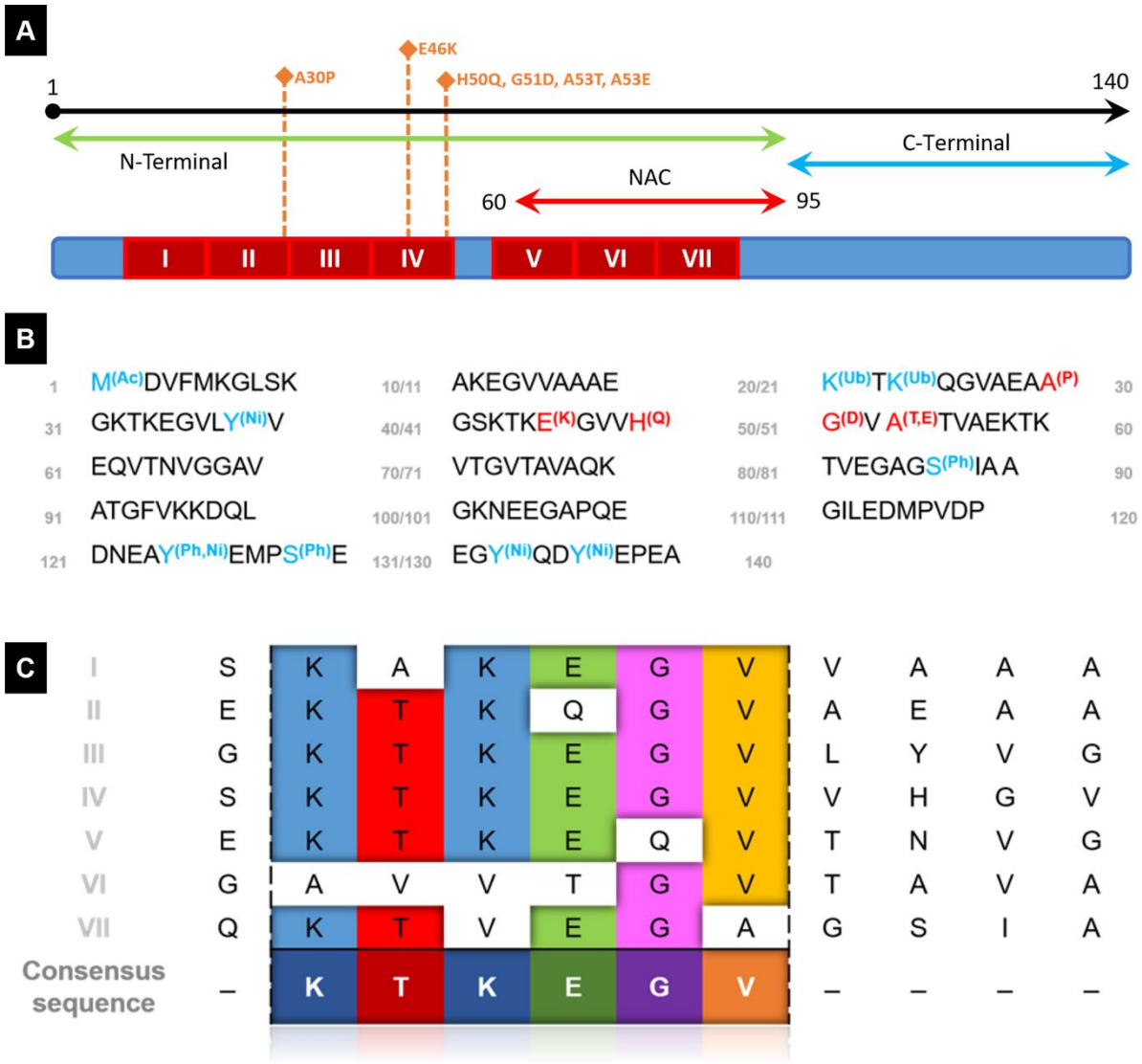

Figure 2 – αS Features

A) Schematic representation of the primary sequence of αS, displaying the organization of the 7 imperfect repeats (presented in red) and all known point mutations related to PD (presented in orange). Protein regions are also highlighted: N-terminal (residues 1 to 95), NAC region (residues 61 to 95), C-terminal (residues 95-140). **B)** Primary sequence of human wild type αS expressed by the SNCA gene. Known point mutations highlighted in red. Most relevant post translational modifications presented in blue (Ac- acetylation, Ph phosphorylation, Ni- nitration, Ub- ubiquitination), adapted from Mor et al.[30] **C)** Aligned repeats and respective consensus sequence.

N-Terminal: Membrane Binding

The N-terminal domain is an amphipathic and highly conserved region of the synuclein family which plays a central role in membrane interactions. This domain is proposed to form a

lysine-rich lipid-binding motif in the presence of negatively charged lipids. The consensus sequence (4 out of 7 repeats) is responsible for conferring α-helical propensity to the amino terminal region as well as regulating the membrane binding. Upon binding the amino-terminal undergoes a radical transition to an α-helical conformation (from 3% α-helical content to 71%) which extends to the NAC component (residues 2 to 89).[42] Lipid binding is initiated by the first 25 residues of the protein and is described as a cooperative and nucleation-dependent process.[43] The N-terminal is acetylated in mammals which further enhances structural alpha helical propensity as well as protects the protein from pathological oligomerization events.

NAC Component: Misfolding and Toxicity

αS shares high sequence similarity with the other members of the synuclein family and yet it is the only member capable of forming amyloids.[3] The most noteworthy example is that of β-synuclein, which shares 62% of the sequence identity of αS but is unable to fibrillate. These observations can be explained by the lack of the NAC region in *β*- and *γ*-synuclein, therefore highlighting the fundamental role of this region in the pathological oligomerization of the protein.[44]

The NAC region was first identified as the minor protein fraction of Alzheimer's plaques.[45] This highly amyloidogenic region (residues 61 to 95) constitutes the hydrophobic core of the protein, which is involved in the pathological transition of unstructured αS into *β*-sheet rich oligomers. The remaining 3 out of the 7 imperfect repeats are found in this region. It is important to note that the NAC region is formally inserted in the N-terminal despite being functionally distinct.

C-Terminal: Solubility and Interactions

Most IDPs use specific primary sequence elements to deter aggregation events. These regions typically contain distinct features such as the enriched in charged residues and prolines as well as a distinct lack of any hydrophobic amino acid stretches.[46] The C-terminal domain (residues 96 to 140) of αS is no different. This highly flexible and acidic region (10 glutamate, 5 aspartate, and 5 proline residues) is responsible for maintaining the solubility and the disordered nature of the protein. This region has been found to transiently establish long range tertiary interactions with the NAC region and N-terminal domain which envelop and thus protect the hydrophobic core of the protein.[40] Curiously, truncated forms of αS (*i.e.,* without the

C-terminal region) are enriched in LBs, further consolidating the protective function of this domain.[10]

The C-terminal is also responsible for establishing protein-protein and protein-ligand interactions in the monomeric and membrane-bound forms of αS. The carboxy-terminal domain has been found to interact with more than 50 different proteins as well as with a myriad of small molecules and proteins.[38] Interestingly, the C-terminal can be found as an independent flexible domain in both physiological and cytotoxic (*i.e.,* amyloid fibril) forms of αS, possibly allowing for unreported interactions.[47] It is also important to note that the C-terminal can be subject to multiple post translational modifications (PTMs), are in some capacity, able to modulate the protective properties of the C-terminal as these forms appear to be selectively enriched in LBs.[48]

1.2.3 Physiological Aspects of αS

Biological Function

Currently, αS's physiological role remains to be fully deciphered despite its direct involvement with PD and high potential as a therapeutic target. This inability to pinpoint the protein's normal functioning greatly hinders the ability to devise effective therapeutic strategies. The difficulty in uncovering αS's real function does not seem to correlate well to the discovery of novel protein and small molecule interactions since several of these have been already cataloged. Instead, the problem seems to be in combining these findings into a robust working theory. It is likely that αS, being an efficient mediator of protein interactions, plays several important physiological roles.

Although no real scientific consensus has been reached, below are some of the most prominent theories.

Synaptic Plasticity and Neurotransmitter Release- Knockout mice studies involving the synuclein family suggest that the synaptic structure is significantly altered in these conditions whilst brain morphology is not.[49] Affected mice demonstrated impaired survival as a result of the knockout which evidences the pro-neurogenic role of αS and related proteins. While several studies link αS to neurotransmitter release[35], the data so far is still very contradictory, with evidences pointing either to an enhancement of neurotransmitter release [50], a decrease in neurotransmitter release [51], or even no relation at all.[35,52]

Recent findings also point to a potential role of αS in the regulation of endocytosis. The protein is described as highly mobile with the ability to disperse from synaptic vesicles upon

stimulation[53], and has been shown to associate into multimers which cluster in synaptic vesicles effectively restricting their motility and attenuating (exo/endo)cytosis.[54] Some studies propose that αS oligomers are formed upon membrane binding and that these multimers act as a chaperone for the soluble NSF attachment receptor (SNARE) complex.[55] αS was found to populate synaptic-vesicle mimics and interacting synaptobrevin-2, resulting in the inhibition of membrane fusion.[36] According to the presented conclusions, αS may be able to interfere with the synaptic vesicle reserves without directly affecting the machinery involved in the fusion process itself.[56]

Molecular chaperone activity- Represents one of the most well-established theories, and it is supported by three main claims: **(i)** αS shares a structural and functional resemblance to the 14-3-3 protein family which are molecular chaperones [57], **(ii)** the C-terminal domain of αS is reported to inhibit the aggregation of (thermally) denatured proteins[58] and **(iii)** αS is able to rescue mice from lethal neurodegeneration caused by cysteine string protein alpha (CSPα) knockout, by acting as a chaperone for SNARE complexes.[35] The chaperone-like function of αS was shown to be essential for long-term neuron function. Recent evidence indicates that triple knockout mice (α-, β-, γ-synuclein) have reduced SNARE-complex assembly, display neuropathological signs, and a shortened lifespan.[35,59]

Dopamine Synthesis and Transport- αS is known to inhibit dopamine synthesis by indirectly regulating the enzyme tyrosine hydroxylase (TH). In this sense, αS is thought to promote the dephosphorylated and inactive form of TH.[60] These findings are in line with an age-related increase of αS expression in the substantia nigra.[61] Moreover, αS promotes the decrease of dopamine from vesicular transporters. Knockdown of αS results in increased vesicular monoamine transporter 2 (VMAT2) density per vesicle, which is integral to the transport of dopamine.[50]

Lipid packing and membrane biogenesis- αS is proposed to detect and correct lipid packing inconsistencies.[62] Phospholipases D1 and D2 are involved in the cleavage of phosphatidylcholine moieties found in lipids and αS is reported to inhibit these enzymes. This may also suggest an additional role in membrane cleavage and biogenesis.[63]

Membrane Bound Structure

Understanding the primary and secondary structure determinants involved in membrane binding is paramount for understanding αS's folding behavior and developing new therapeutic strategies. The membrane bound state of αS represents the most common protein conformation.[64] αS requires negatively charged lipids (e.g., phospholipids) to initiate the

membrane binding process. Namely, a minimum requirement of 30% anionic lipid content must be met for binding to take place.[55] As previously mentioned, lipid binding is initiated by a nucleation step where the initial portion of the amino-terminal is rearranged (first 25 residues). αS contains a set of primary sequence features which promote membrane binding. Noticeably, the initial portion of the N-terminal displays a deliberate disposition of positive, negative, and hydrophobic residues which is thought to direct αS in the membrane binding process. Upon nucleation, lysine residues are proposed to rearrange themselves to better engage with acidic lipids. Conversely, negative charges migrate to the opposite end of the alpha helix. Hydrophobic residues are positioned between residues with similar charges in order to stabilize the α-helix.[65] Additionally, this region is unusually rich in glycine residues which are responsible for conferring plasticity to the α-helix.[42] This rearrangement results in the formation of a small α-helix which cooperatively propagates well into the NAC component.

Membrane bound αS presents an extended α-helix as the only structural hallmark. The helix extends from residues 2 to 89 in a total of 25 turns. The seven imperfect repeat sequences roughly dictate the residues involved in the secondary structure element. Repeats IV and V are separated by a 4-residue insert which deviates the helix's periodicity from the ideal 3,67 residues per turn. This deviation is responsible for displacing pseudo repeats V to VI 32º from the helix axis.[66] Two major models describe αS's likely confirmation as a result of membrane binding: **(i)** the "extended helix" model, where αS is assumed to make a continuous α-helical structure spanning for approximately 100 amino acid residues[67], and **(ii)** the "horse-shoe" model **(Figure 1B)**, where αS forms 2 antiparallel helices (H1 and H2) separated by a small kink at residues 42 to 44.[68] Currently, this is the most popular and accepted model due to the additional stabilization created between helices as well as allowing for the insertion in membranes with high curvature.

Recent studies indicate that the extent of the α-helix is dependent on membrane composition.[65] When binding to nanodiscs, αS presents a sequential binding behavior amongst protein regions: **(i)** residues 1 to 38, are able to weakly interact at 25% anionic lipid content, strong interactions are established at 50% anionic lipid content, **(ii)** residues 38 to 60, only start interacting at 50% anionic lipid content, **(iii)** residues 60 to 98 (roughly corresponding to the NAC region), which display moderate interactions at 75% anionic lipid content, **(iv)** residues 90 to 120, which are partially affected at 100% anionic lipid content, and finally, **(vi)** residues 120 to 140, which are not affected at any concentration. These results are in line with the above-mentioned cooperative and nucleation-dependent models presented for αS. These findings indicate that binding is substantially expanded because of increasing the anionic lipid content.

The binding behavior can be explained by the electrostatic model of αS **(Figure 3)**. The first 60 amino acids have a net positive charge and contain the most pseudo repeats thus being the first to interact. The NAC region takes second preference as mostly neutral region containing the last 3 pseudo repeats. The C-terminal is the last region to bind due to the net negative charge and the lack of pseudo repeats.[47] Previous studies involving small unilamellar vesicles (SUVs) corroborate these findings which suggests that differences in both models such as membrane curvature and spatial boundaries, may not be as relevant.

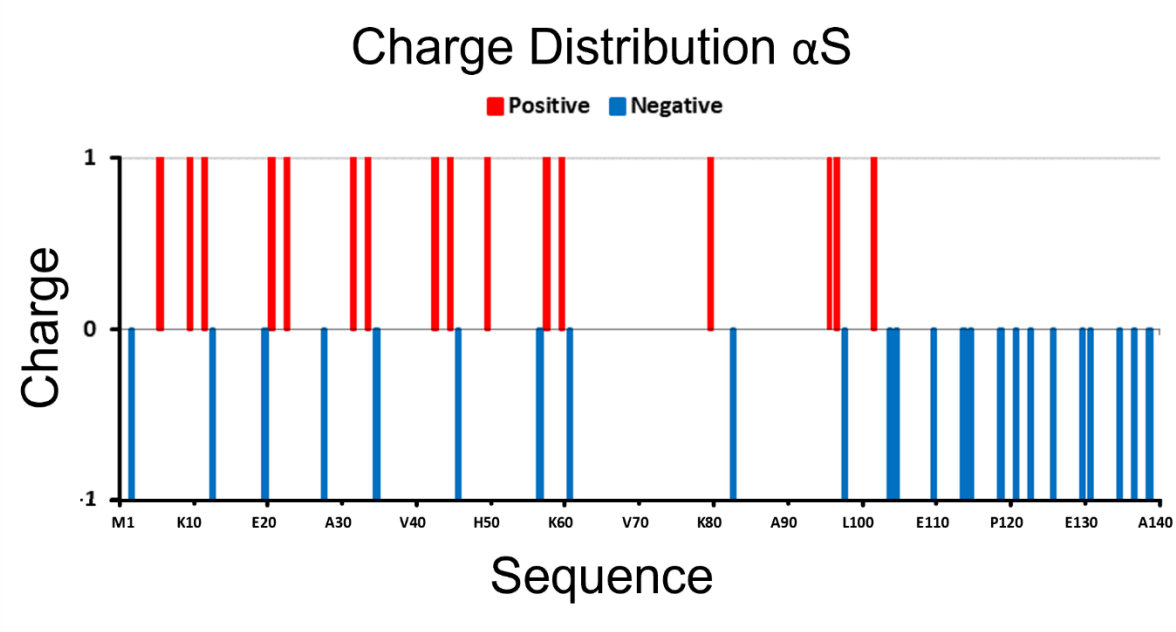

Figure 3 – The Electrostatic Model of αS

Schematic representation of charge distribution along the primary sequence of αS. Adapted from Munishkina et al.[44]

Post Translational Modifications

αS is subject to multiple PTMs, which are well distributed throughout the protein's sequence. Still, a significant part of modifications can be found in the carboxy-terminal domain **(Figure 2A and B)**. PTMs have a great impact on αS by shifting the regional hydrophobicity, net charge, or polar character of the protein. These changes may also affect more complex behaviors such as protein structure, folding outcomes, misfolding events, and binding to small molecules. It is important to note that most PTMs are made in accordance with protein localization within the cell (*e.g.,* presynaptic environment), and thus not all modifications occur at the same time or with the same frequency. It is unclear, for the most part, which PTMs are physiologically

relevant, and which are directly implicated in cytotoxic processes. Some of the most relevant PTMs are described below.[3]

Acetylation- It is considered one of the most important post translational modifications. αS is constitutively acetylated in mammalian cells[6], with acetylation occurring at the amino-terminal end of the protein (*i.e.,* at the methionine residue). This modification is physiologically relevant as it promotes α-helical folding in the amino acid region involved in nucleation, thus increasing αS's membrane affinity and aggregation resistance.[3] Additionally, acetylation can be found in both healthy individuals and patients diagnosed with PD.

Phosphorylation- Regarded as the most well reported PTM. This modification is proposed to regulate key aspects of αS's structure and normal functioning such as membrane binding, oligomerization, fibril formation, and neurotoxicity.[69] While αS is constitutively phosphorylated at sites S87 and S129, other phosphorylation sites undergo multiple phosphorylation cycles during the protein's life span. The effect of this PTM on αS stability is highly dependent on location, with some sites been shown to suppress aggregation whereas others have the opposite effect. Phosphorylation at residues S129 and S87 was shown to inhibit aggregation. Analogously, phosphorylation at residues Y125, Y133, and Y135 are associated with diminished aggregation.[4]

Proteolysis- C- and N-terminally truncated variants of αS can be found in either PD patients or healthy individuals suggesting that truncation is a naturally occurring event.[70] αS was found to have autoproteolytic properties, thus being able to create a variety of smaller fragments. Recent studies suggest that αS (14.46 kDa) can generate 12.16 kDa (residues 14 to 133), 10.44 kDa (residues 40 to 140), and 7.27 kDa (residues 72 to 140) fragmentation variants. The 7.27 kDa fragment contains most of the NAC region, which is exposed. This fragment was shown to aggregate considerably faster than the full-length protein due to a disruption of protective mechanisms. C-terminally truncated versions of αS are more commonly found in Lewy Bodies (LBs) possibly suggesting a role of these autoproteolytic products as cofactors in the aggregation of αS.[71]

Ubiquitination- The role of this PTM in αS regulation is still poorly understood. It is not clear if ubiquitination is a primary event in αS aggregation or just a consequence of natural protein degradation. Nevertheless, ubiquitination retains some relevancy as ubiquitin fragments are found in LBs and Lewy neurites (LNs).[72] Major ubiquitination sites are positioned at K21, K23, K32, and K34. Other relevant ubiquitination sites include K43, K96.[73]

Nitration- LBs have been found to be nitrated. It is not known if nitration is a primary event in αS aggregation or rather just a consequence of oxidative stress. Nitration is known to

have a protective effect against fibril formation.[74] All of the tyrosine residues may be subjected to nitration (*i.e.,* Y39, Y125, Y133, and Y136), however, Y39 and Y125 are the most frequently nitrated.[70]

1.2.4 Pathological Aspects of αS

Synucleinopathies

Synucleinopathies are defined as a group of neurodegenerative disorders that are prompted by an abnormal accumulation of αS aggregates. These aggregates may take the form of Lewy bodies (LBs) and Lewy neurites (LNs), which are described as ubiquitin-positive αS inclusions that accumulate within neurons. All synucleinopathies accelerate the deterioration of dopaminergic neurons resulting in a failure to produce and release dopamine, which is critical for controlling the start and stop of voluntary and involuntary movements.[75] It is important to note that αS pathological importance is not restricted to synucleinopathies and has been found to play an important role in other neurodegenerative disorders. For instance, αS is a significant component of the protein plaques that are created in Alzheimer patients.[76]

Parkinson's disease (PD)- currently represents the second most common neurodegenerative disease, being only surpassed by Alzheimer's disease. PD is estimated to affect 1 to 2% of adults over the age of 65 and 4% of adults over the age of 80.[77] This disease is characterized by the loss of dopaminergic neurons in the substantia nigra pars compacta (SNc).[78] PD's etiology is likely to be complex and triggered by a variety of genetic and environmental factors.[79] The existing clinical symptoms can be divided in: **(i)** motor symptoms such as bradykinesia, muscular rigidity, resting tremor, and postural and gait impairment, and **(ii)** non-motor symptoms such as olfactory dysfunction, cognitive impairment, psychotic symptoms, sleep disorders, autonomic dysfunction, unexplained pain, depression, apathy, and fatigue.[80]

Lewy body dementia (LBD)- shares many of the pathological traits of PD, but as the disease develops at the cerebral cortex level Alzheimer-like symptoms become more pronounced in some patients (*e.g.,* dementia).[37]

Multiple systems atrophy (MSA)- is described as the build-up of αS in the cytosolic fraction of oligodendrocytes.[57] MSA can be manifested in two distinct forms: **(i)** a PD-like variant, which shares many of the pathological traits of PD, and **(ii)** a cerebral variant, where symptoms similar to ataxia are present (*i.e.,* impaired coordination, balance problems, and alterations in the speech and swallowing).[81]

Pure autonomic failure (PAF)- is the most recent addition to the synucleinopathy family. PAF is characterized by the presence of αS-positive LBs and LNs in the sympathetic nervous system, symptoms associated with the disorder resulting in urinary and sexual dysfunction.[82]

Familial Parkinson

In humans, αS is the product of the SNCA gene which is located at position 21 in the long arm of the chromosome 4.[83] To date, six missense mutations **(Figure 2 and B)** have been linked to familial PD (*i.e.;* A30P, E46K, H50Q, G51D, A53E and A53T).[84–87] Fibrils from different mutations display small morphological variations as a function of mutations (*e.g.*, diameter, periodicity, and length), creating distinct "fibril strains".[88]

Point mutations are thought to exert subtle destabilizing changes on native αS instead of directly promoting major structural changes of monomeric αS. These changes may reduce protein solubility, compromise stabilizing long-range interactions, change global protein flexibility, and disrupt α-helical propensity.[89] The aggregation kinetics of αS is highly sensitive to mutations. In these instances, aberrant internal contacts may be formed, contributing to the stabilization of partially folded intermediates, which are critical for self-assembly.[89] Mutations E46K, H50Q, and A53T have been found to increase aggregation propensity whereas variants G51D and A53E display decreased aggregation propensity. A30P appears to favor oligomerization, at the expense of fibrillization.[90]

All mutations except for to A30P (found membrane-binding domain) are located within the core of the fibril structure, further highlighting the region's importance in fibril formation.[10] These changes in primary sequence have been found to exert distinct influences on PD's overall progression, ranging from more mild forms of the disease (*i.e.;* A30P) to more severe variants (*i.e.;* A53T).[91] The localization of the mutations in the N-terminal points to a possible compromise between the membrane-binding properties and fibrillation propensity. Noticeably, mutations A53T and H50Q were shown to more effectively interact with membranes whereas A30P, G51D and A53E display lower propensity.[92] These findings can be explained by the inability of A30P mutant to bind to membranes resulting in an overall increase in cytosolic αS which might, in turn, promote oligomerization. At the same time, the hydrophobic core remains unaltered and prone to fibrillate.

More uncommon mutations have been associated with a higher predisposition to develop PD. Duplications and triplications of the SNCA gene result in an overexpression of αS raising the available protein that can oligomerize. Polymorphisms in regulatory elements of the SNCA gene may exert a similar effect.[93]

Misfolding Behavior and Kinetics

The fibrillation of αS is classically described as a nucleation-dependent event *in vitro*. The process can be divided into three separate stages **(Figure 4)**: **(i)** the lag phase, which corresponds to an initial nucleation event, **(ii)** the elongation phase, which is characterized by the exponential self-assembly of αS building blocks, and **(iii)** the stationary phase, where the growth rate significantly decreases as a result of monomer availability.[7,8]

The lag phase is defined by major structural changes to multiple αS monomers generating partially folded intermediates with exposed hydrophobic regions. Intermediates coalesce into an insoluble critical nucleus (thermodynamically unfavorable process). In the elongation phase, the exponential self-assembly of αS building blocks result in the formation of highly ordered and insoluble amyloid fibrils (thermodynamically favorable process). In the stationary phase an equilibrium is reached between the soluble and insoluble fractions of αS.[7,8]

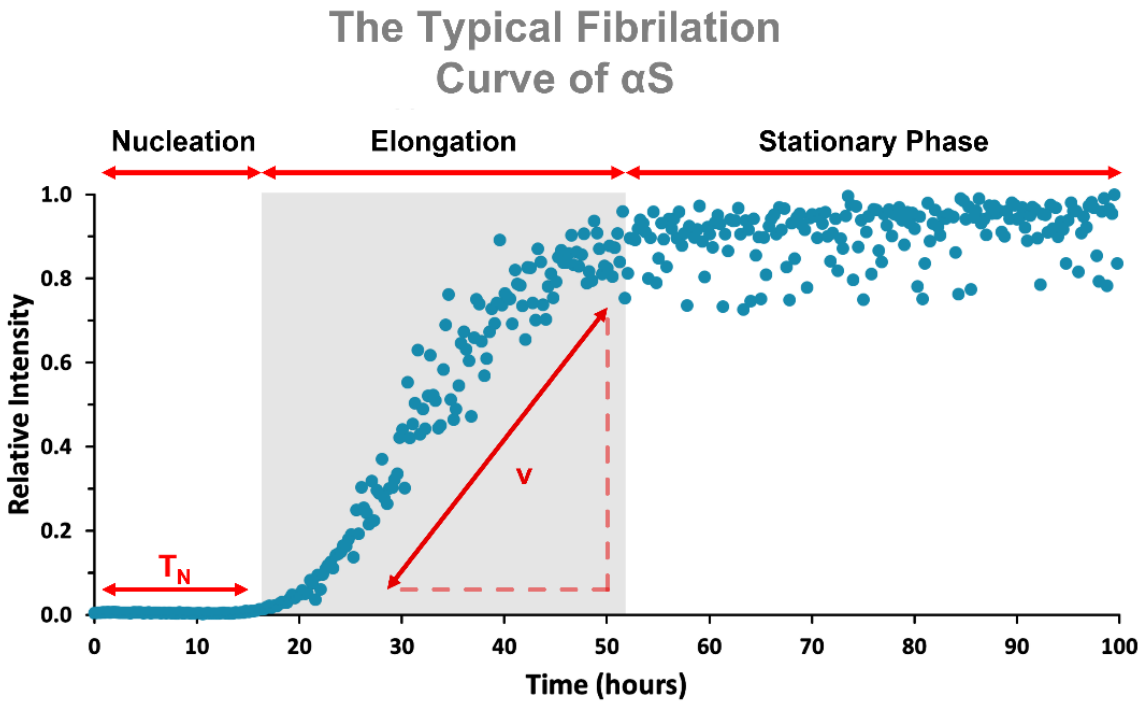

Figure 4 – The Aggregation Profile of αS

The phases of the fibrillation process as well as the respective kinetic parameters are Identified in a typical fibrillation curve of αS.

Fibril Structure and Morphology

αS is particularly susceptible to misfolding events due to the lack of a stable tertiary structure. Under the right conditions, the protein is capable of transitioning into a β-sheet

conformation, with these structures being capable of forming highly ordered fibrils. Structurally, the standard β-sheet conformation is composed of 8 parallel β-strands **(Figure 5A)**: β1: residues 42 to 46, β2: residues 48 to 49, β3: residues 52 to 57, β4: residues 59 to 66, β5: residues 69 to 72, β6: residues 77 to 82, β7: residues 89 to 92, and β8: residues 94 to ~102. Beta strands are flanked by glycine residues (*i.e.,* G41 before β1; G47 between β1 and β2; G51 between β2 and β3; G67 and G68 between β4 and β5; G73 between β5 and β6; G84 and G86 between β6 and β7; and G93 between β7 and β8). β-strands β2 to β7 create a hydrophobic core, composed of mostly alanine and valine residues. These organization patterns create multiple GAV motifs (i.e.,66VGGAVVTGV74) which further contribute to the fibrillation process.[94]

αS's fibrils display variable morphology with the archetype fibril varying in length (500 nm to 3 μm) and diameter (5 nm to 10 nm). αS amyloids can be hierarchically organized into protofibrils (diameter of 3,8 ± 0,6 nm), protofilaments (diameter of 6,5 ± 0,6 nm), and fibrils (diameter of 9,8 ± 1,2 nm).[95] αS protofibrils are composed of several layers. A cross sectional cut of this structure reveals that each layer is composed of 2 αS monomers arranged in a "Greek Key" topology **(Figure 5B)**. Protofibrils display rotational symmetry about the fibril axis, which can be roughly organized into a hydrophobic core which is encapsulated by a mostly hydrophilic layer. The outer layer contains two highly hydrophobic regions (residues L38 and V40, and residues F94 and V95). Another important feature of the fibril structure is the dense mesh of N-terminal and C-terminal tails surrounding the fibril, these tails are composed by the first and last 20 protein residues (approximately).[10]

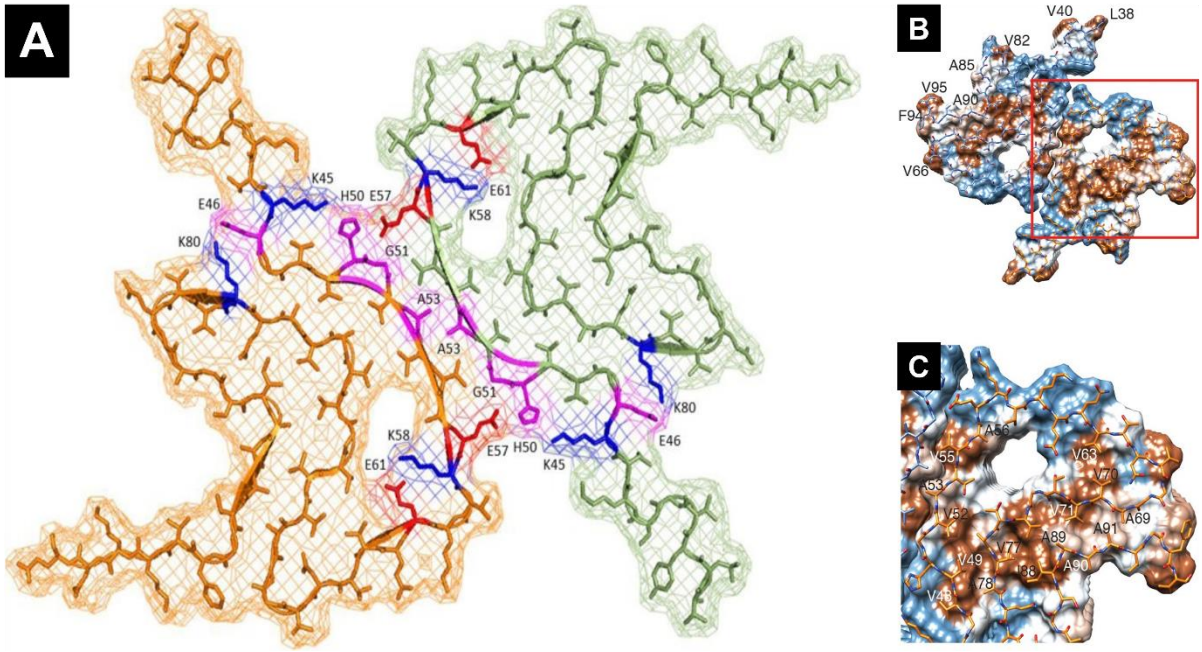

Figure 5 – αS's Fibril Topology

A) CryoEM structure of a Cross-section of the fibril structure displaying the so-called 'Greek Key' topology with rotational symmetry about the axis of the fibril. Protofibrils are highlighted (orange and green). Familial mutations localized within the fibril are evidenced (E46K, H50Q, G51D/E, A53T; highlighted in pink;). **B)** Hydrophobicity scores, ranging from hydrophilic (-4,5 units, in blue) to hydrophobic (4,5 units, in brown), for the trans sectional cut of a typical fibril. **C)** Close-up of the core region highlighted in B. The hydrophobic core (brown) is composed of mostly alanine and valine residues. A hydrophilic region (blue) can be seen surrounding the hydrophobic region of the core.[10,96]

1.2.5 Macromolecular Crowding

Macromolecular crowding occurs when a high concentration of macromolecules, such as proteins, leads to a change in behavior of a given molecule.[97] This phenomenon is also proposed to affect protein folding and chemical reaction rates[8], and is dependent on macromolecules occupying a set volume that cannot be shared with other macromolecules, therefore becoming unavailable (*i.e.,* excluded volume).[98]

The excluded volume has two contributions: **(i)** hard-core, steric repulsions which are always stabilizing interactions resulting from an entropic process, and **(ii)** soft (or chemical) interactions, which are governed by enthalpy and can be repulsive and or attractive in nature.[99] It is important to note that small molecules, even at very high concentrations do not show excluded volume effects due to their small size.[44] The excluded volume is of extreme importance since it is responsible for modulating macromolecular stability, association behavior, and equilibria.[100]

High concentrations of macromolecules are routinely found in cells, meaning that most proteins are optimized for these specific conditions. However, most experiments are performed in idealized (*i.e.,* dilute) solutions. Low concentrations of salts and proteins result in an activity coefficient comparable to 1. In other words, the species' behavior is unaltered. Idealized conditions are unable to model the intracellular milieu **(Figure 6)**, which is a complex and densely packed environment.[99] As an example, *E. coli* cells present a cytoplasmic concentration of macromolecules that may reach as high as 400 g/L and occupy up to close to 40 % of the cell volume.[98] This sort of solution is defined as "crowded" because no particular molecule is present at high concentration at any given time.[101] To mimic this, several polymers can be used as crowders such as: "inert" proteins, polysaccharides, and polyethylene glycols. Besides excluded volume effects, other factors are relevant to molecular crowding, such as solvent viscosity, which reduces diffusion rates and decreases water activity. In the case of αS, this makes the protein less soluble and, therefore, more aggregation-prone.[44]

αS has been shown to aggregate under macromolecular crowding conditions, when in the presence of high concentrations of polymer.[7] Due to excluded volume and viscosity, αS shows different aggregation tendencies in crowded solutions. αS fibrillation is favored by increasing polymer concentration and polymer size. Low polymer concentrations (approximately up to 100 mg/ml) favor excluded volume effects, whereas higher concentrations start to evidence opposing effects from viscosity contributions.[44] These observations suggest that αS fibrillation is predominantly governed by volume exclusion which promotes αS association[44].

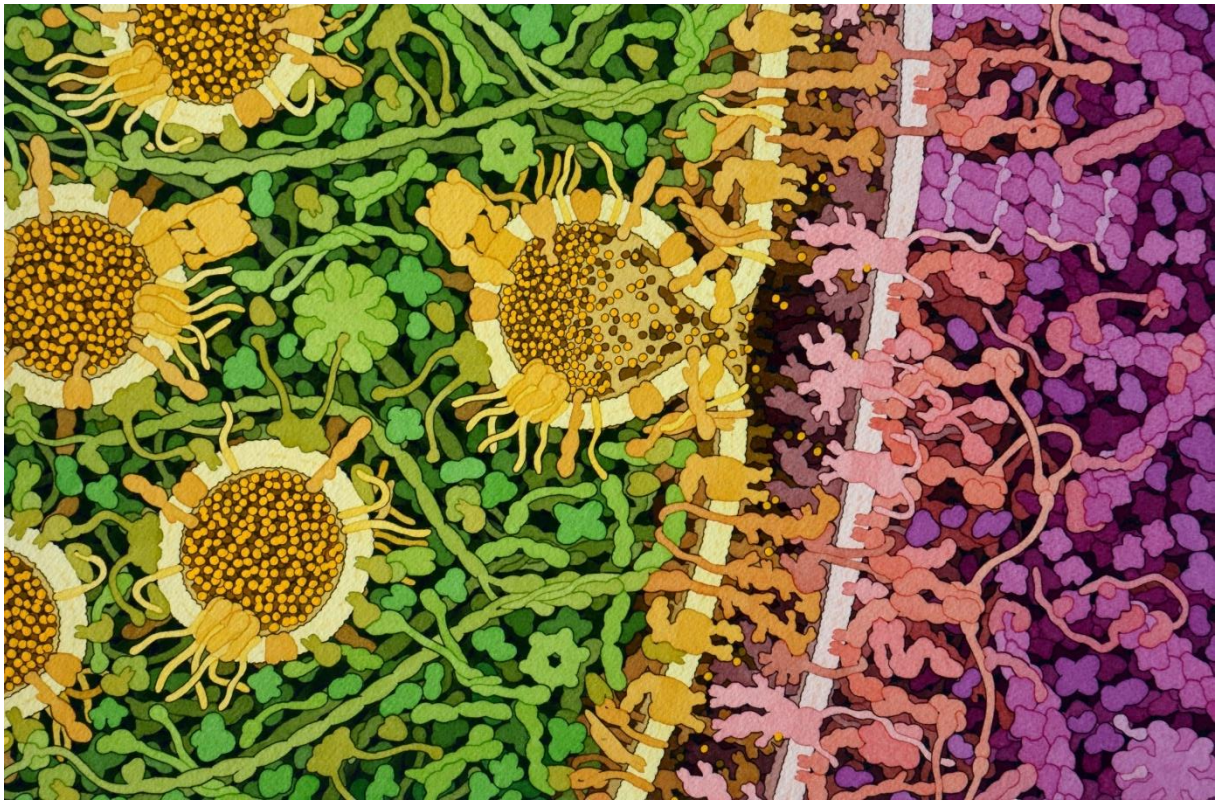

Figure 6 – Representation of the Synaptic Milleu

Up to scale representation of an excitatory synapse. Relevant features include synaptic vesicles containing the neurotransmitter Glutamate, SNARE complex proteins which are associated with vesicles and promote vesicle fusion. Image was made available by David Godsell (Doi: 10.2210/rcsb_pdb/goodsell-gallery-016).

1.3 Ionic Liquids

Over the last decades, frontier ionic liquid (IL) research has impacted a wide range of scientific areas (*i.e.,* chemistry, biology, and physics) by delivering on many promises in academia and industry. Such a positive footprint is reflected in the exponential growth of related publications **(Figure 7)**. These compounds are valued as sustainable alternatives to volatile organic solvents as they benefit from an inherent clean, efficient, and eco-friendly nature. These properties can be coupled with a unique set of (often) tunable, physicochemical and biological properties. ILs are currently associated with synthesis, catalysis, cell biology, material science, physical chemistry, electrochemistry, genetics heredity, nuclear physics, medicinal chemistry, engineering, and many more areas.[11] Noticeably, over the last few years, biologically active (*i.e.,* third generation) ILs have been the subject of several reviews in connection to pharmaceutical and biological applications.[102–105]

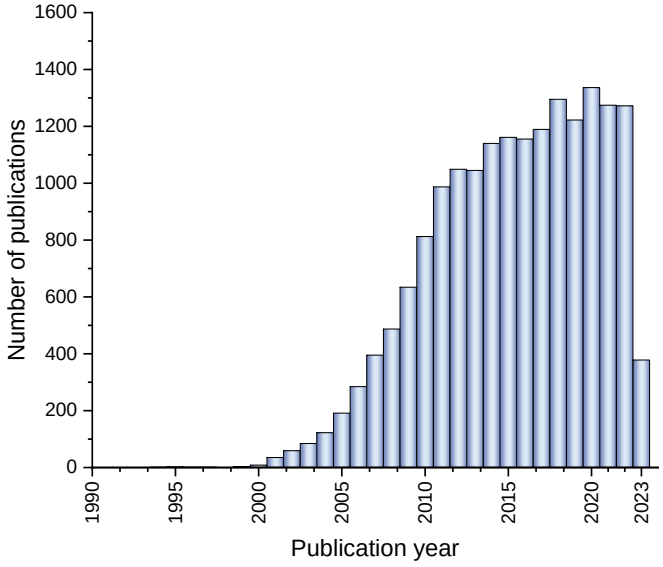

Figure 7 – IL Related Publications

Number of publications dealing with "ionic liquids" as a function of the publication year (according to the PubMed database).

1.3.1 Properties

Fundamental aspects of ILs

ILs are formally defined as molten salts, typically composed of bulky and asymmetrical organic cations (*e.g.,* N,N'-substituted imidazolium, N-substituted pyridinium, tetra-alkylated ammonium, or tetra-alkylated phosphonium derivatives) with melting points below 100 °C (373 K). ILs are an assorted class of compounds that do not fit into the conventional description of molecular fluids as they are reported to have a set of unique and unifying physicochemical features (*i.e.,* low melting temperatures, negligible volatilities, reasonable surface tension, extended liquid state temperature ranges, wide electrochemical windows, high thermal and chemical stabilities, or excellent dissolving capabilities)[12,13,106,107], as well as a set of tunable properties (*i.e.,* viscosity, biological activity, hydrophobicity, acid-base character, polarity, solvent power, higher-order organization, phase equilibria, etc.).[13,14,107] Therefore, ILs are referred to as "designer solvents" due to their tailorable properties that can be easily changed by implementing different anion-cations combinations, introducing a controllable amount of solutes, and/or ion restructuring.[12,106]

Green Aspects of Ionic Liquids

The United States EPA (Environmental Protection Agency) defines green or sustainable chemistry as the "design of chemical products and processes that reduce or eliminate the use or generation of hazardous substances". This movement aims to reduce pollution and waste in laboratory and industrial settings, while also focusing on the development and optimization of eco-friendly techniques that improve yields and decrease waste generation.[108] Truly "green" solvents must minimally burden the environment over the life cycle of a chemical product[109], which is the case when we compare ILs to traditional organic solvents. In this sense, ILs are considered benign alternatives due to their overall lower E-factors, hydrophilic nature, tunable acid-base character, and excellent biopolymer solubilization capabilities.[11] Other factors such as toxicity, biodegradability, and recyclability are also of great importance. Recent studies have risen some concerns if ILs are really eco-friendly solvents.[110,111] When analyzing the sustainability of ILs not only the process must be considered but also their synthesis, and the recovery and recycling process. Few ILs are found to be toxic and non-biodegradable, based on their LCAs (Life Cycle Assessments).[112] However, comparing the number of ILs with the number of LCA studies the latter are scarce and still limited to specific IL classes and limited to the characterization of the IL structure.[111]

Ionic Bonding

Tunability is one of the most well-known and captivating aspects of ILs. This property partially reflects the intrinsic versatility of the ionic interactions found in ILs. Ionic bonds are created when significant differences in electronegativity amongst coordinating atoms result in complete or almost complete incorporation of the electron pair by the more electronegative atom, thus creating ions bound by electrostatic interactions.[102] Conventional inorganic salts are formed by small anions that display a high localized charge density, which in turn creates strong bonds and promotes a closely packed crystal lattice, when in a solid phase. Conversely, ILs are formed by bulky, organic cations and weakly coordinating anions. In these instances, cation charge is distributed over a large volume and is often delocalized (*i.e.,* smaller charge density). Depending on the organic nature of the cation, several weaker but cooperative interactions like hydrogen bonding, hydrophobic interactions, and/or van der Waals interactions which in turn all destabilize the crystal lattice and contribute to the unique IL liquid nanostructure.[113,114] These differences in structure explain some of the differences in the behavior between ILs and inorganic salts as the lower charge density and the charge delocalization in the

former suggests an apparent weaker coulombic interaction, which not only results in lower melting points but also affects ion pair formation.[114]

Ionic compounds are also deeply affected by the solvent medium. The potential of ionic compounds is best employed in the liquid phase, as ionic compounds tend to rearrange in the presence of a solute disrupting previously established interactions formed between solvate shells and respective ions. The structuring effect of water is so significant that small fractions of water are known to alter the molecular interaction network of ILs, and thus some of IL's properties (*e.g.,* biocatalytic activity, acidity, density, viscosity, electrical conductivity, enthalpy, surface, or interfacial tensions). The extent of the perturbation is dependent on the structural size of the cation and anion.[14]

Ion Pairing

Ion pairing is a highly debated feature of liquid phase domain ILs. These interactions are proposed to be a result of strong attractive forces established between counterions. ILs are proposed to exist in a complex equilibria where ions can be found as fully solvated species (*i.e.,* C^+A^-), solvent-separated ion pairs (*i.e.,* $C^+||A^-$), and/or contact ion pairs (*i.e.,* CA).[115] Hydrogen bonding is suggested to play a key role in the process[116], as are some milieu conditions (*i.e.,* large concentrations, low dielectric media, small ionic radii, and low temperatures).[14,117]Several encouraging studies were made over the decades but the topic remains to be settled as ion pair formation in ILs is still poorly understood, yet some studies suggest that ion paring is responsible for physical properties of ionic liquid-solvent mixtures.[118]

One noteworthy example is the putative ion pairing found in aaILs (amino acid based ILs) which were sustained by molecular dynamic studies. Woo and co-workers[119] found that most of the studied imidazolium-based aaILs [C_2mim][AA] were in a strongly coupled regime suggestive of ion pairing. Furthermore, the strength of ion pairing in these ILs was found to increase when polar side chains were present.

Higher Order Structuring

Historically, ILs were taught to behave like a homogeneous and coherent system akin to highly concentrated salt solutions.[117] However, recent findings using NMR spectroscopy[120], theoretical modeling[121], and thermal techniques[122] suggest that they may act as structured solvents displaying dynamic nanoscopic (*e.g.*, ion pairs, ion clusters) to microscopic (*e.g.,* H-bond networks, and micelle-like morphologies) levels of organization, which sets them apart

from the conventional homogeneous and heterogeneous (*i.e.,* phase separated) solvent−solute systems. Microstructures are thought to provide stable "cage structures" capable of capturing substrate molecules and facilitating chemical reactions.[123] It is thought that ionic interactions, hydrogen bonding, and hydrophobic interactions are the major players in these types of IL organization.[117]

Noticeably, a recent electron microscopy study demonstrated the micro structuring effects of imidazolium based ILs. Kashin's group[124] reported the formation of stable water compartments of various morphologies in IL−water mixtures (*e.g.,* droplets, aggregates, 2D meshworks). Moreover, these same water compartments were found to improve upon the selectivity and yield of the biomass conversion reaction of D-fructose into 5-(Hydroxymethyl)furfural.

1.3.2 Classification

General Classification According to ion structure and origin

The classification of ILs is dependent on several features (*e.g.,* anion/cation origin, physicochemical properties, structural aspects). Consequently, multiple classification systems exist, and class types are often confluent.[125] Below it is presented a classification system based on the structural elements of cation-anion pair as well as the origin of said components.

(a)Protic (PILs/APILs) - ILs are primarily divided into protic or aprotic depending on the presence of redeemable Brønsted acidic proton(s).[11] Typically, PILs are formed through a neutralization reaction whereas APILs are created by a quaternization reaction followed by anion exchange.[126] An example of a PIL is ethyl ammonium nitrate $[EtNH_3][NO_3]$ while 1-Butyl-3-methylimidazolium dicyanamide [Bmim][dca] constitutes a typical example of APIL.

Chiral ionic liquids (CILs) - Another fundamental feature of ILs is chirality. An IL is considered chiral when at least one of its counterions is chiral. As commonly known, biologically active molecules (*e.g.,* amino acids, nucleic acids, and sugars) are chiral, and many biological systems rely on this property to function (*e.g.*, enzymes). Hence it is only natural that chiral molecules are indispensable to the fields of biochemistry and pharmacology. CILs are also relevant to the fields of organic and analytical chemistry.[127] Amino acid containing ILs are examples of CILs.

Bioinspired ionic liquids (BILs) - Commonly used counterions such as imidazolium are potentially toxic and poorly biodegradable. BILs were designed to overcome these limitations by being more recyclable, sustainable, minimally toxic, environmentally friendly, and biodegradable. Typically, compounds like cholinium, amino acids, sugars, lactate, and acetate are

among the most used ions.[11] An example of a BIL is choline glutamate [Cho][Glu] which is of particular importance to this work and will be discussed later **[Section 1.3.6]**.

Task specific ionic liquids (Ts-ILs) - The first report of a Ts-IL is accredited to Coles's group (2002).[128] These compounds gained recognition over the years due to an increased tunability when compared to conventional ILs. This special class of ILs requires the functionalization of anion and/or cation (*i.e.,* covalent insertion of a functional group) in order to impart particular properties or reactivities.[129]It is important to note that Ts-ILs also present important disadvantages such as the need for additional complex synthesis steps.[130] There are several reported instances of the functionalization of ions with the goal of improving the chelating properties of ILs.[131]

Classification According to Properties

Alternatively, ILs can be categorized into generations depending on their physical, chemical, and biological properties. This organization results in three distinct groups.

First Generation ILs (1914) are air- and water-sensitive, which limits their research potential. ILs from this generation are essentially composed of combinations of metal halides (anions) with dialkyl imidazolium or alkyl pyridinium derivatives (cations).[104]

Second-generation ILs (circa 1990) present an air- and water-stable nature, but are more expensive and toxic. These are the most extensively reviewed compounds and are of interest not only because of their physical and chemical properties (*i.e.,* melting points, solubilities, viscosities, etc.), but also because they display important biocatalytic properties. The most common cations include dialkyl imidazolium, alkyl pyridinium, ammonium, and phosphonium whereas halides, tetrafluoroborate, and hexafluorophosphate are among the most common anions.[104]

Third-generation ILs (circa 2000) also known as advanced ILs. These ILs surpass past generations by employing natural and readily available ions such as choline, amino acids, and sugars. They are of special importance in biological studies as they are often more compatible with biological systems. These compounds are biodegradable, nontoxic, inexpensive, recyclable, and simpler to prepare. It is important to note that novel solvent systems such as deep eutectic solvents (DES) and Ts-ILs are also encompassed in this generation of ILs.[104]

1.3.3 Applications

ILs are remarkable chemical compounds that have delivered several predicted applications and are currently employed in varied areas of science and technology. Such relevance is attributed to a significant diversity of possible compounds, a unique set of physicochemical properties, and high biological activity. In the following segment, relevant mentions are highlighted.

Biological Applications

ILs can have an extensive impact on biological systems, ranging anywhere from the simpler ionic liquid-macromolecule interactions all the way to higher complexity living organisms.[132]This impact on the functioning of biological systems is dependent on biological activity which has been shown to correlate with bioavailability and be strongly dependent on the organism under study.[133]

Antibacterial and Antifungal Agents - Several ILs are known to inhibit the growth of pathogenic species with implications in the fields of medicine. Imidazolium, pyridinium, pyrrolidinium, based ILs were shown to hinder the growth of pathogenic bacteria and fungi. Some examples include the infamous *Clostridium sp.* bacterium which is susceptible to pyridinium-based ILs (N-ethyl pyridinium tetrafluoroborate) [134], and the multidrug-resistant fungus *Candida tropicalis,* whose growth is strongly inhibited by low concentrations of an imidazolium-based IL (1-n-hexadecyl-3-methylimidazolium chloride).[135] Consequently several instances of IL-coated surfaces with antimicrobial properties are known.[136]

Anticancer Agents - Considered a novel, yet important, avenue of research, several studies have been focused on the development of ILs as therapeutic agents with reduced toxicity toward humans.[137] The so far encouraging results on numerous cancer cell lines have shown ILs to be cytotoxic and/or cytostatic by promoting oxidative stress, DNA damage, and ultimately apoptosis.[138] Unfortunately results are highly dependent on cell lineage[139] and a consensual mechanism of action is yet to be established, effectively hindering further developments in the area.

Industrial Applications

Many of the physicochemical advantages of ILs are already being explored in the industrial setting owing to specific hydrogen bonding, coulombic, and van der Waals interactions after the widespread commercialization of said products.

Pharmaceutical Applications - One of the main bottlenecks in active pharmaceutical ingredient (API) development is the solubility optimization. In this sense, API-IL constructs are of particular interest as an alternative to crystalline salts. ILs can be used as adjuvants contributing to solubility and enhancement and drug delivery. ILs are capable of tuning the properties of active molecules (*e.g.,* solubility, polymorphism, delivery, release rates, handling, therapeutic efficacy, and adverse reactions) effectively optimizing therapeutic performances.[140] Some examples of potential API-IL constructs include the solubilization of N-Acetyl-L-cysteine in the [C2MIM][OTf] based IL or the solubilization of ibuprofen in [C10MIM][NTf2] based IL.[141]

Food and Biomass Processing - Extraction and separation processes are essential to many fields of science and industry, allowing for the selection of an interesting compound from a complex matrix.[142] In this sense, ILs present a novel and often more efficient approach to the already established organic solvents.[143] These compounds can disrupt the strong intermolecular hydrogen bonding networks found in weakly soluble biopolymers. In fact, ILs are already being applied in the dissolution of keratin[144], lignin[145], the decrystallization of cellulose[146], or the extraction of piperine from pepper.[147]

Chemical Applications

Many of the physicochemical advantages of ILs are already used in the laboratorial setting.

Organic Chemistry - The use of ILs as greener alternatives to conventional solvents in the fields of organic chemistry and the chemical industry remains the most significant application to date.[148] Applications in this area are a function of the excellent physicochemical properties found in ILs. These have been successfully used as solvents in a series of assorted reactions: electron transfer reactions, acid-base reactions, substitutions, elimination, addition, base or nucleophilic reactions, and many more. When it comes to catalysis ILs present an alternative to the common limitations found in conventional catalysts (*i.e.,* yield, selectivity, and reaction conditions).[149]

Electrochemistry - ILs have gained increasing interest in the field of electrochemistry due to their unique array of properties (*i.e.,* high conductivity, a wide span of electrochemical potentials, non-volatility, high viscosity)[150] which renders them as safer electrolytes to be used in metal electrodeposition, batteries, fuel cells, and sensors among other examples.[151]

Physical/Analytical Chemistry - ILs are currently being incorporated in essential analytical processes such as high-performance liquid chromatography, spectrometry, sensing, and analysis of metal ions and organic environmental pollutants.[152] The field of physical chemistry

has also gained interest in these kinds of compounds. Their tunable physicochemical properties has the potential to expand the current boundaries of conventional molecular solvents.[153]

1.3.4 Ionic Liquid Protein Interactions

Although it may be obvious, conventional inorganic salts cannot be used as biocompatible solvent media due to their relatively high melting temperatures (*e.g.,* NaCl presents a Tm of 801°C). Conversely, ILs display reduced melting temperatures opening novel avenues of investigation in biological systems.[149] For instance, the area of protein stabilization is paramount issue in several areas of research, with reports on this area dating back to the 1980's.[154] One noteworthy example is the pharmaceutical industry, where proteins are used in drug formulations. Proteins as active principles must remain stable in order to retain function, and minor changes in their microenvironment (*i.e.,* temperature, solvent composition) may lead to unfolding and inactivation. Native proteins are often marginally stable as folding intermediates and misfolded protein states may promote irreversible protein aggregation. Several strategies were developed to promote protein stability in non-native conditions with minor success (*i.e.,* chemical modification, immobilization, and genetic modification).[155] Some examples of stabilizing agents (*e.g.,* amino acids, sugars, and salts) being used as excipients are also reported, these prevent the denaturation and aggregation of therapeutic proteins. Currently, lyophilization or freeze-drying is one of the most employed strategies to increase protein shelf life. In this sense, ILs are a vast class of organic salts, which show high affinity to proteins and other biomolecules.[156] ILs (pure or as a mixture) are regarded as a novel approach as they can be designed to maintain the three dimensional structure of a protein by promoting hydrogen bonding, hydrophobic interactions and ionic interactions.[157] Over the last decade the impact of IL-water mixtures on protein stability[158], activity[159], refolding[160], and aggregation[161] has been studied. Selected examples report the ability of ILs to induce unfolding, misfolding and refolding on assorted proteins.[161]

Ion Specific Effects

Salt-protein interactions in water have been extensively reviewed[162] as ion-induced effects are ubiquitous to biology and chemistry alike. This phenomenon is described as the restructuring of the hydrogen bonding network of water when in the presence of ions (*i.e.,* bulk phenomenon).[163] Aqueous electrolytes display a predictable protein solvation behavior classically described in the Hofmeister series **(Figure 8)**. Ions are qualitatively classified as

kosmotropes (*i.e.,* structure and salting-out promoters) or chaotropes (*i.e.,* structure breakers and salting-in promoters). Kosmotropes are densely charged ions (*i.e.,* dihydrogen phosphate, sulfate, ammonium, etc.) which promote vicinal electrostatic ordering (breakage of nearby hydrogen bonds), thus being strongly hydrated. Chaotropes, on the other hand, are typically single charged and bulky ions (*i.e.,* dihydrogen phosphate, sulfate, ammonium, etc.) which minimally interfere with the surrounding water network promoting hydrogen bonding in surrounding water molecules (weakly hydrated), these ions tend to destabilize proteins.[164]

More recently ion-protein interactions have been described as an interfacial phenomenon which is not necessarily dependent on water perturbation. Instead, the interactions of ions with the aqueous interface of the macromolecule are regarded as central to the thermodynamic and kinetic properties of proteins.[163,165] ILs display a more balanced range of interactions when compared to conventional salts, as electrostatic interactions are comparable to hydrophobic interactions and hydrogen bonding. In this sense the solvation tendency among ILs is similar, but not identical, to conventional inorganic salts and must be further assessed on the grounds of hydrophobicity, charge/polarity, polarizability, and acid-base character.[163] It is important to note that protein nature, and consequently specific solute-ion interactions, are also crucial to describe the expected solvation behavior, as the protein backbone profile will dictate interaction tendencies with a given ion.[166]

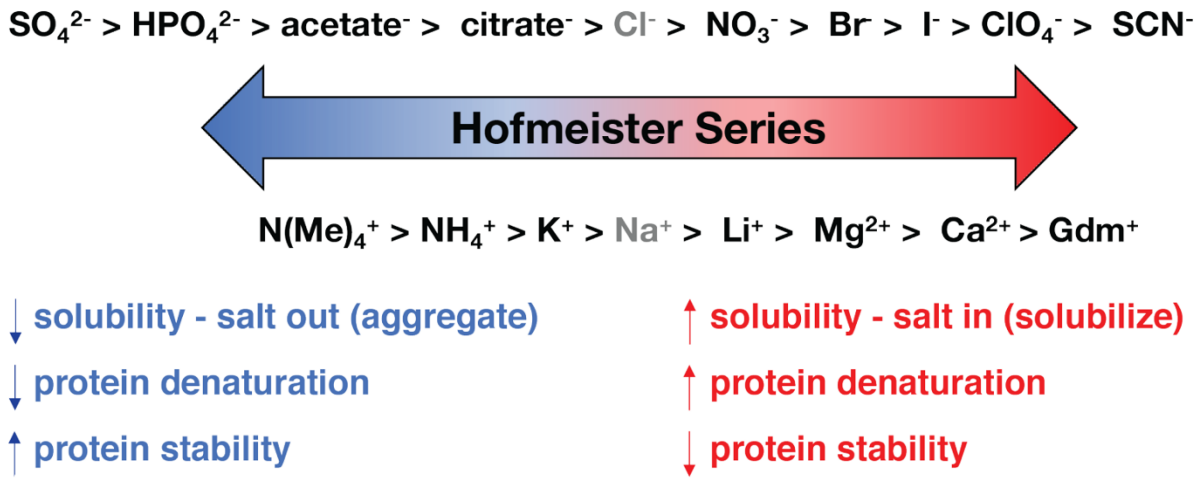

Figure 8 – Modernized Hofmeister Series

Anionic and cationic elements (top and bottom respectively) are grouped by series and accompanied by the respective properties. Adapted from Zhang and Cremer.[167]

Ionic Liquids and Amyloid Formation

Several proteins can form amyloid aggregates (*e.g.,* alpha synuclein, lysozyme, insulin or tau protein), which are often involved in disease processes. Over the decades several drugs were explored as potential anti-amyloidogenic agents.[21] Akin to these compounds, some ILs have been reported to modulate fibril formation and stability. Depending on ILs nature, amyloidogenesis may be favored or inhibited. Some cases can even result in the dissolution of mature fibrils, effectively restoring original protein structure and function.[21,156,168] These compounds are thought to influence major molecular interactions found within amyloid aggregates (*i.e.,* hydrophobic interactions, hydrogen bonds, and salt bridges) which are responsible for the characteristic thermodynamic stability of the protein structure.[168] Additionally, water content is key to predict the inhibitory effects of a given IL as it often ties to higher ordering structuring in more hydrophobic ILs.[156]

Relevant examples of fibrillation modulation by ILs include: **(i)** the role of tetramethylguanidinium acetate [TMG][Ac] as a partial inhibitor of Chicken egg-white lysozyme fibrils[169], or **(ii)** Stimulation of αS amyloid fibril formation in the presence of 1-butyl-3-methylimidazolium based ILs.[170,171]

Cholinium based ILs ([Cho] ILs) are of special importance to the present discussion due to their reported effects on protein (de)stabilization. These ILs exhibit an increased propensity to suppress the formation of mature fibrils. Overall, inhibition efficiency is not only dependent on the hydrogen bonding and kosmotropic nature of cholinium but also on the properties of the selected counterion. Although literature related to [Cho] ILs and amyloid formation is scarce, some noteworthy examples include: **(i)** the conservation of secondary structure and function of Chicken egg-white lysozyme by choline dihydrogen phosphate [Cho][DHP] and choline bitartrate [Cho][Bit] when in the presence of fibrillation prone conditions (i.e., acidic pH and high temperature)[21], **(ii)** the dissolution of recombinant cellulase fibrils from Escherichia coli by [Cho][DHP][156], **(iii)** the stabilization of the domain B1 of protein G (GB1) from *Streptococcus sp.* by [Cho][Glu][24], and **(iv)** the stabilization of collagen and Human Serum Albumin (HSA) by [Cho][DHP] when acting as a cosolvent.[21,172,173]

1.3.5 Osmolytes as potential Ionic Liquids

Osmolytes are low-molecular weight organic salts that exhibit protective properties against denaturing and/or osmotic stress. These compounds exhibit high intracellular concentrations and are primarily tasked with the preservation of cell integrity by regulating key

features of biological solutions (*e.g.,* viscosity, melting point, and ionic strength) in response to specific stress signals (*e.g.,* osmotic pressure, temperature, salinity and pH).[16,17,174] Akin to conventional inorganic salts, osmolytes exert significant effects on macromolecules and have been found to influence protein folding and stability.[16–18] Osmolytes regulate protein structure by means of: **(i)** direct mechanisms, which include the co-solvent interactions with the peptide backbone and/or side chains (i.e., hydrogen bonding, charged, and polar interactions), and **(ii)** indirect effects, referring to the solvation of hydrophobic portions of the protein or changes in bulk water structure when in the presence of co-solutes.[175] The indirect effects play a major role in influencing protein structure.[176] More traditional ionic liquids (*e.g.*, 1-Butyl-3-methylimidazolium based) tend to have a strong hydrophobic character, thus resulting in a (de)stabilization of the protein structure through indirect effects. Biocompatible ILs are on the other hand water friendly, creating a more nuanced balance between direct mechanisms and indirect ones. Stabilizing bioinspired ILs (*i.e.,* Cholinium-based ILs) have been shown to exert more subtle protein interactions that allow for the inclusion of water in the protein surface. These osmolytes are also capable of mimicking the hydrogen-bond strength of interfacial water acting as a biocompatible osmolyte that minimally interfere with water-protein interactions.[175]

Because these compounds are derived from natural sources, they yield biocompatible ILs with much lower toxicities than traditional ILs.[164] Naturally occurring osmolytes are reported to have an osmoprotectant effect towards proteins (*i.e.,* γ-aminobutyric acid, glycerophosphorylcholine, taurine, betaine, myo-inositol, trimethylamine-N-oxide).[177,178] These compounds exist intracellularly at concentrations that range from 100 to 300 mM, which can be defined as general upper and lower limits for protein IL interactions.[174,179]

1.3.6 Design of the Bioinspired Ionic Liquid [Ch][Glu]

The osmolytes found in the intracellular milieu stand out as well-suited candidates for the development of biocompatible ILs. These candidate ions may reach molar concentrations *in vivo*[19] and are inherently biodegradable and biocompatible, often displaying important roles on cellular processes such as regulation of diffusion, reaction rates, biochemical processes, cellular organization, and protein stability.[19,180] The possibility of combining physiologically relevant charged metabolites into ILs is strengthened by the first report of a naturally occurring IL. Chen's group.[20] identified several formate-based ionic liquids in the neutralized venom mixtures created by hostile interaction between *S. invicta* and *N. fulva*. By combining these findings with the broader cellular context mentioned earlier, one can conclude that there is a significant possibility that some charged metabolites can form naturally occurring ILs. The

implications of which for protein stability in physiological conditions are still unpredictable and the effects may extend far beyond the traditional Hofmeister series. Therefore, a representative IL must be selected from the available metabolites and studied in the context of protein stabilization.

For solution protein studies, the cation-anion pair should result in an IL that displays inherent buffering capabilities when in aqueous solution. Cation-anion combinations should result in an IL with a buffering range that encompasses the physiological pH.[181] Human metabolome databases were used to identify biologically relevant charged metabolites with implications in protein conformational diseases. The resulting a metabolite pool consisted mostly of anions (*e.g.,* 5-oxoproline, acetate, aspartate, bicarbonate, citrate, formate, glutamate, glutarate, glycolate, glycerate, homovanillic acid, kynurenic acid, lactate, malate, maleate, malonate, oxoglutarate, propionate, pyruvate, salicylate, and succinate) and a few cations (*e.g.,* acetylcholine, arginine, choline, diethanolammonium, dopamine, ethanolammonium, and lysine).[182]

Choline is an ideal cationic component for naturally occurring ILs. The cholinium ion can be found in relatively high concentrations in the CNS despite values varying significantly with the patient and the studied brain tissue. This cation is estimated to reach concentrations of 1.83 mM in the basal ganglia, up to 1.4 mM in the frontal lobe white matter, and as much as 76.5 mM in cerebrospinal fluid.[183,184] It is important to note that the cholinium ion may be found in higher concentrations in synaptic vesicles. Choline is an essential micronutrient that is required for the normal functioning of most cells. The cholinium ion is an important component of several important metabolites which play important roles in the maintenance of membrane integrity (*i.e.,* phospholipid synthesis), transmembrane signaling and transport, labile methyl group metabolism, and is also the precursor of the neurotransmitter acetylcholine [185–187] Choline is well reported as a stabilizing agent in the field of ILs with most of the selected anions (*e.g.,* lactate, levulinate, carbohydrate derivatives and amino acids) being already explored as biocompatible cholinium-based ILs. The presence of additional hydroxyl, carboxylic acid, and amide groups on cholinium-based ILs has been shown to improve the thermal stability of proteins and extend their long-term storage.[188]

Glutamate is the most abundant amino acid and one of the most abundant intracellular metabolites found *in vivo*, being able to reach concentrations of 96 mM in *E. coli* specimens, for instance.[19,180] In the Human brain this metabolite is estimated to have a concentration of 12.5 mM, with synaptic vesicles reaching concentrations of close to 60 mM.[189,190] The glutamate anion is of extreme importance physiologically by acting as an intermediary of the carbon

nitrogen metabolism (energy reserve, nitrogen source). Glutamate is also an important precursor of glutathione (redox balance) and the important neurotransmitter GABA (Gamma-Amino-Butyric Acid). Despite not being as well studied as choline, some glutamic acid analogs such as bitartrate and α-ketoglutarate have reported to have stabilizing properties towards proteins.[28,191,192] Like the cholinium cation, glutamate also benefits from the additional interactions of carboxy and hydroxy groups.

The ionic liquid [Cho][Glu] **(Figure 9)** (Choline Glutamate) inherits many of the favorable biological activity traits found in cholinium and dicarboxylic acid based ILs, thus becoming a prime candidate for promoting protein stabilization. Earlier studies in the group have already reported on the stabilizing influence of this IL on the stability of different protein models[23], including: αS (alpha-synuclein), lysozyme, GB1 (B1 domain of staphylococcal protein G), and SH3 domain (Drosophila signaling N-terminal protein drk).

αS is expected to directly interact with cholinium and glutamate, as the compounds are for the most part colocalized. Moreover, the concentrations of αS, cholinium, and glutamate are maximized in the presynaptic area and vesicles.[189,190] These findings suggest a possible stabilizing role of choline glutamate as a potential stabilizing agent for alpha-synuclein.

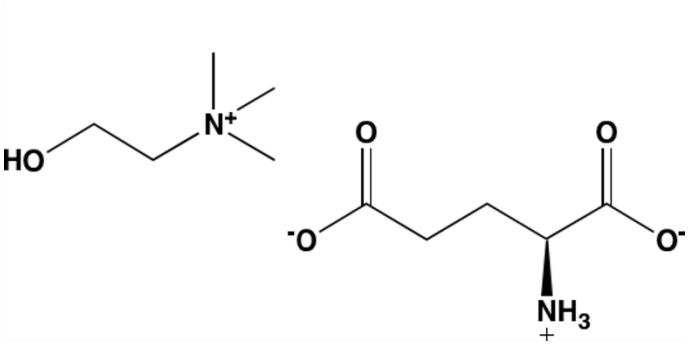

Figure 9 – Structural Features of the Ion Pair [Ch][Glu]

The structures at physiological pH for cholinium and glutamate ions are represented on the left and right, respectively

1.4 Hypothesis, Objectives, and Outline of the Thesis

Synucleinopathies are neurodegenerative diseases characterized by the presence of intracellular deposits containing the protein alpha-synuclein (αS) within patients' brains.[3] A pathological hallmark of synucleinopathies, particularly Parkinson's Disease (PD), is αS misfolding into pathogenic conformers, which has been proposed as an early trigger of PD.[3] These

findings support the development of PD therapies that reduce αS gene expression or block its aggregation.

An increasing pool of knowledge has shown that intracellular metabolites/osmolytes have the potential to modulate protein folding, particularly those that are charged and whose concentrations are sensitive to aging and lifestyle (*e.g.*, choline and glutamate).[19] Additionally, in its native form, αS exists exclusively in its N-terminal acetylated form (Ac-αS), with this feature being proposed to modulate its function and aggregation into amyloid fibrils.[3] Yet, the great majority of studies are conducted with its non-acetylated form. Thus, the research plan aims to investigate the influence of common metabolites on the aggregation of αS and Ac-αS, as well as to characterize possible interaction sites. For this, the work focused on structural aspects, using nuclear magnetic resonance spectroscopy (NMR) and fluorescence studies (thioflavin T, ThT) to study the interaction between alpha synuclein (αS and Ac-αS) and the ionic liquid choline glutamate ([Cho][Glu]).

The objectives of the presented work are to understand, with atomic detail: **(i)** if/how intracellular metabolites and osmolytes can modulate αS stability, and aggregation; **(ii)** the consequences of this modulation in terms of the protein's structure; **(iii)** evaluate if the obtained results have physiological relevance.

Taking the proposed objectives in to account, the work was divided into four tasks: **1)** Production and purification of [Cho][Glu] and αS and Ac-αS (non-labeled and 13C,15N-labeled). **2)** Aggregation kinetics of αS and Ac-αS in the presence and absence of [Cho][Glu]. **3)** Interaction studies of αS and Ac-αS with [Cho][Glu].**4)** Study of the influence of [Cho][Glu] on αS and Ac-αS structure.

Task 1 involved **(i)** the expression and purification of αS variants (acetylated and non-acetylated) through a hybrid heat-shock/precipitation technique; and **(ii)** the synthesis of [Cho][Glu] via an ion exchange. The obtained samples were used in the following tasks. Because of this, αS variants were also produced isotopically labeled with ^{13}C and ^{15}N.

In task 2, the effect of [Cho][Glu] on αS variants was explored. High throughput fluorescence spectroscopy was used to study the stability of αS in the presence of [Cho][Glu] and sodium chloride (NaCl), aiming at unraveling any underlying mechanism(s). αS variants were tested under increasing concentrations of [Cho][Glu] or NaCl, with thioflavin T (ThT) being used as an indirect reporter of amyloid fibril formation.

In tasks 3 and 4 we used solution state NMR spectroscopy to gain atomic insights on potential interactions of αS residues and [Cho][Glu] and to infer on eventual structural modifications caused by the presence of the IL. Isotopically labeled (^{13}C,^{15}N) αS variants were titrated

with increasing concentrations of [Ch][Glu] or NaCl. A series of bidimensional spectra (*i.e.,* $^{1}H,^{15}N$-HSQC) were collected in order to identify the residues affected by the ionic liquid. Moreover, histidine specific HSQC's were also acquired to follow the protonation behavior of H50 (a key residue involved in αS fibrillation propensity). In parallel, tridimensional spectra (*i.e.,* HNCACB, HN(CO)CACB, HNCO, and HNCACO) were also acquired at specific points to not only facilitate the assignment of the HSQC peaks, but also to infer about the protein secondary structure propensity (SSP).

In this way, we established an *in vitro* protocol for studying αS-IL interactions, capable of linking the protein's aggregation behavior (stability) to the affected residues, further highlighting possible structural propensity changes.

2
MATERIALS AND METHODS

In the present work, four protein samples were prepared in the labeled and unlabeled forms, corresponding to: **(a)** Alpha-synuclein. **(b)** Acetylated alpha-synuclein. **(c)** Double-labeled alpha-synuclein. **(d)** Double-labeled acetylated alpha-synuclein. Non-labeled samples were used for fluorescence studies whereas double-labeled protein samples were used for NMR studies. The labeling of αS is controlled by the composition of the medium, while acetylation is controlled by selecting the desired plasmids. Non-labeled samples were prepared by expressing transformed cells in conventional LB growth medium, whereas double-labeled protein samples (*i.e.,* uniformly labeled with ^{15}N, and ^{13}C) are obtained by expressing cells in M9 minimal medium. The latter uses $U^{15}N$-labeled ammonium chloride (3.0 g/L) and $U^{13}C$-labelled D-glucose (1.52 g/L) as sole sources of nitrogen and carbon, respectively. Regarding the αS acetylation state, in brief, if only pT7-7*****[1] (ampicillin resistance, always supplemented at a concentration of 100 mg/mL) is used, non-acetylated αS is formed. Conversely, if pT7-7 and pNatB*****[2] (chloramphenicol resistance, always supplemented at a concentration of 25 mg/mL) are combined, Ac-αS is formed. The detailed experimental protocols provided below are for the double-labeled Ac-αS.

2.1 Plasmid Replication and Purification

Equipment. ES-20 Compact Shaker-Incubator; Grant-Bio (ES-20). 5804R Bench Top Centrifuge; rotor F34-6-38, Eppendorf (5804R). MIKRO 120, rotor 1242; Hettich (MIKRO). **Materials & Reagents.** NZYMiniprep kit, NZYTech (MB010). Ampicillin, NZYTech (97.8%, MB021). Chloramphenicol, NZYTech (99.6%, MB02402). Glycerol, Scharlau (99,5%, GL00261000). **Buffers & Media.** The Luria Bertani agar (LA) and Luria Bertani Broth (LB) media were formulated according to the specifications provided in Tables S8 and S9, respectively. **Strains & Plasmids.**

Competent DH5α *E. coli* cells, ThermoFisher Scientific (TableS5). pT7-7 (Addgene #36046). pNatB (Addgene #53613).

2.1.1 Overview

Expression of recombinant αS requires the production of highly concentrated and purified plasmid samples to be used in subsequent steps. Plasmids related to αS (pT7-7) and the NatB complex (pNatB) were individually cloned in competent DH5α *E. coli* cells. Purification was accomplished through the NZYMiniprep kit.

2.1.2 Protocol

The NZYMiniprep kit protocol was followed with minor modifications.*[3] First, a stock of competent DH5α E. coli cells was used to streak a LA plate and incubated for 12 h, 37 °C, supplemented with ampicillin and chloramphenicol. A single colony was extracted and used to inoculate 12 mL of LB culture medium supplemented with ampicillin and chloramphenicol, which was then incubated for 12 h (37 °C, 200 rpm | ES-20). Then 10 mL of the resulting sample was pelleted (12000xg; 1 min | 5804R). A glycerol stock*[4] was created for long-term use. Each pellet was resuspended in 500 µL of Buffer A1 by vigorous vortexing. Buffer A2 (500 µL) was added and mixed by tube inversion (6-8 times) followed by a 4-minute incubation. Buffer A3 (600 µL) was also added and mixed by inversion (6-8 times). The resulting mixture was centrifuged for 10 min (10000 rpm | MIKRO). The supernatant was loaded into an NZYTech spin column previously mounted on a 2 mL collecting tube. Buffer AY (500 µL) was added to the column followed by centrifugation (1 min; 10000 rpm | MIKRO) and the flow-through was discarded. Buffer A4 (600 µL) was added to the column followed by centrifugation (1 min; 10000 rpm | MIKRO), and the flow-through was discarded. The NZYTech spin column was placed in a new 2 mL collecting tube and centrifuged (2 min; 10000 rpm | MIKRO). The column was transferred to a 1.5 mL tube, 50 µL of preheated (80 °C) ultrapure water*[5] was added. Next, the column was incubated for 1 min and subject to centrifugation. The final step was repeated*[6] to obtain 2 samples (100 µL, 65 pg/mL) of pT7-7 and pNatB. Samples*[7] were later stored (-20 °C).

2.1.3 Relevant Notes (✱)

[1] The pT7-7 plasmid (high copy number) encodes human WT αS and was provided by Hilal Lashuel (Addgene plasmid # 36046).[193] Further information and plasmid sequence can

be found in **Figure SM1**. **[2]** The pNatB plasmid (pACYCduet-naa20-naa25, high copy number) was provided by Dan Mulvihill (Addgene plasmid # 53613).[194] pNatB encodes for the N-α-terminal acetyltransferase B complex (NatB) that is composed of a catalytic subunit (Naa20, 23 kDa) and an auxiliary subunit (Naa25, 92 kDa). Further information and plasmid sequence can be found in **Figure SM2**. **[3]** Two modifications were done to the NZYMiniprep kit protocol. The first refers to the reduction of purification runs in the original protocol. A combined (10 ml) purification run was used instead of the recommended 2 runs (5 ml), and buffer volumes were doubled to accommodate the changes mentioned. The second adjustment can be found in the final stage of plasmid purification; the column is incubated twice with MQ water to maximize the plasmid yield. **[4]** A small volume (1-2 mL) is reserved to create glycerol stocks, which are created by combining 75% (v/v) of transformed cells with 25% (v/v) of glycerol. All glycerol stocks are flash-frozen and stored at -80 °C. Upon usage, glycerol stocks should not defrost completely, instead cells should be collected on the melted surface using a sterilized toothpick (or equivalent). **[5]** The pH was maintained in the 7.0 to 8.5 range for optimal results. **[6]** The step was repeated to increase the yield. Samples resulting from the 1st and 2nd elutions were combined to guarantee a homogeneous solution. **[7]** Samples of both plasmids were sequenced to ensure that the protein of the primary sequence of interest was present, and sequence analysis was performed with the ExPASy Translate Tool.[195]

2.2 Transformation

Equipment. AccuBlock™ Digital Dry Baths; Labnet International (AccuBlock). ES-20 Compact Shaker-Incubator; Grant-Bio (ES-20). MIKRO 120, rotor 1242; Hettich (MIKRO). **Materials & Reagents.** Ampicillin, NZYTech (97.8%, MB021). Chloramphenicol, NZYTech (99.6%, MB02402). **Buffers & Media.** Luria Bertani agar (LA) and Luria Bertani broth (LB) media were formulated according to the specifications provided in Tables SM7 and SM8, respectively. **Strains & Plasmids.** Competent BL21-DE3 E. coli cells, ThermoFisher Scientific (Table SM5). pT7-7 (Addgene #36046). pNatB (Addgene #53613).

2.2.1 Overview

Here, competent BL21-DE3 *E. coli* cells incorporate the plasmids created in the previous section. Therefore, we created cells capable of expressing all αS variants. Transformation was performed via the heat shock method. The following protocol was adapted from previous work by Fauvet and Johnson.[5,194]

2.2.2 Protocol

The desired plasmid (1 µL, 65 pg) was added to 50 µL of a stock of competent BL21-DE3 E. coli cells, which was then cooled on ice for 15 min. The sample was incubated in a thermal block (40 s, 42 °C | AccuBlock), followed by another 15 min of refrigeration on ice. LB medium (500 µL, 37 °C) was added and incubated (200 rpm, 1 h, 37 °C | ES-20). The bacterial culture was pelleted (10000 rpm, 1 min, room temperature | MIKRO) and resuspended in 200 µL of LB medium.*[8] Two 20 mL LA plates, supplemented with ampicillin and chloramphenicol, were streaked with 100 µL of the resulting sample. The plates were then incubated (12 h, 37 °C | ES-20) and stored at 4 °C.

2.2.3 Relevant Notes (✱)

[8] The concentration of the bacterial culture contributes to a more efficient transformation. This process is especially important when co-transforming. In these cases, the number of colony-forming units is particularly low (*i.e.,* 2 to 5 CFUs) due to the use of 2 selection antibiotics.

2.3 Expression and Purification of αS

Equipment. ES-20 Compact Shaker-Incubator; Grant-Bio (ES-20). UV-1280 UV-VIS Spectrophotometer; Shimadzu (Shimadzu). Avanti J-26 XPI, fixed-angle rotor JA-10; Beckman Coulter (Avanti). 5804R Bench Top Centrifuge, rotor F34-6-38; Eppendorf (5804R). ÄKTA™ start; Cytiva (*ÄKTA*). NanoDrop ND-1000 UV-Vis spectrophotometer; Thermo Fisher Scientific (*NanoDrop*). Edwards Modulyo Freeze Dryer, Artisan Technology Group (Modulyo). **Materials & Reagents.** SnakeSkin™ dialysis tubing, 7 K MWCO; ThermoFisher Scientific (SnakeSkin). HiTrap Q HP 5 mL column, Cytiva (HiTrap). Whatman Puradisc Syringe Filter (0.2 µm); Cytiva (Puradisc). Glycerol, Scharlau (99,5%, GL00261000). Isopropyl β-D-1-thiogalactopyranoside (IPTG), nzytech (>99%, MB026). Ammonium Sulfate, May and Baker LTD Dagenham England (99%, CAS: 7783-20-2). Ampicillin, NZYTech (97.8%, MB021). Chloramphenicol, nzytech (99.6%, MB02402). **Buffers & Media.** Lysis Buffer (Lys | Table SM14). Ion Exclusion Chromatography Buffer (IEC | Table SM16). Buffer A (BA | Table SM17). Buffer B (BB | Table SM18). The Luria Bertani Agar (LA), Luria Bertani Broth (LB), and M9 minimal media were formulated according to the specifications provided in Tables SM8, SM9, and SM10, respectively. **Strains & Plasmids.**

Competent BL21-DE3 E. coli cells, ThermoFisher Scientific (Table SM5). pT7-7 (Addgene #36046). pNatB (Addgene #53613).

2.3.1 Overview

αS variants were expressed in 1 L (4 x 250 mL) batches by utilizing transformed BL21-DE3 *E. coli* cells. Bacterial cultures resulting from protein expression were lysed (by boiling the cells) and purified in a three-step system. The first step consists of precipitating protein with ammonium sulfate, followed by anion exchange chromatography and a final polishing and concentration step via ammonium sulfate precipitation. The developed protocol was based on previous works of Viennet, Hoyer, and Wördehoff.[65,196,197]

2.3.2 Protocol

First, a single transformation plate colony was used to inoculate 12 mL of LB medium supplemented with ampicillin and chloramphenicol for 12 h (37 °C, 200 rpm | ES). This step was repeated 2 times, and the starter cultures were combined*[9] (final volume of 24 mL). Supplemented culture medium (250 mL) was inoculated with 5 mL of the starter cultures. This step was repeated 4 times. Glycerol stocks were created for long-term use. The resulting 1 L of culture medium was inoculated and incubated (37 °C, 180 rpm) until an OD_{600} in the range of 1 to 1.2 was reached (Shimadzu), at which point protein overexpression was induced by adding IPTG to a final concentration of 1 mM.*[10] Cells were incubated for another 4h, collected by centrifugation (15 minutes, 6000xg, 4 °C | Avanti), and stored at -20 °C.*[11] Bacterial pellets containing αS were resuspended in 30 mL of LyB (preheated to 75 °C). The resulting sample was incubated for 20 min in a double boiler system (90-95 °C)*[12], allowed to cool on ice for 10 minutes and then centrifuged (15000xg; 30 min; 4 °C | 5804R).*[13] The supernatant was subjected to precipitation with a saturated ammonium sulfate solution*[14], while under magnetic agitation.[198] During precipitation, 5 mL of ammonium sulfate was added at a time until the final concentration of 0,36 g/mL (70% saturation at 0 °C) was reached.*[15] The sample was incubated on ice for 20 min and then centrifuged (1,5000xg; 30 min, 4 °C | 5804R). The pellet was then resuspended in an adequate volume of IEC (approximately 20 mL) and dialyzed against 4,5 L of BA for 12 h at 4 °C (SnakeSkin).*[16] As a second purification step, the dialyzed fraction was subjected to anion exchange chromatography (ÄKTA).*[17] In both cases, the samples were divided into two separate runs of equal volume and injected with a flow rate of 3 mL/min. The column was equilibrated with 40 ml of BA. A 0-50% gradient of BB was created, with a flow of

2 ml/min (lasting for 40 mL) followed by a 50-100% gradient of BB (lasting for 10 mL at the same flow rate). As a final step, 100% of BB was eluted at the same flow rate until Abs_{280} resumed the initial value. Elution fractions containing the protein of interest were again subjected to precipitation with ammonium sulfate, while under magnetic agitation. During precipitation 5 mL of ammonium sulfate was added at a time until the final concentration of 0.36 g/mL (70% saturation at 0 °C) was reached. The sample was incubated on ice for 20 min and then centrifuged (1,5000xg; 30 min; 4 °C | 5804R). The pellet was then resuspended in an adequate volume of BA (approximately 5 mL) and dialyzed*[18] against 4,5 L of BA for 12 h at 4 °C.*[19] The resulting samples were flash-frozen in liquid nitrogen, lyophilized (Modulyo), and stored at -20 °C.*[20]

2.3.3 Relevant Notes (✱)

[9] Mixing ensures sample homogeneity. **[10]** IPTG induces both the expression of αS and NatB. **[12]** High temperatures result in bacterial membrane destruction. Non thermoresistant proteins precipitate while αS remains in solution. **[11]** The act of freezing bacterial pellets promotes cell lysis. **[13]** During this process, the lysate should be completely covered in the LyB solution. **[14]** αS, being thermoresistant, will not precipitate like most proteins. **[15]** The ammonium sulfate solution is 100% saturated when a 3.9 M concentration is reached at 0 °C.[198] **[16]** At 70% saturation (2.72 M, 0 °C) αS precipitates. **[17]** HiTrap was used as an anion exchange column. All tampons were filtered before usage (Puradisc). **[18]** Step intended to remove cellular salts and ammonium sulfate. **[19]** Protein concentration was estimated by measuring Abs_{280} values (NanoDrop). The molecular weight is available in (Table SM6). The ProtParam ExPASy software.[195](was used to estimate the molecular extinction coefficient (Table SM6). **[20]** Studies have shown that storage conditions can significantly affect the aggregation dynamics of α-Syn.[199]

2.4 Tris-SDS-PAGE electrophoresis

Equipment. AccuBlock Digital Dry Baths; Labnet International (AccuBlock). MIKRO 120, rotor 1242; Hettich (MIKRO). PowerPack Universal Power Supply, Bio-Rad (Power Supply). Mini-PROTEAN Tetra hand-cast systems (PROTEAN). **Materials & Reagents.** Acrylamide gel consists of a stacking and running gel (Table SM1). NZYTech Colour Protein Marker II, NZYTech (MB090). **Buffers & Solutions.** Tris-tricine Buffer (TB | Table SM12). Sample Buffer (SB | Table SM3). Staining and destaining solutions (Table SM4).

2.4.1 Overview

Electrophoresis was made under denaturing conditions (SDS-PAGE). A tricine-SDS (Tris-SDS)*[21] buffer system was used for protein separation. Acrylamide gels allowed qualitative monitoring of the αS at different time points of the expression and purification process.

2.4.2 Protocol

A discontinuous acrylamide gel system, consisting of a stacking and running gel (4% and 12%, respectively), was prepared*[22] (PROTEAN). Briefly, the separating gel was poured into the gel mold (2/3 of the height) and then gently overlaid with a stacking gel solution, the gel comb was introduced, and the gel was left to polymerize (4 hours). Regular samples were prepared by mixing 5 µL of SB to 15 µL of sample and then incubated (1 min, 100 °C | AccuBlock). Gels were loaded with 15 µL of the sample mixture. Bacterial samples (1 mL) were centrifuged (14000 rpm, 10 min | MIKRO) and the pellet*[23] resuspended in 70 µL of SB, incubated (10 min, 100 °C | AccuBlock), and centrifuged again (14000 rpm, 30 min | MIKRO). Gels were loaded with 10 µL*[24] of the sample mixture. Molecular markers (NZYTech Colour Protein Marker II; NZYTech) were added to monitor the electrophoretic process (11 to 245 kDa). All gel runs were made at 200 Volts, 50 Watts for 45 minutes (variable amperage). The resulting acrylamide gels were stained (30 minutes) and destained (minimum of 4 hours) to reveal results (using premade solutions).

2.4.3 Relevant Notes (✱)

[21] The discontinuous Tris-SDS-PAGE system is more effective when resolving low molecular weight proteins such as αS (14,4 kDa). It is used to obtain better separation in the molecular ranges of 5-20 KDa (5-20 KDa; capable of separating in the range of 1 to 100 KDa).[200] **[21]** Acrylamide gels can be stored for up to 2 weeks in TB (4 °C). **[23]** May be stored at -20 °C for later use. **[24]** The sample mixture should be collected on the solution surface which is considerably less viscous.

2.5 Choline Glutamate Synthesis

Equipment. Docu-pH_{Meter}, Sartorius (Docu-pH). Buchi R-114 Rotary Vap System, Marshall SCIENTIFIC (Rotavapor). Edwards Modulyo Freeze Dryer, Artisan Technology Group (Modulyo). **Materials & Reagents.** Choline chloride ([Ch][Cl]), Alfa Aesar (>98%, A15828). L-glutamic

acid (GluAc), Panreac (99%, A1704). Amberlyst® A-26(OH), Alfa Aesar (Amberlyst | A17361). Nitric acid, Sigma-Aldrich (70%, 438073). Silver nitrate, Panreac (>99.8%, 131459).

2.5.1 Overview

The IL [Ch][Glu] was synthesized in a 2 steps reaction **(Figure 10)**: **(a)** An ion exchange resin was used to form choline hydroxide from the precursor choline chloride. **(b)** Choline hydroxide and L-glutamic acid were combined to form IL in a neutralization reaction (potentiometric titration).

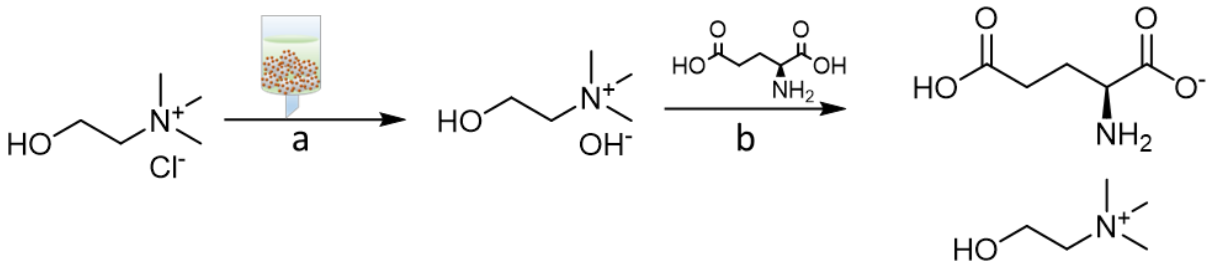

Figure 10 – Synthetic route for the formation of [Ch][Glu]

2.5.2 Protocol

Choline Hydroxide Preparation. We used the method reported in the literature.[201,202] A column (1 cm in diameter, 30 cm in length) was packed with 43 mL (36 g) of Amberlyst resin*[25] on a cotton base. BD water (0.2 drops/s) was passed through the column until pH 7.0 was reached (Docu-pH). 50 mL of a [Ch][Cl] solution (4.75 g, 34 mmol) was added to the column (0.1 drops/s). The resin was then washed with 150 mL of water to collect the [Ch][OH] solution. The absence of chloride ions was confirmed by a qualitative silver nitrate test.*[26] Briefly 1 mL of sample is combined with 0.5 mL of concentrated nitric acid (70% v/v) followed by the same volume of silver nitrate (0.1 M), to ensure that no precipitate is formed.

Choline Glutamate Preparation. This synthetic step was based on the work by De Santis et al.[203] The freshly prepared [Ch][OH] solution*[27] (175 mL, 31 mmol) was used to titrate 100 mL of L-glutamic acid (4.5 g, 31 mmol) under agitation. The progress of the titration was monitored by pH readings, the reaction was stopped when the equivalence point (pH=7.0) was reached.*[28] The sample was left to incubate in the dark under agitation (12 h). Finally, the solvent was evaporated under reduced pressure (3 h, 60 °C | Rotavapor) and the samples were flash-frozen and lyophilized (overnight | Modulyo).

2.5.3 Relevant Notes (✱)

[25] Amberlyst is a basic anion exchange resin capable of exchanging halide ions for hydroxide ions. Amberlyst may be regenerated with 10% NaOH. The resin should be packed in a dark and well-ventilated environment. The slow exchange of the resin only allows for small fluxes. **[26]** The nitrate test allows the detection of chloride ions in the solution. Nitric acid not only acidifies the solution but also removes interfering ions (e.g., carbonate). The absence of precipitate indicates that the solution contains minimal chloride traces (≤ 10 ppm). **[27]** May be stored for up to 2 days (4 °C). **[28]** At this point, the [Ch] to [Glu] stoichiometry is 1:1.

2.6 Fibrillation Assays

Equipment. 5804R Bench Top Centrifuge, rotor F34-6-38; Eppendorf (5804R). Infinite 200 Pro, Tecan (Tecan). **Materials & Reagents.** Whatman Puradisc Syringe Filter (0.2 μm); Cytiva (Puradisc). Amicon® Ultra-4 Centrifugal Filter Units (Amicon | UFC810024). MICROPLATE, PS, 96 WELL, F-BOTTOM, Greiner (655076). Glass beads, 2,85 - 3,45 mm; Carl Roth (A557). Microseal 'B' Adhesive Sealing Film; Bio-Rad (Microseal | MSB1001). Sodium Chloride (NaCl), Panreac (>99.5%, A2942). Sodium Azide (NaN_3), Panreac (>99%, A1430). Thioflavin-T; Sigma-Aldrich (>65%, T3516). **Buffers.** Phosphate Buffer (PB | Table SM19).

2.6.1 Overview

The stability and aggregation kinetics of αS variants were monitored in the presence of increasing concentrations of [Ch][Glu], and NaCl. The Thioflavin-T (ThT) probe was used as a reporter of amyloid formation. The protocol was adapted from the works of Wördehoff and coworkers.[204] Titrations are divided into protein samples, resulting in two microplates, one for alpha-synuclein in IL/NaCl and another for acetylated alpha-synuclein in IL/NaCl. Individual microplates can be organized into sample groups: **(a)** IL and NaCl arrays, which range from 10 mM to 1 M (triplicates, cells D1 to F6 and F7 to H12, respectively). Here, the aggregation conditions of αS (50 μM) are tested in the presence of ThT (10 mM) and NaN_3 (0.02 % w/v). **(b)** The αS reference (triplicates, cells A1 to A3). This group is used to monitor protein behavior when neither IL nor NaCl is present. **(c)** The IL and NaCl controls range from 10 mM to 1 M (cells B2 to B11 and C2 to C11, respectively). The controls ensure that neither IL nor NaCl interferes with the ThT fluorescence. **(d)** The NaN_3 control ranges from 0.005% to 2% (cells A4 to A12). The

control ensures that NaN_3 does not interfere with ThT fluorescence. **(e)** Sample blanks correspond to water, PB, ThT in water, and ThT in PB (cells B1, B12, C1, and C12).

2.6.2 Protocol

Microplate Preparation. Non-labeled Ac-αS solutions (200 µM, pH 7.2)*[29] were titrated with previously established concentrations of IL or NaCl (i.e., 0 mM, 15 mM, 25 mM, 50 mM, 100 mM, 200 mM, 300 mM, 500 mM, 600 mM, 800 mM, and 1 M of solute concentration). The protein samples were then filtered*[30] (Amicon) in 5 min cycles (1 min, 100 °C | 5804R) and stored at 4 °C. Stock solutions of PB*[31], NaCl (2 and 0.3 M), IL (2 and 0.3 M), and ThT+NaN3*[32] (10 mM and 0.02 % w/v, respectively) were prepared, filtered (Puradisc), and stored (4 °C) until further use. The aggregation assay was made in a black full bottom medium binding 96 well microplate*[33]. Briefly, 180 µL samples were prepared from stock solutions (pipetted in the following order: phosphate buffer solution, ionic liquid or NaCl, NaN_3, ThT, and finally αS).*[34] Glass beads were added to each well.*[35] The microplate was sealed*[36] (Microseal) and preheated (37 °C, 30 min). The composition of individual microplates can be found in Figures SM20.

Data Acquisition. Kinetic fluorescence measurements were carried out on the 200 Pro microplate reader. The incubation was initiated by 5 min of vigorous orbital agitation (3 mm amplitude, 37 °C). Data points were collected over a total of 560 kinetic cycles with a duration of 15 min (140h in total). 25 measurements were taken at the end of each cycle (settle time: 100 ms; integration time: 50 µs). The gain was set to 20. The extrinsic fluorescence was monitored by exciting ThT at 448 nm, the emission wavelength was collected at 480 nm. The spectral slit widths employed were 20 nm for excitation and 7 nm for emission. The gain was adjusted to 20.

Estimation of Kinetic Parameters. Quantitative insight regarding the effect of ionic compounds on fibrillation was gained through the fitting of experimental data to a two-parameter sigmoidal function. Initially, curves resulting from the fibrillation assays were normalized to the end point fluorescences (100 hours). Data was analyzed according to a simplified version of the "two step" Finke-Watzky (F-W) model.[205] This model correlates the fractional concentration of product (θ) with the time needed to reach 50% fibrillation ($t_{1/2}$ (h)) and ν is the fibrillation growth rate (h^{-1}). The results were fitted to a two-parameter sigmoidal function **(Eq. 1)**:

$$\theta(t) = \frac{1}{1 + e^{-4\nu(t - t_{1/2})}} \qquad \text{[Eq.1]}$$

The parameter T_N (h) represents the nucleation time (dependent variable) obtained from the following equation **(Eq. 2)**:

$$t_N = t_{1/2} - \frac{1}{2v} \quad \text{[Eq.2]}$$

All the data was fitted using Origin 2021 software and the error of the nucleation time was determined by error propagation of the error obtained from the model fitting with the following equation **(Eq. 3)**:

$$\Delta t_N = \sqrt{\left(\Delta t_{1/2}\right)^2 + \left(\frac{2}{(2v)^2}\Delta v\right)^2} \quad \text{[Eq.3]}$$

2.6.3 Relevant Notes (✱)

[29] According to the protocol, the PB concentration will vary depending on the expression yield. PB concentrations for unlabeled αS and Ac-αS were 77.14 mM. Protein stock solutions must be dissolved in filtered water since they were previously lyophilized in a PB solution. Protein samples should be kept on ice when used. **[30]** Protein stocks were filtered to remove aggregates formed during the storage process. **[31]** The concentration of the PB stock was matched to the stock solution of αS. **[32]** NaN_3 prevents undesired microbial growth. **[33]** Medium binding plates reduce protein adsorption to the well, resulting in more consistent assays. **[34]** A multichannel pipette was used to prepare the microplates. **[35]** The glass beads are selected for homogeneity in size and morphology and then washed with BD water before usage. **[36]** Covering the microplate prevents water losses due to condensation.

2.7 NMR spectroscopy

Equipment. Bruker Avance III™ HD 500 MHz NMR spectrometer, Bruker BioSpin (Avance III), equipped with a 5-mm inverse detection triple resonance z-gradient TCI cryoprobe. **Materials & Reagents.** Sterile Syringe Filter (0.22 µm); Branchia (Syringe Filter | SFPE-22E-050). 2,2-Dimethyl-2-silapentane-5-sulfonic acid (DSS), Eurisotop (97%, DLM-32-1). Sodium Azide (NaN_3), Panreac (>99%, A1430). **Buffers.** Phosphate Buffer (PB | Table SM19).

2.7.1 Overview

Solution-state NMR was used to monitor IL-protein interactions with atomic resolution. A total of 4 titrations were made, these correspond to **(a)** Alpha-synuclein in IL. **(b)** Alpha-

synuclein in NaCl, **(c)** Acetylated alpha-synuclein in IL. **(d)** Acetylated alpha-synuclein in NaCl. Each titration consisted of subjecting αS variants to increasing concentrations of ligand. Each titration point was used for the collection of a standard [^{1}H,^{15}N]-HSQC spectra. At selected titration points additional Histidine [^{1}H,^{15}N]-HSQC, [^{1}H,^{15}N,^{13}C]-HNCACB, HN(CO)CACB, HNCO and HN(CA)CO spectra were recorded. Two-dimensional spectra were used to follow the chemical shift perturbations of individual amino acids, whereas three-dimensional spectra were used to monitor eventual structural changes through secondary structure propensities (SSPs).

2.7.2 Protocol

Protein Sample Preparation. A stock solution of DSS was prepared in D_2O (0.5% NaN_3, 500 μM DSS) and used as a reference for NMR samples. αS samples intended for NMR applications were prepared in ultrapure water (200 μM of protein, 10% D_2O v/v, 0.05% NaN_3 v/v, and 50 μM DSS).*[40] For each titration point, an adequate volume of solutions A and B is combined, these solutions differ only in ligand concentration (0 M and 1 M of ligand, respectively). Solutions A (SA) and B (SB) are referenced with the stock solution mentioned earlier (10% v/v). Briefly, titration points ranging from 0 to 100 mM were obtained by incrementally adding 30 μL of SB to 500 μL of SA. The points 200 and 300 mM were made by creating an intermediate solution of 200 mM and then adding 72 μL of SA. Similarly, points 500 and 600 mM were made by creating an intermediate solution (500 mM) and then adding 125 μL of SA. Titration points of 800 and 1000 mM were prepared directly from the stock solutions. All experiments were carried out in 5 mm NMR tubes. The final pH of the sample was adjusted with the addition of negligible volumes of HCl and/or NaOH solutions.*[41]

Data Acquisition and Processing. All NMR spectra were acquired at 288 K (15 °C) using the Avance III spectrometer. This spectrometer is equipped with a 5-mm inverse detection triple resonance z-gradient TCI cryoprobe. The proton chemical shifts were referenced against the internal standard DSS while the nitrogen and carbon chemical shifts were indirectly referenced to the internal standard through the absolute frequency ratio.[206] Data points were processed with Bruker TopSpin 4.0.8 (Bruker BioSpin) and analyzed with the software Computer Aided Resonance Assignment (CARA), version 1.9.1.7.[207]

Amide Backbone Assignments. The BMRB database provides comparable ^{1}H, ^{13}C, and ^{15}N chemical shift assignments for αS; these experiments use similar experimental conditions to the present work. Assignments for αS and Ac-αS (0 M, and 1 M NaCl) were based on

previously published works of Kang and Mariño[208,209] and can be found under the accession codes 27796 and 19350, respectively.

Choline Glutamate characterization. A single choline glutamate sample was prepared in ultrapure water (1.8 M of IL, 10% D2O v/v, 0.05% NaN3 v/v, and 50 µM DSS) for characterization. All experiments were carried out in 5 mm NMR tubes. The final pH of the sample was adjusted with the addition of negligible volumes of HCl and/or NaOH solutions. The structure of the resulting [Ch][Glu] IL was confirmed by ^{1}H spectroscopy. The chemical shifts are the following: ^{1}H NMR (400.15 MHz, D2O, 25 °C) δH (ppm): 1.84 – 2.02 (m, 2H, CH2, Glu), 2.20 (apparent q, 2H, CH2, Glu), 3.05 (s, 9H, CH3, CH3, CH3, Ch), 3.37 (apparent t, 2H, CH2, Ch), 3.60 (q, J = 4.87, 7.12 Hz, 1H, CH, Glu), 3.88 – 3.93 (m, 2H, CH2, Glu).

Backbone chemical shift titrations and Acetylation State. As previously mentioned, experiments were collected for αS with increasing concentrations of [Ch][Glu] and NaCl (control for ionic strength). A solution of uniformly labeled αS (^{15}N/^{13}C) was titrated individually at previously established concentrations of either IL or NaCl (i.e., 0 mM, 2.5 mM, 5 mM, 10 mM, 15 mM, 25 mM, 50 mM, 100 mM, 200 mM, 300 mM, 500 mM, 600 mM, 800 mM, and 1 M of solute concentration), to maintain the protein concentration constant throughout the titration procedure. A standard two-dimensional [^{1}H,^{15}N]-HSQC spectrum was acquired at each solute concentration point. The acetylation state of αS was confirmed by comparing the standard two dimensional [^{1}H,^{15}N]-HSQC spectra of reference Ac-αS to αS (0 M of ligand).*[42] Spectra were collected using the Bruker hsqcetfpf3gpsi2 pulse sequence. The acquisition required 16 scans and was made in a 2048 (^{1}H) x 512 (^{15}N) complex point matrix with a 2346.53 (^{1}H) x 6033.18 (^{15}N) Hz spectral window. The ^{1}H dimension is centered on water, and the ^{15}N dimension is centered on 119 ppm.

The Combined ^{1}H-^{15}N chemical shift differences were calculated for each standard 2D [^{1}H,^{15}N]-HSQC spectra using the initial point as a reference (*i.e.,* 0 M of solute concentration). Chemical shift perturbations ($\Delta\delta_{comb}$), were calculated as follows **(Eq. 4)**:

$$\Delta\delta_{comb} = \sqrt{(\Delta\delta_H)^2 + (\omega_i \Delta\delta_N)^2} \qquad \text{[Eq.4]}$$

The ΔδHN and $\Delta\delta_{NH}$ variables represent the chemical shift differences of αS in the presence of solute minus the equivalent resonances in the absence of added species. The variables are normalized with the scaling factor α (α is 0.14 for most residues but 0.2 for glycine).[210] A threshold is created to objectively differentiate between the interacting and non-interacting residues. This cutoff value represents the corrected standard deviations in reference to zero and is based on the method provided by Schumann's group.[211] Given that the total

concentrations of ligand ([L]t) and protein ([P]t) are known during the titration, it is possible to calculate the dissociation constant (Kd) for residues that are above the cutoff threshold.[210] This process is made possible by the non-linear regression analysis of the following equation **(Eq. 2.12)**:

$$\Delta\delta_{comb} = \Delta\delta_{max}\frac{(K_d + [L]_t + [P]_t) - \sqrt{(K_d + [L]_t + [P]_t)^2 - (4[P]_t + [L]_t)}}{2[P]_0} \quad \text{[Eq.5]}$$

The variable $\Delta\delta_{comb}$ represents the combined chemical shift deviation from the free state defined in Eq. 2.11 and $\Delta\delta_{max}$ is the maximum chemical shift change on saturation. Data points are fitted to a single site binding model, using a least square fitting search of Microsoft Excel™ Solver™ to find the values of Kd and the chemical shift of the fully saturated protein.

Identification of histidine tautomers. Previously selected concentration points (i.e., 0 mM, 15 mM, 100 mM, 300 mM, and 1 M of solute concentration) were used to acquire 2D Histidine ^{1}H-^{15}N HSQC spectra. Spectra were collected using the Bruker hsqcetfpf3gpsi2 pulse sequence. The acquisition required 16 scans and was made in a 2048 (^{1}H) x 512 (^{15}N) complex point matrix with a 2346.53 (^{1}H) x 6033.18 (^{15}N) Hz spectral window. The ^{1}H dimension is centered on water, and the ^{15}N dimension is centered on 119 ppm. To accommodate for the small two-bond spin-couplings in the histidine imidazole ring ($^{2}J_{NH} \approx 11$ Hz)[212], the ^{1}H-^{15}N HSQC INEPT delay (CNST XX in the Bruker experiment) was set to 22 ms.

Secondary structure propensity (SSP). Previously selected concentration points (i.e., 0 mM, 15 mM, 100 mM, 300 mM, and 1 M of solute concentration) were used to acquire 3D [^{1}H, ^{15}N, ^{13}C]-HNCACB, HN(CO)CACB, HNCO, and HN(CA)CO spectra. The $^{13}C\alpha$ and $^{13}C\beta$ chemical shifts of αS were used to calculate the SSPs using the standalone script (SSP protocol) provided by Marsh's group.[29] The SSP values are indicative of the secondary structure propensity of a given protein. Positive values (ranging from 0 to 1) represent α-helical propensity, whereas negative ones (0 to -1) indicate β-sheet propensity.*[43] Reference values for random coil, secondary structure chemical shifts, and standard deviations were provided by Zhang et al.[213] The HNCACB and HN(CO)CACB experiments were collected using the standard Bruker hncacbgp3d and hncocacbgp3d pulse sequences, respectively. Acquisitions required 32 scans. These were made in a 2048 (^{1}H) x 64 (^{13}C) x 256 (^{15}N) complex point matrix with a 2346.53 (^{1}H) x 6033.18 (^{13}C) x 5284.04 (^{15}N) Hz spectral window. The ^{1}H dimension is centered on water, the ^{13}C dimension is centered at 42 ppm, and the ^{15}N dimension is centered at 119 ppm. The HNCO and HN(CA)CO experiments were collected using the standard Bruker hncogp3d and hncacogp3d pulse sequences, respectively. Acquisitions required 16 scans. These were made in a 2048 (^{1}H)

x 64 (^{13}C) x 256 (^{15}N) complex point matrix with a 2346.53 (^{1}H) x 6033.18 (^{13}C) x 5284.04 (^{15}N) Hz spectral window. The ^{1}H dimension is centered on water, the ^{13}C dimension is centered at 174 ppm, and the ^{15}N dimension is centered at 119 ppm.

2.7.3 Relevant Notes (✱)

[40] The concentration of PB will vary according to expression yields; concentrations for each titration are as follows: 105 mM for αS in IL, 106 mM for αS in NaCl, 104 mM for Ac-αS in IL, and 54 mM for Ac-αS in NaCl. **[41]** Samples are stored (4 °C) when not used and are discarded preventively after 3 days to ensure that αS does not aggregate. **[42]** Correlations for the first 2 aa (M1 and D2) are only present in Ac-αS, in addition to significant variations in chemical shift aa 3 to 10. The pH of solutions A and B are matched to ensure no pH variations during titrations. **[43]** ^{13}Cα and ^{13}Cβ chemical shifts were used in the determination of SSPs, these are found to be more reliable than ^{13}CO.

3 RESULTS

The current study is primarily focused on the investigation of the IL-protein interactions established between αS and [Cho][Glu]. Protocols for protein expression, purification, and characterization as well as IL synthesis and characterization have been already established and optimized in previous studies from our group.[24] As a result, a limited emphasis will be placed in these topics. Due to the similarity of results amongst available protein samples (*i.e.,* αS, Ac-αS, $^{13}C^{15}N$-αS, $^{13}C^{15}N$-Ac-αS), αS will be chosen as a representative sample for displaying results unless stated otherwise.

3.1 Expression and Purification of αS

3.1.1 Heterologous Protein Expression

The cellular growth curves can be used as an objective metric for the global expression effectiveness of a system **(Figure 11)**. As expected, the curve profiles for LB growth media display reduced incubation times suggesting that non-labeled media is best suited for the expression of αS in *E. coli* cells when compared to M9 minimal media. These incubation divergences can be explained by the differences in composition of the provided nutrient matrixes. The rich LB medium provides an ideal support for microbial growth whereas the M9 minimal medium is sub optimal. Additionally, the exclusive use of isotopically labeled sources of carbon (^{13}C) and nitrogen (^{15}C) in minimal medium is expected to negatively contribute to the expression efficiency. Naturally, biological systems are optimized for the assimilation of the most common naturally occurring isotopes, and as a result the differences in mass are expected to hinder cellular growth. Another expected outcome would be the diminished expression efficiency of acetylated samples The simultaneous expression of an additional acetylation complex

is responsible for diverting and consequently limiting the cellular resources dedicated to the expression of αS, as denoted by the relative reduction of incubation times.

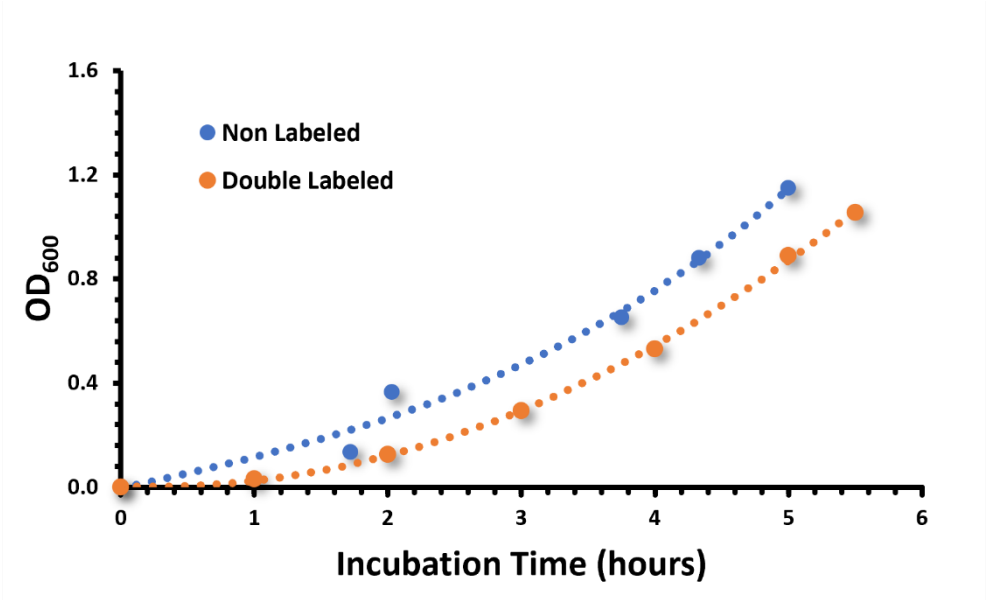

Figure 11 – Cellular Growth Curves for the Expression of αS

Representation of the *E. coli* growth curves in LB medium (presented in blue, non-labeled samples) and M9 minimal medium (presented in orange, double-labeled samples). Batches of 1 L were used in both cases, at 37°C. Growth was monitored at OD at 600 nm.

The efficiency of the *E. coli* expression systems was also evaluated through Tris-Tricine SDS-Page **(Figure 12)**. Cellular pellets were analyzed before and after the induction with IPTG (at set intervals, corresponding to 1, 2, and 4 hours after induction). A faint band of approximately 17 kDa is visible at hour after induction, this band corresponds to αS (14.4 kDa). The differences in expected and experimental molecular weight can be explained by the highly acidic nature of the protein (pI of 4.5) which translates into a wealth of negative charges. These charges hinder the migration of the protein creating an apparent excess in molecular weight. After 4 hours of induction, αS's band reaches optimum intensity are reached at these time points, respectively). SDS-Page outlines are similar amongst protein samples (*i.e.,* αS, Ac-αS, $^{13}C^{15}N$-αS, $^{13}C^{15}N$-Ac-αS), suggesting comparable proteomic profiles even in the presence of different media. A significant difference is the presence of NatB complex proteins in acetylated samples.

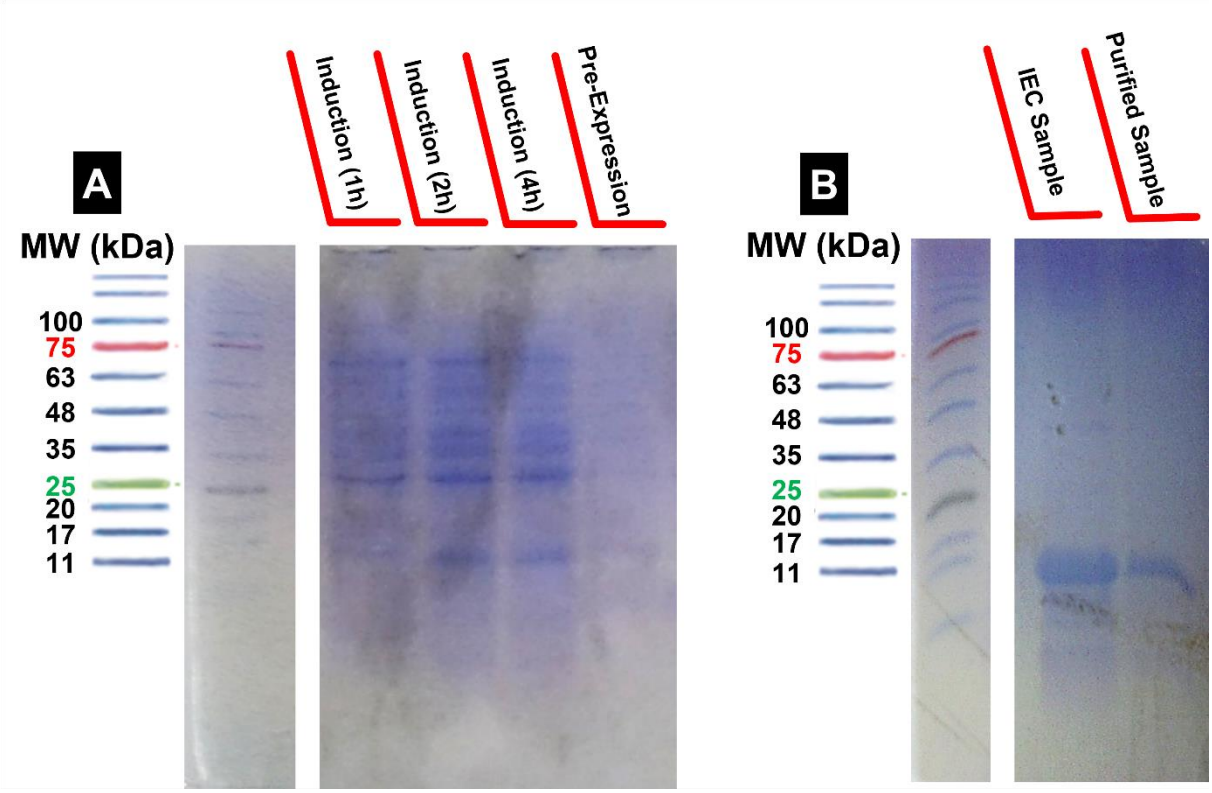

Figure 12 – SDS-PAGE Monitorization of the Expression and Purification of αS

A) SDS-Page samples relative to the expression of αS. First well corresponds to the molecular weight marker (NZYColour Protein Marker II). Second well corresponds to the bacterial culture at 1hour of incubation. Third well corresponds to the bacterial culture at 2 hours of incubation. Fourth well corresponds to the bacterial culture at 4 hours of incubation. Fifth well corresponds to the bacterial culture before expression. **B)** SDS-Page samples relative to the purification of αS. First well corresponds to the molecular weight marker (NZYColour Protein Marker II). Second well corresponds to the protein sample after IEC purification. Third well corresponds to protein sample after purification. Each well was loaded with 15 µL of sample or 2 µL of molecular marker. Samples correspond to non labelled αS.

3.1.2 Purification by Ion Exchange Chromatography

Anion exchange chromatography (IEC) was used as the third purification step. Chromatogram analysis **(Figure 13)** indicates an effective separation of the αS peak from the remaining impurities, which correspond essentially to additional thermoresistant proteins at this point. Although not shown, it is important to note that the chromatographic profiles are analogous amongst protein samples (*i.e.,* αS, Ac-αS, $^{13}C^{15}N$-αS, $^{13}C^{15}N$-Ac-αS), displaying comparable peak distribution and elution rates. This is indicative of a relatively similar sample composition.

The monitoring of the elution at 280 nm allowed for the detection of a series of cationic protein contaminants (1st peak at 18-35 mL) in the column equilibration step (corresponding sensibly to the 15 mL to 35 mL region). These cationic compounds are unable to adsorb to the

column and are consequently the first to be eluted. Upon the development of an ionic force gradient anionic proteins are separated according to adsorption strength (correlates with charge density). At approximately 17% gradient of buffer B a second weakly bound contaminant is eluted (2nd peak at 55 to 67 mL). SDS-Page analysis confirmed the presence of an αS peak, eluted at approximately 40% gradient (3rd peak at 75 to 85 mL highlighted by a gray bar). A third contaminant can be found at 50% gradient (peak 4 at 90 to 100 mL). Finally, a series of strongly bound anionic contaminants can be found at 100% gradient, these compounds typically display high absorbances and often surpass the detection limit.

SDS-PAGE gel analysis **(Figure 12)** of the final sample resulting from IEC reveals a strong αS band accompanied by minor contaminants (faint bands bellow 11 kDa). The findings are consistent with similar purification protocols which report a final purity of 99%. The resulting protein yield was 29.04 mg/L for αS in LB medium. Results for other αS samples are available at Table SM7.

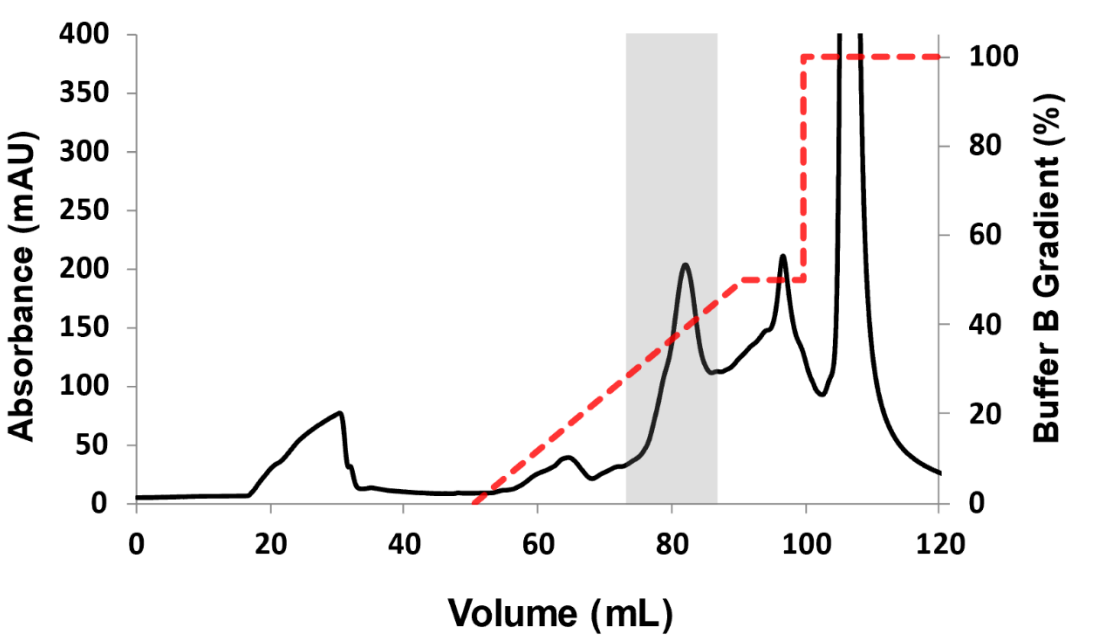

Figure 13 – Purification of αS by Anion Exchange Chromatography

Chromatographic profiles resulting from IEC. Primary and secondary axis represent respectively variation of absorbance at 280 nm (continuous line) and the gradient of buffer B (dotted line). Ac-αS was eluted at 40% of buffer B corresponding to 70 to 90 mL. Peak corresponding to Ac-αS is highlighted in gray.

3.2 Synthesis and Characterization of [Ch][Glu]

Choline Glutamate ([Cho][Glu]) was prepared via the potentiometric titration of Choline hydroxide (31 mmoles, 150 mL) and L-glutamic acid (31 mmoles, 4.5 g) following a previously reported protocol. The resulting product was lyophilized for 24 h to yield a slightly yellow and oily substance (7.84 g, >97%). The yield is comparable to reported studies that employ an identical methodology (>99%). The structure of the resulting IL was confirmed by ^{1}H NMR spectroscopy **(Figure 14)**. As expected, the [Ch] to [Glu] ratio is close to 1 and no impurities can be found.

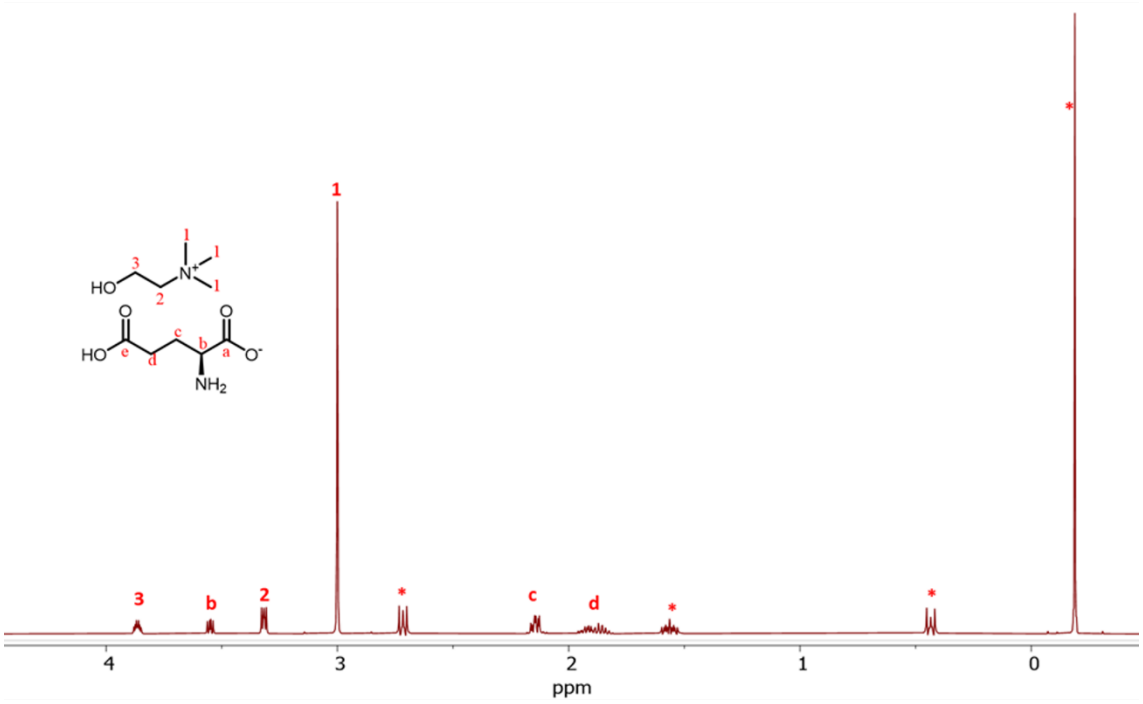

Figure 14 – ^{1}H Spectra of [Ch][Glu] in Solution

Unidimensional ^{1}H NMR spectra of a [Ch][Glu] solution. A sample corresponding to 100 mM of [Ch][Glu] was prepared in 20 mM of phosphate buffer, 0.1 %NaN3, and 100 µM of DSS, ensuring a 9 to 1 H2O/D2O ratio. The identifying structural elements of choline are identified in the spectra (represented by the numbers 1 to 3) as well as structural elements of glutamate (represented by the letters a to e). Peaks corresponding to the internal standard DSS are also highlighted (represented by the * symbol). Experiments were acquired at 288 K (15 ºC).

3.3 Fluorescence Spectroscopy

3.3.1 Thioflavin-T as an Amyloid Reporter

The fluorescent probe Thioflavin T (ThT) is commonly used to monitor amyloid formation. This fluorophore shows affinity towards *β*-sheet elements commonly found in amyloid fibrils. Binding to these structures results in a considerable increase in fluorescence intensity as well as a bathochromic shift of excitation and emission wavelengths (from 342 nm to 442 nm and from 430 nm to 482 nm, respectively).[214] Such a behavior can be justified by the organization of the structural elements of ThT **(Figure 15)**. Structurally, this fluorescent probe is divided into two moieties: **(i)** a benzothiazole ring, and **(ii)** a dimethylaminobenzene ring. These elements form two rigid planes that can freely rotate about the C-C bond when in solution, the torsion angle formed between planes is designated as Φ. In its fundamental state Φ is approximately 37º.[215]

When bound to amyloid fibrils ThT loses all of its conformational freedom as the torsion angle is restricted to 90º.[216] When the molecule is excited in this state energy is unable to dissipate via non-radiative processes. As a result, this ThT is obligated to fluoresce (a radiative process) in order to liberate energy. Such a behavior when restricted is responsible for considerably increasing the quantum yield of the molecule.[217]

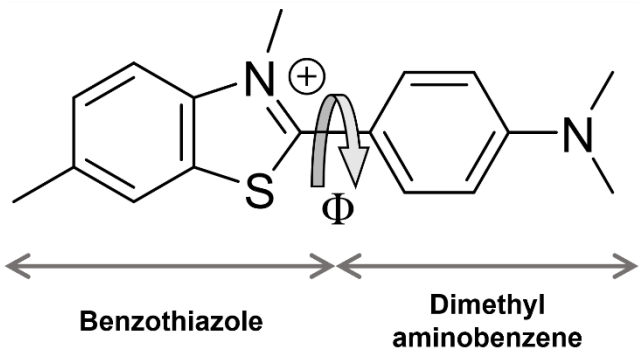

Figure 15 – Structural Features of ThT

The fluorescent probe Thioflavin-T is composed of two moieties (highlighted in the figure), a benzothiazole ring and dimethylaminobenzene ring. These two rigid planes can freely rotate n solution forming a torsion angle designated as Φ. When bound to amyloid fibrils the two planes cannot rotate conferring fluorescent properties to the molecule.

3.3.2 High Throughput Screening in Amyloidogenesis

Amyloidogenesis is classically defined as a stochastic process where nucleation may not take place despite ideal conditions being present. This problem is aggravated by the high sensitivity of fibrillation to different experimental parameters that can affect aggregation behavior such as pH, temperature, buffer composition, sample heterogeneity, molecular crowding, and the presence of small molecules (*e.g.,* charged metabolites and lipids).[199,218] These findings prompt the need for high throughput screening (HTS) as an approach capable of delivering efficient and reproducible characterization of "drug-like" compounds and/or screening of multiple experimental conditions *in vitro*.[219] In this sense, aggregation assays were designed to monitor the interference of [Ch][Glu] on the aggregation behavior of αS and Ac-αS. NaCl was used as a control for ionic strength ensuring that the observed effects (if present) are specific to [Ch][Glu] and not just a result of electrostatic forces. Negative controls for ThT fluorescence were also created to ensure that the fluorescent probe only interacts with αS and not with other utilized compounds (*i.e.,* [Ch][Glu], NaCl, NaN_3), thus producing potential false positives.

3.3.3 The Aggregation Profiles of αS

As previously mentioned, two microplates were created for the study of αS and Ac-αS. The resulting data from each aggregation microplate was corrected and normalized, which allowed for the evaluation of the general aggregation behavior of the protein variants.

When αS is titrated **(Figure 16A and E)** with low concentrations of NaCl (*i.e.,* 10 and 25 mM), some aggregation is visible. The following concentrations (*i.e.,* 50, 100, 200 mM) are unable to yield a similar effect. Significant aggregation is only apparent at intermediate concentrations (*i.e.,* 300 mM). At the concentration of 300 mM the maximum fluorescence intensity (I/I_{MAX}) is reached for the entire microplate, the fluorescence intensity appears to stabilize at 500 mM. The fluorescence intensity directly correlates with the amyloid fraction present in the sample suggesting the formation of fibrils. Therefore, these concentrations correspond to the optimal fibrillation conditions. As the concentration of NaCl is further increased a steady decline in fluorescence intensity is observed suggesting a progressive decrease in amyloid fraction.

When αS is titrated with IL **(Figure 16C and E)**, all the low concentrations of [Ch][Glu] (*i.e.,* 10, 25, 50, 100 mM) can trigger aggregation. Significant aggregation can only be found at the intermediate concentration of 300 mM. The maximum fluorescence intensity for [Ch][Glu] samples is reached at the concentration of 300 mM. Progressive decrease can be observed until 600 mM followed by a moderate increase in fluorescence intensity for 800 and stabilization at 1000 mM of IL.

When Ac-αS is titrated **(Figure 16B and F)** with low concentrations of NaCl aggregation is visible at low to moderate concentrations (*i.e.,* 50 and 100 mM). Significant aggregation is only found at 200 mM, this is an incomplete process as the plateau is not reached. At the concentration of 300 mM the maximum fluorescence intensity is reached for NaCl samples. A steady decrease in fluorescence can be observed until 600 mM followed by an increase in fluorescence intensity for 800 and a final reduction 1000 mM.

When Ac-αS is titrated **(Figure 16D and F)** with [Ch][Glu], aggregation is present at low concentrations (*i.e.,* 10, 25, 50 and 100 mM). Significant aggregation is only found at 300 mM. At the concentration of 300 mM the maximum fluorescence intensity is reached for IL samples. Progressive decrease can be observed until 600 mM followed by a moderate increase in fluorescence intensity for 800 and stabilization at 1000 mM of IL.

The aggregation profile of αS is significantly altered by the interactions with ionic compounds. Samples in the presence of NaCl are minimally affected in low range concentrations (*i.e.,* 10 to 200 mM) whereas the aggregation is already initiated in the presence of [Ch][Glu].

NaCl displays considerably larger fluorescence intensities (2-to-3-fold increase) in the mid to high range concentrations (*i.e.,* 300 to 800 mM). In these cases, the IL is more efficient in promoting fibril formation in the low and high range concentrations (*i.e.,* 10 to 200 mM and 800 to 1000 mM, respectively). Ac-αS presents a similar shift in aggregation behavior to αS. The aggregation behavior in the presence of IL is comparable for both forms. Samples are minimally affected by NaCl in low range concentrations (*i.e.,* 10 to 100 mM) whereas the aggregation is immediately initiated in the presence of [Ch][Glu]. NaCl displays considerably larger fluorescence intensities (4-to-5-fold increase) in the mid to high range concentrations (*i.e.,* 300 to 800 mM). In these cases, the IL is more efficient in promoting fibril formation in the low and high range concentrations (*i.e.,* 10 to 200 mM and 800 to 1000 mM, respectively).

When comparing the aggregation profile of αS and Ac-αS, significant differences can be found. While αS can initiate the aggregation process when no ionic compounds are present (*i.e.,* NaCl or [Ch][Glu]), Ac-αS samples do not aggregate in these conditions. This observation suggests an additional stability of the acetylated form of the protein. Ac-αS significantly aggregates at 200 mM of NaCl whereas αS is only able to do so at 200 mM. In these cases, the IL is more efficient in promoting fibril formation in the low range concentrations (*i.e.,* 10 to 100 mM).

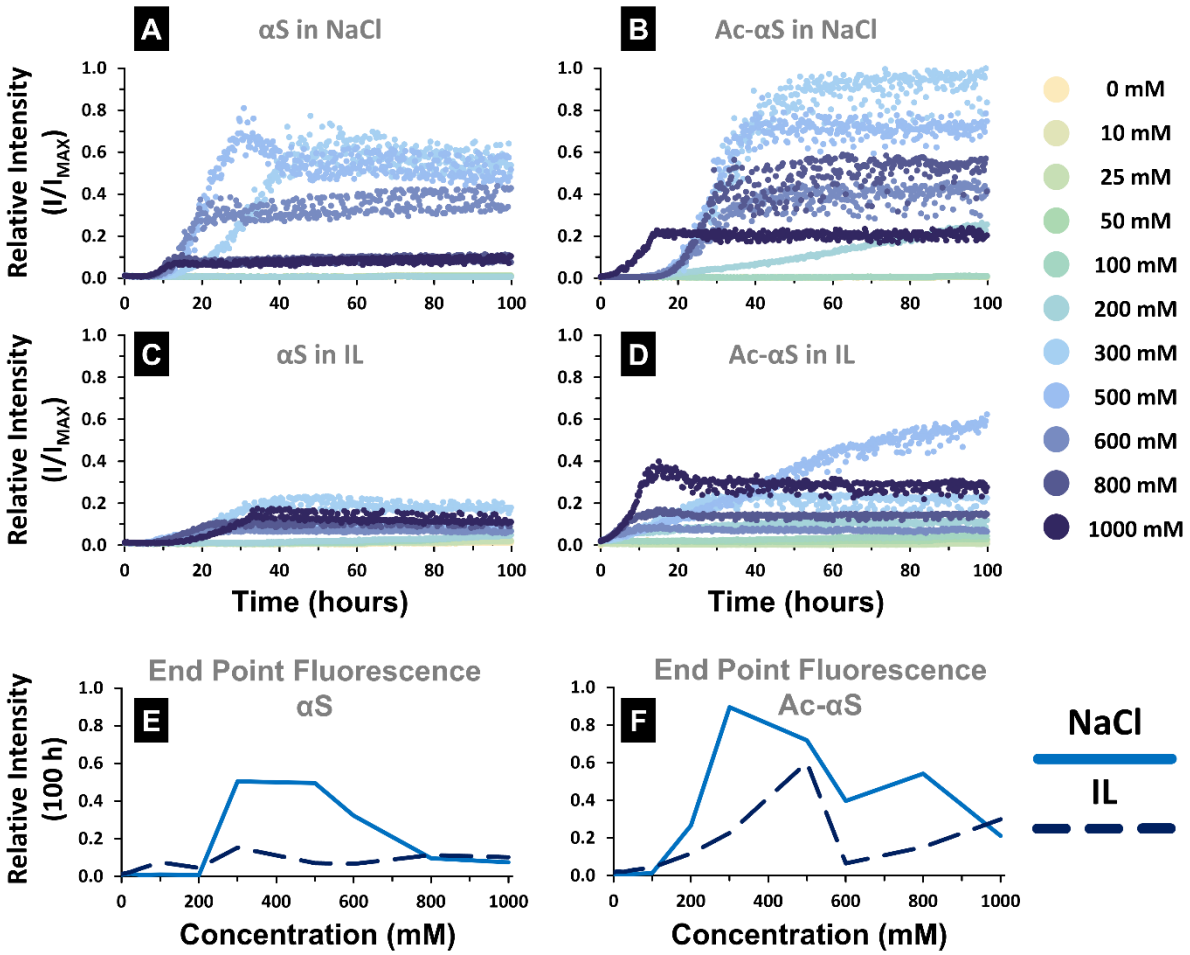

Figure 16 – The Fibrillation Profiles and End Point Fluorescences of αS Variants

Fluorescence spectroscopy analysis of αS's interaction with ionic compounds. **A)** The aggregation curves of αS in the presence of increasing concentrations of NaCl (0 to 1 M). **B)** The aggregation curves of Ac-αS in the presence of NaCl. **C)** The aggregation curves of αS in the presence of IL. **D)** The aggregation curves of Ac-αS in the presence of IL. Each aggregation assay (A to D) is composed of several aggregation conditions (11 in total) which differ from each other in terms of ionic compound concentration. Concentration points are color coded according to the legend found in the top right-hand corner of the figure. **E)** Comparison of the end point fluorescence results for αS in the presence of IL and NaCl. **F)** End point fluorescence results for Ac-αS in the presence of IL and NaCl. End point fluorescence values correspond to the normalized and corrected fluorescence intensities at a fixed time point (corresponding to 100 hours). End point fluorescence analysis is an effective toll for describing the aggregation tendencies of found in aggregation assays A to D. Experiments were monitored over 100 hours at 37 °C, fibril formation is monitored by the fluorescence of ThT. Samples (200 µM of protein) were prepared in 77 mM of phosphate buffer (pH 7.2), 200 µM of ThT, and Protein samples (200 µM) were prepared in 77 mM of phosphate buffer (pH 7.2), 200 µM of ThT, and 0.02% NaN3.

3.3.4 The Aggregation kinetics of αS

As previously mentioned, the fibrillation of αS is classically described as a three-stage process involving a lag phase, an elongation phase, and a stationary phase. This aggregation

profile depicts a simplified aggregation behavior that can be objectively analyzed through the Finke−Watzky (F−W) two-step model.[205] Here the complex molecular steps involved in the aggregation are combined into two pseudo-elementary constants, k1 and k2, which represent the nucleation and elongation, respectively. Due to its simplicity the F−W model can be successfully applied to a whole range of kinetic aggregation data.

The F−W model depicts a sigmoidal function that describes the relative concentration of the product as a function of time, θ(t), which corresponds to the normalized fluorescence. Two sets of independent parameters can be used for the F−W model, these are: **(i)** Pseudoelementary rates k1 and k2. **(ii)** The time required to produce half the total product ($t_{1/2}$) and the rate of growth at time $t_{1/2}$ (v). The latter representation was used to describe aggregation kinetics of αS due to the ease of interpretation of the kinetic parameters. A third (dependent) parameter T_N is used as an indicator of the duration of the nucleation phase.

The objective kinetic characterization of alpha synuclein variants is only possible in samples where significant aggregation was present and a plateau is reached (i.e., 300 to 1000 mM). The kinetic parameters associated concentration points of 800 and 1000 mM (αS in NaCl) as well as 600 mM (AcαS in IL) are not presented due to poor fitting. In general, poor fitting is associated with the medium binding nature of microplates and or high viscosity.

αS in the presence of NaCl **(Figure 17A and C)** displays several oscillations in growth rate, the maximum growth rate can be found at 500 mM (0.13±0.01 h^{-1}). A progressive decrease in nucleation time can be observed as the concentration of NaCl grows. The minimum nucleation time is reached at 600 mM (9.0±0.6 h).

Ac-αS when in the presence of NaCl **(Figure 17A and C)** exhibits a relatively stable growth rate from 300 to 800 mM, an increase in growth rate is found in the final concentration. The maximum growth rate can be found at 1000 mM of NaCl (0.123±0.007 h^{-1}). A progressive decrease in nucleation time can be observed as the concentration of NaCl grows. The minimum nucleation time is reached at 1000 mM (5.3±0.3 h).

αS in the presence of [Ch][Glu] **(Figure 17B and D)** displays relatively stable growth rates, the maximum growth rate can be found at 600 mM of IL (0.098±0.009 h^{-1}). The nucleation time suffers a decrease in the transition from 300 to 500 mM followed by a stabilization of the nucleation times. The minimum nucleation time is reached at 500 mM (6.1±0.7 h).

Ac-αS when in the presence of [Ch][Glu] **(Figure 17B and D)** variable nucleation times can be observed through the series. The minimum nucleation time is reached at 600 mM (10.4±0.4 h).

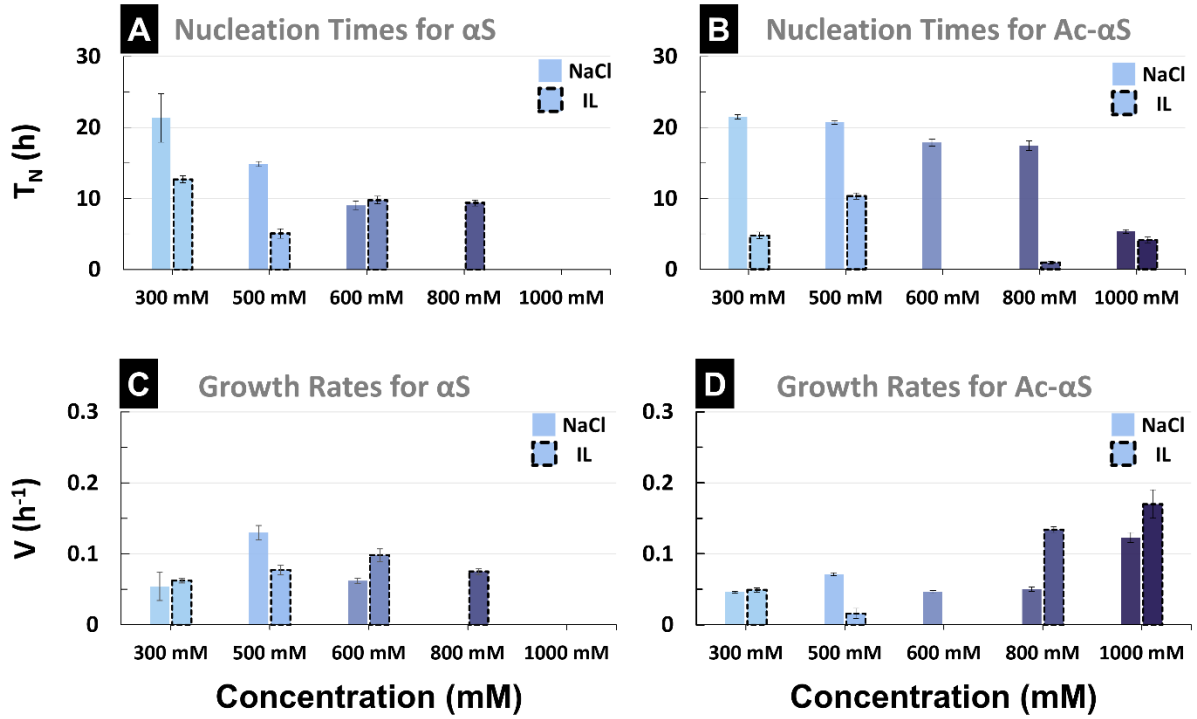

Figure 17 – The Fibrillation Kinetics of αS Variants

A) The nucleation times (T_N) for αS in response to IL and NaCl. **B)** Nucleation times for Ac-αS in the presence of IL and NaCl. **C)** The growth rates (v) for αS in response to IL and NaCl. **D)** Growth rates for Ac-αS in the presence of IL and NaCl. The kinetic fibrillation parameters (T_N and v) were estimated using the aggregation curves found in the base aggregation profiles which are depicted in figure 16 (A to D). Individual curves were fitted (using Origin 2021) to the FW two step model to yield two independent kinetic parameters. The represented error bars correspond to the error associated with the fitting of the curve.

3.4 Biomolecular NMR spectroscopy

3.4.1 Ligand Binding Monitored by NMR Spectroscopy

Nuclear magnetic resonance (NMR) spectroscopy is extensively used to evaluate protein interactions due to a wealth of analyzable parameters that convey structural information with atomic resolution (*i.e.,* chemical shifts, coupling constants and relaxation times).[220] The present study NMR spectroscopy was used to describe the interactions of [Ch][Glu] with (Ac-)αS, providing information on the nature (*i.e.,* specific binding or nonspecific binding) and location of binding.

Double labeled protein samples were used to study protein-ligand interactions, correlations were initially followed through Heteronuclear Single Quantum Correlation (HSQC) experiments. In this type of experiment, cross peaks represent the correlation between N-H pairs of amide groups of amino acids (*i.e.,* peptide backbone).[221] Each amino acid can be

characterized by a specific chemical shift which is dependent on protein structure as a function of the chemical environment. The chemical environment is, in turn, modified by changes in protein structure and nearby atoms (*e.g.,* ligands). These spectra are often regarded as protein "fingerprints".

Triple resonance spectra (*i.e.,* HNCO, HNcaCO, HNcoCACB, and HNCACB) were collected to link active nuclei (*i.e.*, 1H,^{15}N, and ^{13}C). These experiments take advantage of the relatively large magnetic couplings created between active nuclei ($^{1}J_{NH}$, $^{1}J_{CH}$, $^{1}J_{CC}$, and $^{1}J_{CN}$) to establish the backbone connectivity of αS. Specifically, the couplings are used to establish the scalar connectivity pathway between nuclei.

3.4.2 Characterization of αS by NMR

Sample quality (*e.g.,* protein aggregation, folding state) was initially accessed from the 1H unidimensional spectra of αS. Ac-αS displays a narrow set of peaks (8 to 9 ppm) characteristic of disordered protein. No protein aggregation is present as peaks remain sharp and intense. The assignment of the resonances in the [^{1}H,^{15}N]-HSQC spectrum was done by comparison with an already deposited data set in the Biological Magnetic Data Bank (BMRB), entry 25227.[222] The original assigned peak list was adjusted to the experimental results. αS variants present a comparable [^{1}H^{15}N]-HSQC spectra **(Figure 18)**. Major differences can be found in the chemical shifts of the first 10 amino acids. The M1 and D2 correlations are not present for αS due to the relaxation of the highly flexible N-terminal. Residues V3 to K10 suffer considerable shifts because of acetylation. This PTM is responsible for conferring neutral charge to the otherwise positive methionine residue promoting the stabilization of this region.[223] As a result, we can visually confirm the success of the acetylation process.

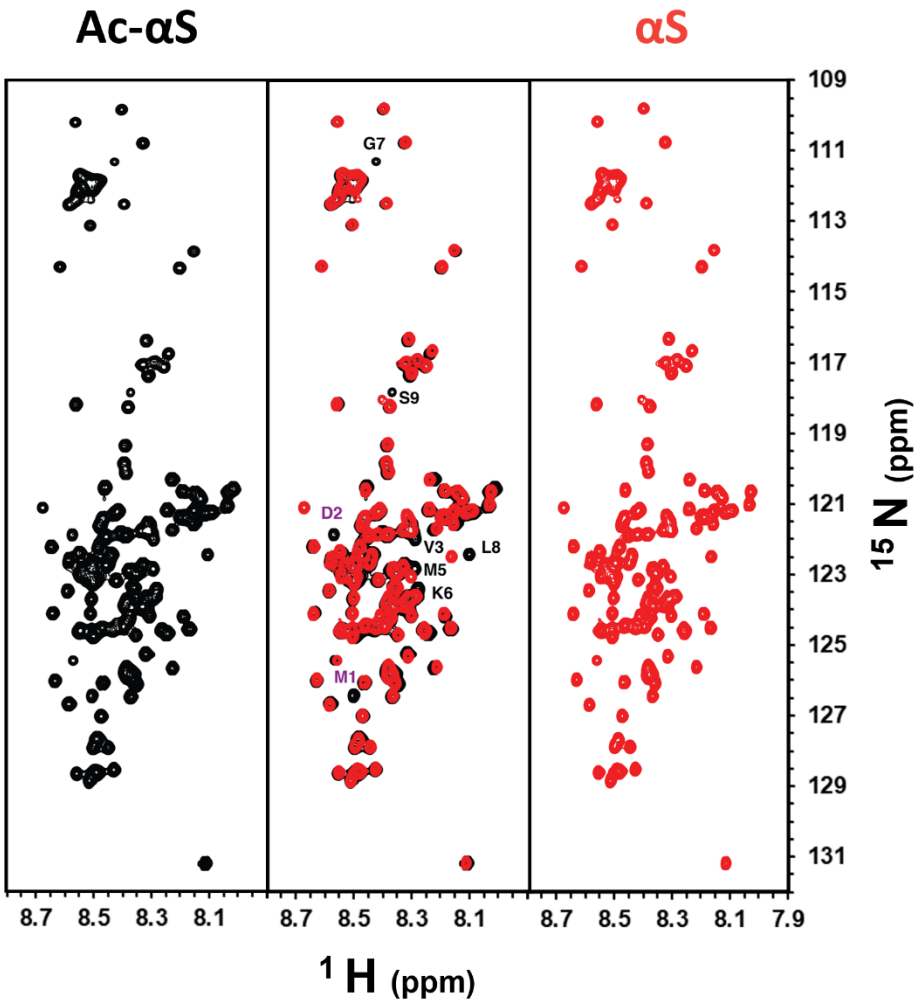

Figure 18 – Spectral Comparison of αS Variants ($^{1}H^{15}N$-HSQC)

A) HSQC spectrum of αS. **B)** Overlay of the HSQC spectra of αS and Ac-αS, most affected residues are highlighted. **C)** HSQC spectrum of Ac-αS. Samples (700 µM) were prepared in 105 mM of phosphate buffer (pH 7.2), 0.1% NaN3, 100 µM of DSS, ensuring a 9 to 1 H2O/D2O ratio.

3.4.3 The Side Chain of Histidine 50

Akin to the backbone of the protein the histidine sidechain can also exhibit NH correlations. The distinctive ^{15}N chemical shifts of histidine can be used as indicators protonation state of the imidazole ring.[224] A neutral imidazole can assume two separate tautomeric states, these are designated as the δ and the ε forms **(Figure 19)**, with the later tautomer being the most common form. Unprotonated nitrogen nuclei display at higher NMR chemical shifts (up to 80 ppm) compared to its protonated counterpart. This behavior pattern allows for the unambiguous assignment of the nuclei and the specification of the protonation state of each nitrogen in the imidazole ring.

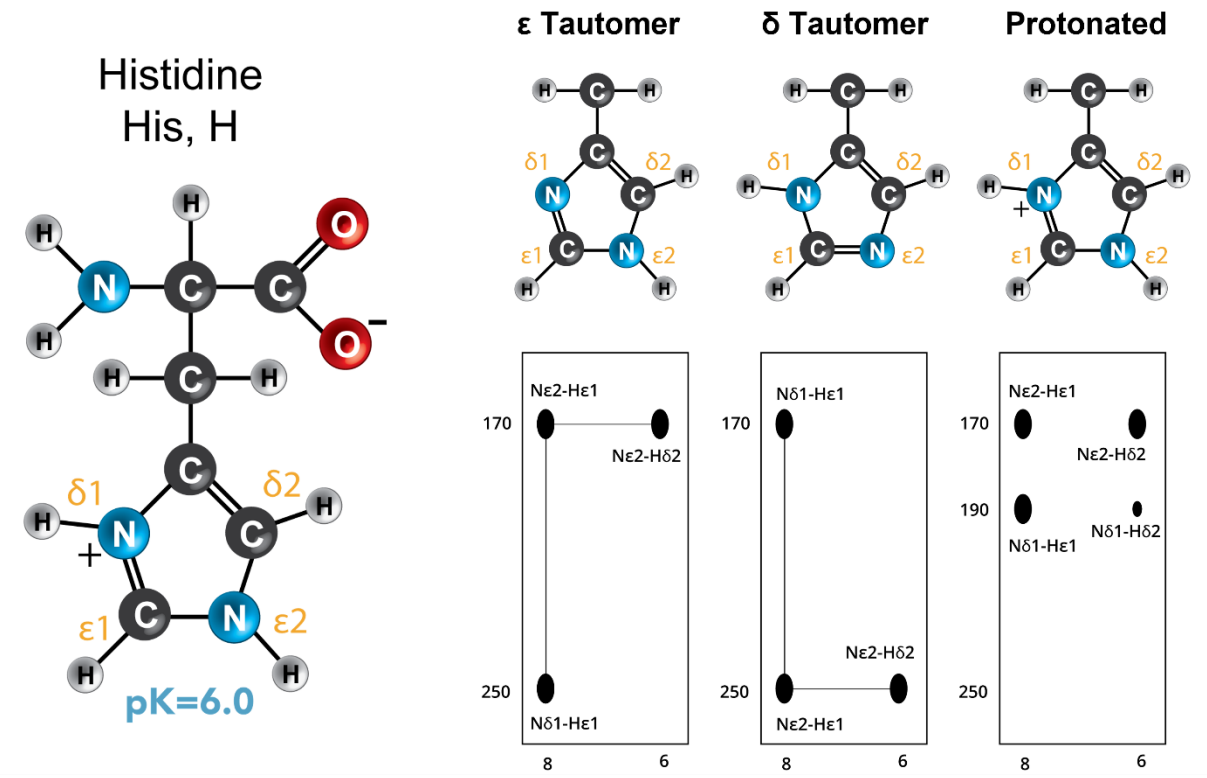

Figure 19 – The tautomeric profiles of Histidine

The imidazole ring found in the side chain of histidine can be found in two tautomeric forms, the δ-tautomer (protonated at ε2 nitrogen) and the ε-tautomer (protonated at the δ1 nitrogen). Histidine can also be found in a fully protonated form with a positive charge.

The concentrations of 0, 50, 200, 500, 1000 mM were used as references for evaluating the changes (if any) in histidine tautomerism. No histidine cross peaks could be identified in the αS titrations. As a result, only Ac-αS behavior can be evaluated. When no ligand is present the imidazole ring of histidine is found in the more common δ form. The addition of NaCl and [Ch][Glu] result in the progressive migration of the Nδ1-Hε1 resonance (212) to higher chemical shifts (196 and 206 ppm, respectively). These changes are indicative of a stronger association between the proton and the nitrogen, NaCl seem to be more effective at promoting association.

It is Important to note that αS only contains one histidine, therefore only one set of correlations should be present. The correlations of H50 are most likely doubled due a poor decoupling of the active nuclei.

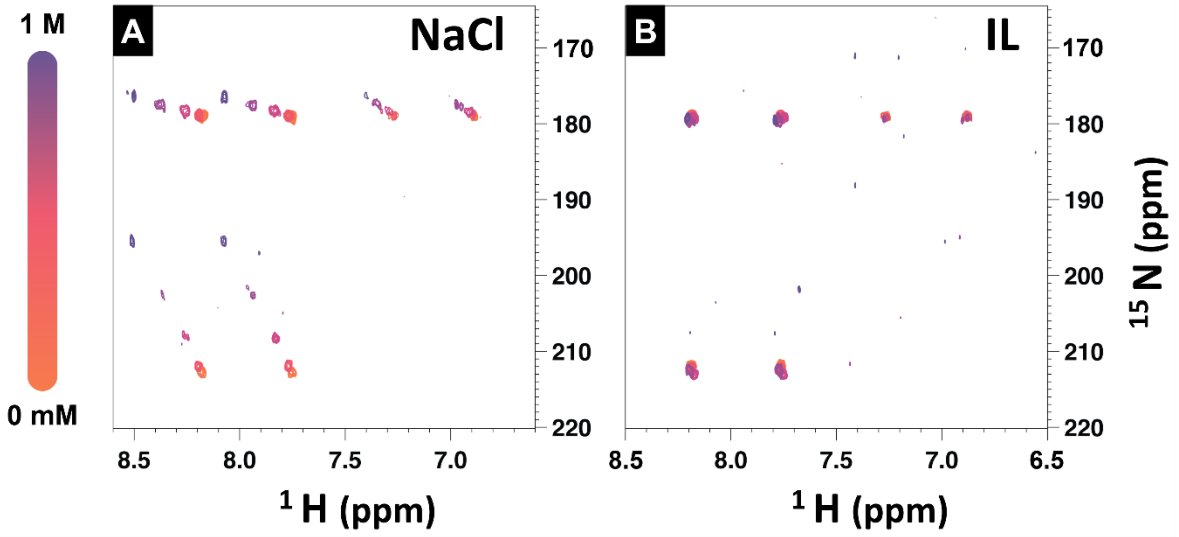

Figure 20 – H50 side chain correlations (Ac-αS)

A) The 2-3 bond NH correlations found in the imidazole side chain of H50 when in the presence of increasing concentrations of NaCl. **B)** NH correlations found in H50 when in the presence of increasing concentrations of IL. Signals are duplicated due to poor uncoupling between active nuclei. Experiments were acquired at 288 K (15 ºC). Samples (200 µM of protein) were prepared in 105 mM of phosphate buffer (pH 7.2), 0.1% NaN3, and 100 µM of DSS, ensuring a 9 to 1 H_2O/D_2O ratio.

3.4.4 Chemical Shift Perturbations

Chemical shift perturbations (CSPs) are a simple and effective technique for the monitorization of protein-ligand binding. The procedure requires the titration of a 15N-labeled protein with increasing concentrations of unlabeled ligand, 15N−1H HSQC spectra are recorded at each concentration point. The variation in the chemical shifts is representative of protein ligand interactions. High CSP values are representative of environmental changes on the protein interfaces and can be associated with binding.[210] The concentrations of 0, 15, 100, 300, 500, and 1000 mM were used as references for evaluating the changes (if present) of CSP for alpha synuclein variants as function of the addition of Ionic compounds. The concentration points of 100 and 1000 mM in the series **Ac-αS in NaCl** were not show due to time constraints of the thesis. The missing titration points were consequently substituted by the concentrations of 200 and 500 mM respectively.

Low concentrations of NaCl (15 mM) **(Figure 21)** cause variations at the N-terminal of αS (residues V3 to M5, and K10) as well as the core of the protein (residues S42 to K43, K45, and N65). Moderate concentrations (300 mM) show variations at the N- and C-terminal (residues V3 to Q24 and K96 to A140) as well as the core of the protein (residues S42 to Q62). Moderate to high concentrations of NaCl (500 mM) affect most regions of the protein, but the

N-terminal (residues form the V3 to K21) and core of the protein (residues form the S42 to K45) are still evidenced. High concentrations (1000 mM) affect most regions of the protein, but the N-terminal (residues form the V3 to K21) and core of the protein (residue K43) are still evidenced.

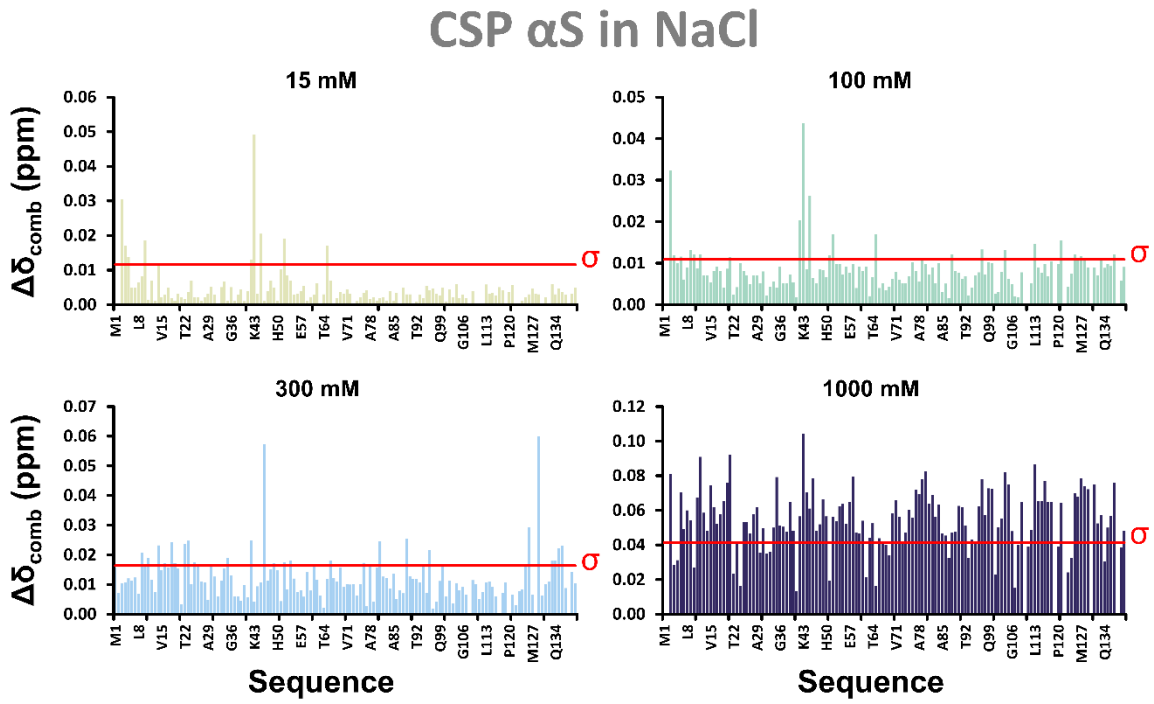

Figure 21 – The CSPs of αS in the presence of NaCl

NMR CSP analysis of the interactions of αS with NaCl at representative concentration points (4 in total). **A)** The CSPs of αS at low concentrations of salt (15 mM). **B)** The CSPs of αS at moderate concentrations of salt (100 mM). **C)** The CSPs of αS at moderate concentrations of salt (300 mM). **D)** The CSPs of αS at high concentrations of salt (1000 mM). The determination of the CSPs of αS variants under several concentration points allows for the identification of the amino acid residues and/or regions that are particularly affected by a given ionic compound. The variable sigma (σ, in red) represents the threshold value for pinpointing potentially interacting residues. Experiments were acquired at 288 K (15 ºC). Samples (200 µM of protein) were prepared in 105 mM of phosphate buffer (pH 7.2), 0.1% NaN3, and 100 µM of DSS, ensuring a 9 to 1 H_2O/D_2O ratio.

For Ac-αS low concentrations of NaCl (15 mM) **(Figure 22)** show variations at the N- and C-terminal (residues G7 to G31 and Y125 to A140) as well as the core of the protein (residues E46, and T59 to A91). Moderate concentrations (300 mM) show variations at the N- and C-terminal (residues S9 to K23 and E126 to Q134) as well as the core of the protein (residues S42 and E46). Moderate to high concentrations of NaCl (500 mM) affect most regions of the protein, but the N-terminal (residue G14) and the C-terminal (residue S129) are still evidenced.

High concentrations (1000 mM) affect most regions of the protein, but the N-terminal (residue G14) and the C-terminal (residue E126) are still evidenced.

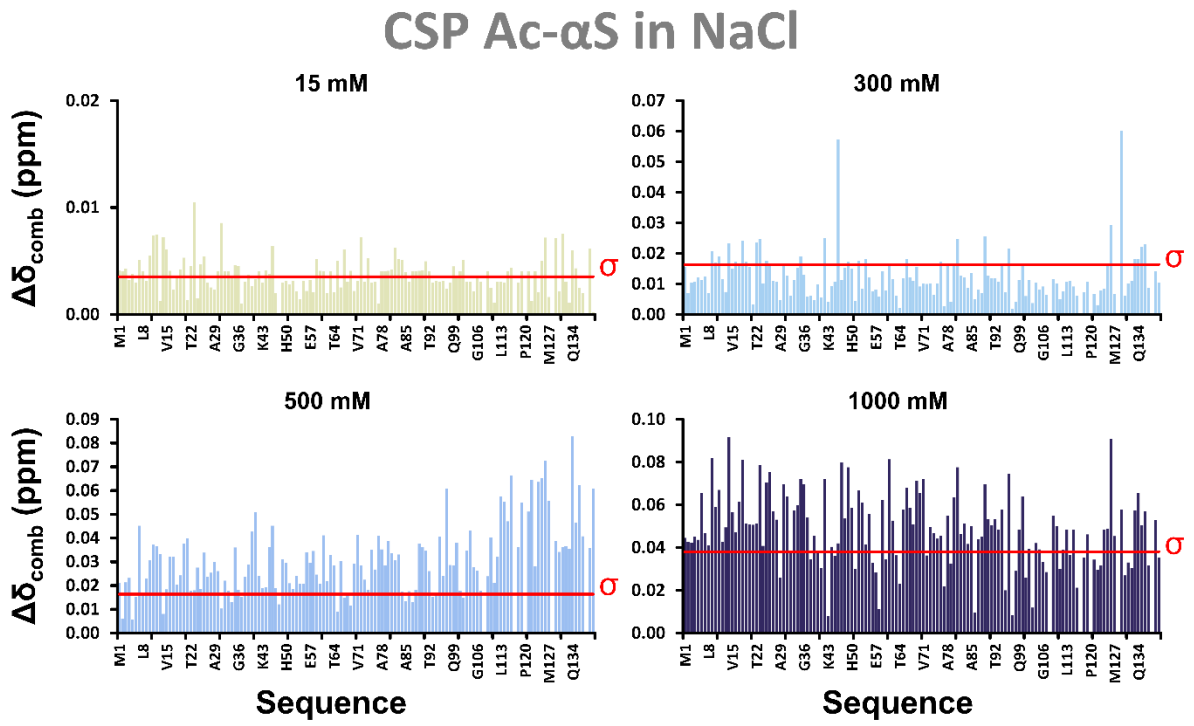

Figure 22 – The CSPs of Ac-αS in the presence of NaCl

NMR CSP analysis of the interactions of Ac-αS with NaCl at representative concentration points (4 in total). **A)** The CSPs of Ac-αS at low concentrations of salt (15 mM). **B)** The CSPs of Ac-αS at moderate concentrations of salt (300 mM). **C)** The CSPs of Ac-αS at high to moderate concentrations of salt (500 mM). **D)** The CSPs of Ac-αS at high concentrations of salt (1000 mM). The variable sigma (σ, in red) represents the minimum threshold value for pin-pointing potentially interacting residues. Experiments were acquired at 288 K (15 °C). Samples (200 µM of protein) were prepared in 105 mM of phosphate buffer (pH 7.2), 0.1% NaN3, and 100 µM of DSS, ensuring a 9 to 1 H_2O/D_2O ratio.

When in the presence of low concentrations of [Ch][Glu] (15 mM) **(Figure 23)** αS shows small, interspersed variations throughout the protein. Moderate concentrations (300 mM) αS show perturbations at the C-terminal (residues L113 to A140) as well as the core of the protein (H50 and vicinal residues). Moderate concentrations (300 mM) αS show perturbations at the C-terminal (residues L113 to A140) as well as the core of the protein (G41 and vicinal residues). High concentrations (1000 mM) affect mostly the N- and C-terminal (residue G14) and the C-terminal (residue E126) are still evidenced.

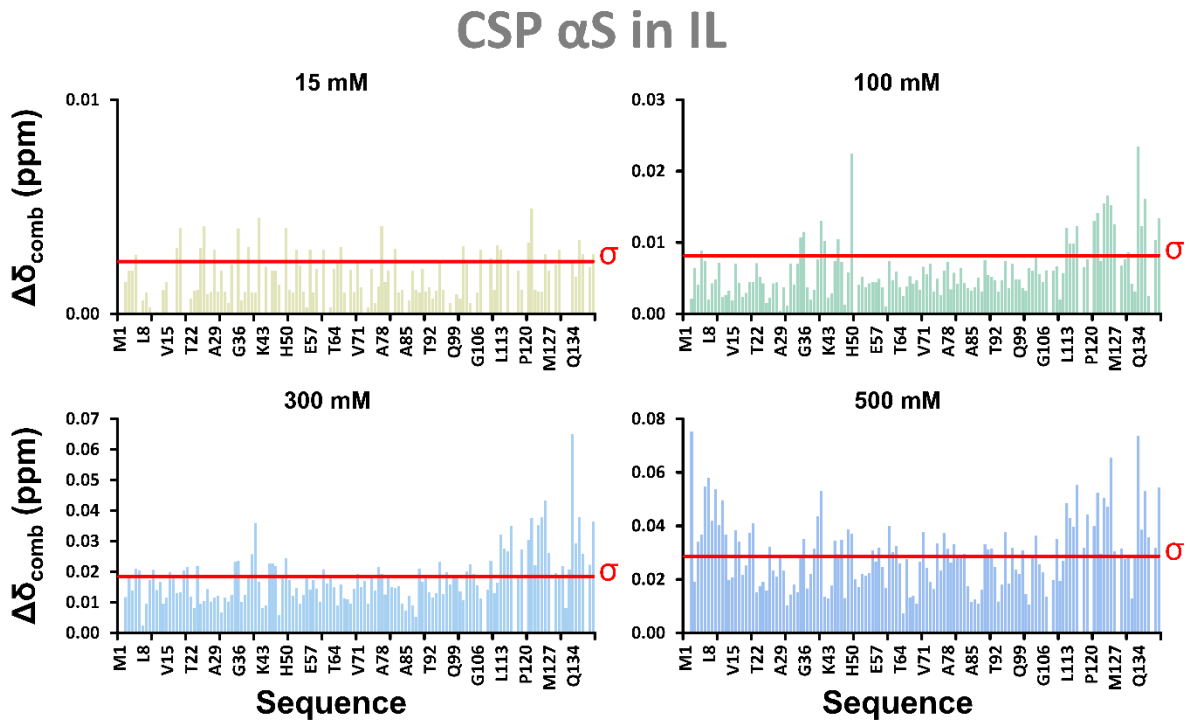

Figure 23 – The CSPs of αS in the presence of [Ch][Glu]

NMR CSP analysis of the interactions of αS with [Ch][Glu] at representative concentration points (4 in total). **A)** The CSPs of αS at low concentrations of IL (15 mM). **B)** The CSPs of αS at moderate concentrations of IL (100 mM). **C)** The CSPs of αS at moderate concentrations of IL (300 mM). **D)** The CSPs of αS at moderate to high concentrations of IL (500 mM). The variable sigma (σ, in red) represents the threshold value for pinpointing potentially interacting residues. Experiments were acquired at 288 K (15 ºC). Samples (200 µM of protein) were prepared in 105 mM of phosphate buffer (pH 7.2), 0.1% NaN3, and 100 µM of DSS, ensuring a 9 to 1 H_2O/D_2O ratio.

When in the presence of low concentrations of [Ch][Glu] (15 mM) **(Figure 24)** Ac-αS shows variations at the N- and C-terminal (residues A11 to G14 and L113 to A140) as well as the core of the protein (residues E35, E46, E61 and K97). Moderate concentrations (300 mM) αS show perturbations at the C-terminal (residues L113 to A140 and residues G7 and K10) as well as the core of the protein (H50 and vicinal residues). Moderate to high concentrations of [Ch][Glu] (500 mM) causes well dispersed perturbations in Ac-αS that are more evident at the at the N- and C-terminal (residues M1 to E20 and A56 to A140) as well as the core of the protein (G41 and vicinal residues). High concentrations (1000 mM) affect mostly the N- and C-terminal (residue G14) and the C-terminal (residue E126) are still evidenced.

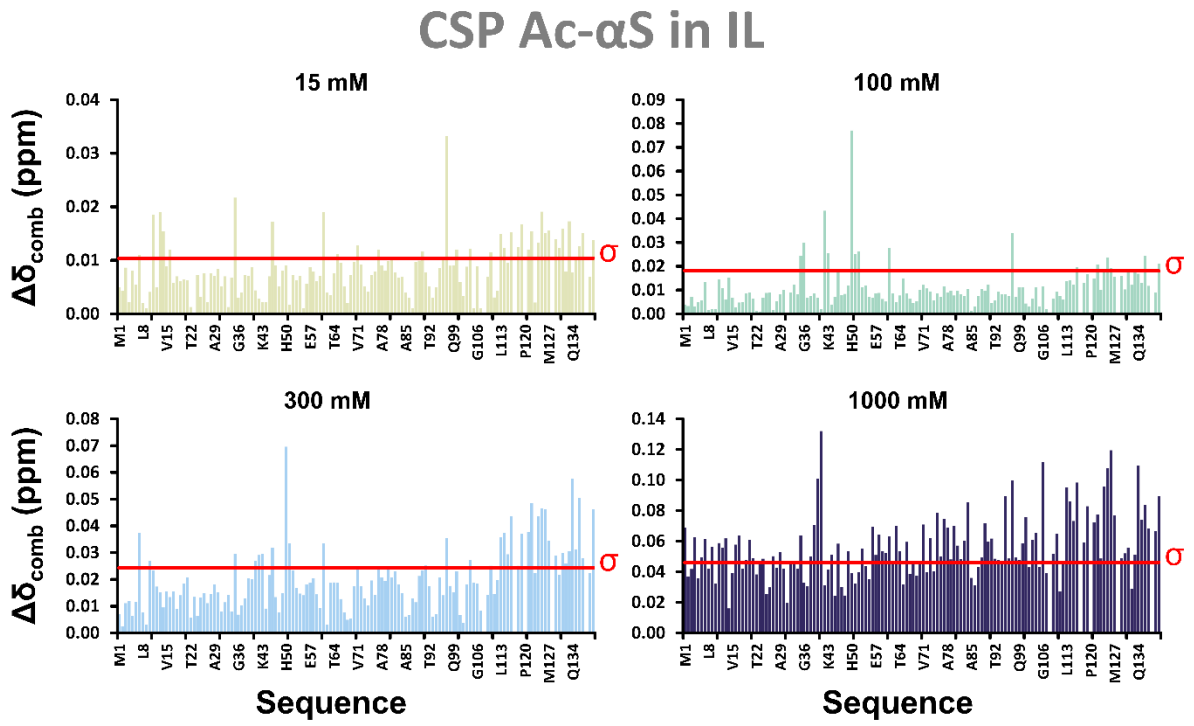

Figure 24 – The CSPs of Ac-αS in the presence of [Ch][Glu]

NMR CSP analysis of the interactions of Ac-αS with [Ch][Glu] at representative concentration points (4 in total). **A)** The CSPs of Ac-αS at low concentrations of IL (15 mM). **B)** The CSPs of Ac-αS at moderate concentrations of IL (100 mM). **C)** The CSPs of Ac-αS at moderate concentrations of IL (300 mM). **D)** The CSPs of Ac-αS at high concentrations of IL (1000 mM). The variable sigma (σ, in red) represents the threshold value for pinpointing potentially interacting residues. Experiments were acquired at 288 K (15 ºC). Samples (200 µM of protein) were prepared in 105 mM of phosphate buffer (pH 7.2), 0.1% NaN3, and 100 µM of DSS, ensuring a 9 to 1 H_2O/D_2O ratio.

3.4.5 Secondary Structure Propensities

Secondary structure propensities (SSPs) represent the intrinsic tendency for the transition of collective amino acid residues into secondary structure elements. The SSP algorithm was initially developed to explain the fibrillation propensities of human α and γ-synuclein [225]. The procedure relies on the experimental calculation of the chemical shifts for a given nucleus, which are then divided by the expected chemical shifts of an equivalent nucleus in a fully formed secondary structure element (*i.e.,* α-helix or β-sheet). At the end of the procedure SSP scores are obtained, these can vary from 1.0 to -1.0 and reflect the formation of α- or β-structure respectively. As an example, a SSP score of -1.0 suggests that 100% of conformers in an ensemble adopt a α-helical conformation at that position. On the other hand, a SSP score of -0.5 would suggest that 100% of conformers adopt a β-structure at that residue. As already mentioned, secondary structure emerges as a collective property of amino acids. Therefore, a

secondary structure element is only present when a minimum of 4 sequential residues with the same score tendency is present. Secondary structure elements separated by a gap are also merged.[225] SSP score can be calculated by a comprehensive set of ^{1}HN, ^{1}Hα, ^{13}Cα, ^{13}Cβ, ^{13}CO, and ^{15}N chemical shifts. For analysis ^{13}Cα, ^{13}Cβ and 1Hα tend to be preferred as ^{13}CO measurements are more inconsistent and ^{15}N chemical shifts are less sensible. Structural propensities are highly sensitive to experimental conditions and can be used to monitor the influence of acetylation and the interaction with ionic compounds on the reference secondary structure propensities of αS.

The reference spectrum for Ac-αS presents reduced SSP scores, in general, indicating a reduced tendency to form secondary structure elements. Although small, SSP scores suggest the presence of 10 distinct regions: **(i)** Residues M1 to K10 represent the region with the most relevant α-helical propensities. **(ii)** Residues A11 to A19 form a buffer region with negligible secondary structure propensities. **(iii)** Residues E20 to A29 create the second region displaying α-helical propensities. **(iv)** Residues A30 to K60 which present reduced β-structure propensities **(v)** Residues E61 to V74 form a buffer region with highly variable secondary structure propensities. **(vi)** Residues V77 to A85 low β-structure propensities. **(vii)** Residues V77 to A85 which present significant β-structure propensities. **(viii)** A third buffering region can be found in residues 86 to 90. **(ix)** Residues A91 to V118 which present significant β-structure propensities. **(x)** Residues N122 to A140 which present the most significant β-structure propensities.

SSP diagrams are highly similar to one another Residues M1 to A29 correspond roughly to the N-terminal region. The only segments with α-helical propensities are found in this region. Residues A30 to A85 roughly corresponds to the NAC domain. Here 2 β-structure prone elements can be found separated by buffer region. Finally, residues A91 to V118 correspond roughly to the C-terminal region. This region contains two β-structure prone elements with considerable SSP scores. The SSP scores for reference αS was not collected due to time constraints of the thesis.

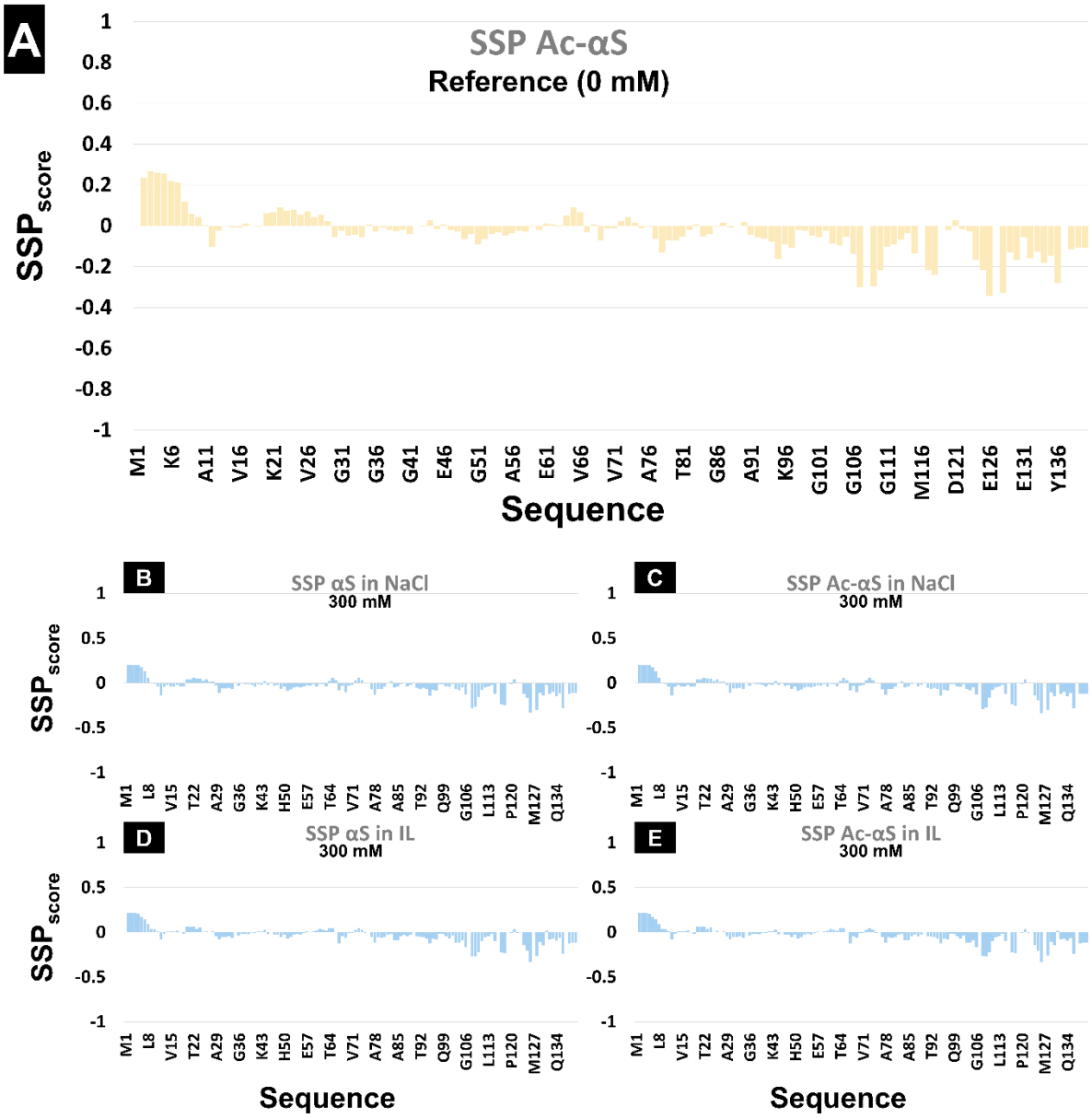

Figure 25 – The SSPs of αS variants

Structural interpretation of αS variants in the presence of ionic compounds. **A)** The propensity of pure Ac-αS (reference propensity plot). **B)** Propensities for αS at moderate concentrations of NaCl (300 mM). **C)** Propensities for Ac-αS at moderate concentrations of NaCl (300 mM). **D)** Propensities for αS at moderate concentrations of [Ch][Glu] (300 mM). **E)** Propensities for Ac-αS at moderate concentrations of [Ch][Glu] (300 mM). Calculations were performed using $^{13}C\alpha$, $^{13}C\beta$ chemical shifts resulting from the in-house assignment of the protein variants. Experiments were acquired at 288 K (15 °C). Samples (200 µM of protein) were prepared in 105 mM of phosphate buffer (pH 7.2), 0.1% NaN3, and 100 µM of DSS, ensuring a 9 to 1 H_2O/D_2O ratio.

4
DISCUSSION

4.1 [Ch][Glu] Acts as a Moderate Destabilizer of αS

4.1.1 αS is Stable in the Absence of Ionic Compounds

The reference samples of (Ac-)αS do not contain NaCl or IL and therefore should be considered baseline indicators of the aggregation behavior for αS variants. In these conditions αS and Ac-αS samples are unable to aggregate over the course of 100 hours of intermittent agitation **(Figure 26)** suggesting that both protein variants are particularly stable under these conditions. Therefore, any alterations on the behavior of the protein variants are a direct consequence of the selected ionic compounds (NaCl or IL). αS variants can aggregate under low concentrations (10 mm) of [Ch][Glu] and moderate concentrations of NaCl (200 to 300 mM) indicating that these ionic compounds are destabilizing the protein and inducing aggregation, albeit through different underlying mechanisms.

Previous studies have already reported on the aggregation propensity of αS under similar conditions.[204] This protein is expected to aggregate without the presence of additional compounds (in as little as 20 hours; for 25 μM of protein and 10 μM in 10 mM of phosphate buffer). The current study offers comparable experimental conditions to those of the study (*i.e.*, fluorescent probe, buffer system, microplate characteristics, and agitation system) yet no autonomous aggregation is observed. Explanations can be derived from minor differences in experimental setups (*i.e.*, αS and ThT concentrations). The concentration of the fluorescent probe ThT is also essential for the success of the fibrillation assays as the reporter molecule exhibits a concentration threshold for fluorescence as well as optimal values of concentration.[226] Another possible justification for this unexpected behavior is the high concentrations of phosphate found in samples **[see section 4.2]**, yet the available literature does not suggest phosphate interference at these concentrations.[227]

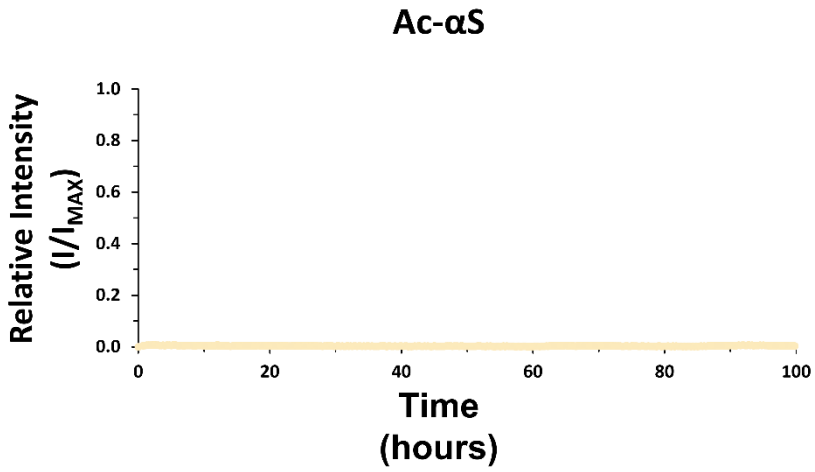

Figure 26 – Reference Aggregation Profiles (Ac-αS)

Ac-αS is unable to fibrillate over the course of 100 hours suggesting that the protein stable in these conditions, αS displayed a similar behavior (date not shown). Protein samples (200 μM) were prepared in 77 mM of phosphate buffer (pH 7.2) and 200 μM of ThT.

4.1.2 [Ch][Glu] Displays Destabilizing Properties Towards αS

Choline glutamate IL promotes the destabilization of (Ac-)αS. This outcome is evidenced by the lack of aggregation in the absence of [Ch][Glu], a similar trend is present for NaCl suggesting that the protein is rather stable at these concentrations. (Ac-)αS can aggregate under low concentrations (10 mM) of [Ch][Glu] and moderate concentrations of NaCl (200 to 300 mM, respectively). These findings are early indicators of a different destabilization mechanism of these compoundsand can be partially explained by the distinct nature of the interacting compounds, as classified by the Hofmeister series. The IL [Ch][Glu] is a combination of a weak (cholinium) and a moderate kosmotrope (glutamate), whereas NaCl is a neutral compound. The resulting ionic compounds are expected to inherit most if not all the properties of the base ions, therefore [Ch][Glu] is expected to be a moderate to weak kosmotrope whereas NaCl is expected to minimally affect kosmotropicity. Kosmotropicity is related to charge density and is a qualitative measure of the structure forming (salting out) properties of the base ions. Kosmotropic ions are strongly hydrated in solution thus contributing to reordering of the water structure around the protein. These effects generally contribute to the stabilization of structured proteins in solution (depending on concentration), but it is important to note that protein-solute interactions are also dependent on the nature of the protein. αS is far from being structured in solution with the added issue of being a highly amyloidogenic protein, in this context structure forming ions act as structural promoters of fibril formation. In this sense [Ch][Glu], as a moderate to weak kosmotrope, is expected to stabilize the protein through a

wealth of protein-IL interactions. [Ch][Glu] is the combination of two bulky naturally occurring ions that promote protein interactions through a variety of mechanisms (at physiological pH): **(i)** ionic bonding provided by the positively charged amine groups and negatively charged carboxylate groups; **(ii)** hydrogen bonding provided by the hydroxyl group (hydrogen bond acceptor and donor) and carboxylate groups (hydrogen bond acceptor); **(iii)** hydrophobic interactions provided by the carbon backbone, which are especially relevant for cholinium. The presence of additional protein-IL interaction mechanisms is likely to have unpredictable effects on the stability of (Ac)-αS.

(Ac-)αS is reported to establish transient, long range tertiary interactions between the N- and C-terminal.[228] Chi et al. reported significant chemical shifts in H50 and the C-terminal of the H50Q mutant suggesting the presence of protective long range interactions in the WT mutant.[229]The core of the protein is also involved in these interactions, with likely residues being: **(i)** E28 to G31; **(ii)** K43 to E46; and **(iii)** H50 to V66.[230] These regions surround and confer protection to the highly hydrophobic NAC domain. Amino terminal acetylation confers neutral charge to the otherwise positive methionine residue promoting the stabilization of the first ten amino acids of the protein. Consequently, this physiological PTM may impart significant physicochemical changes to the near N-terminal region of the protein with likely implications for transient long-range contacts.[5,223]

The effects of increasing concentrations of NaCl on the conformation of αS are well reported.[231] Moderate concentrations of NaCl are known to disrupt protective intramolecular contacts established between the flexible terminal domains of the protein. These alterations lead to the fibrillation of the protein due to an exposure of the NAC core. Charge screening of the flexible terminals of the protein are reported to be the likely mechanism of αS destabilization. High concentrations of NaCl lead to a more compact (and aggregation prone) conformation of the protein which is dominated by unspecific ionic interactions.[231]

4.1.3 Aggregation is Modulated by Acetylation and Ionic Compound

[Ch][Glu] and NaCl are responsible for destabilizing (Ac-)αS albeit through distinct processes. Analysis of the general aggregation dynamics suggest differentiated fluorescence profiles and kinetic parameters for αS variants. The variations in mechanism of action are reflected in the end point fluorescence (100 h) of the protein.

αS presents a maximum fluorescence at 300 to 500 mM for NaCl whereas IL presents optimal fluorescence 300 to 500 mM. Fluorescence intensities are an indirect measure of fibril growth, in general Ac-αS presents larger fluorescence intensities which reach maximal values at 300 mM of NaCl and 500 mM of IL. Therefore, fluorescence intensities can be used to determine the most favorable fibrillation conditions as well as being a helpful early indicator of the protein's aggregation patterns.

The end point fluorescence is comparable for αS and Ac-αS when in the presence of NaCl, relevant differences for the acetylated variant include the early onset of aggregation (from 300 to 200), narrowing of the optimal values (which changed from a plateau to a single peak at 300 mM), and the slower decline in intensities at medium to high concentrations of salt (500 to 1000 mM). These findings suggest that NaCl is more efficient at promoting and sustaining amyloid fractions at higher concentrations of salt. Interestingly the endpoint fluorescence is considerably different for Ac-αS when in the presence of IL. In general, Ac-αS presents larger fluorescence intensities in the presence of [Ch][Glu] further strengthening the link of acetylation to sustained amyloid fractions. Moreover, the optimal fibrillation concentration shifts from 300 to 500 mM for Ac-αS suggesting an alteration of the driving forces of fibrillations as a result of intrinsic properties of the protein.

The kinetic profiles of the fibrillation curves provide further insights into the aggregation mechanisms of the protein. αS presents comparable growth rates in the ranges of 300 to 500 mM and significantly smaller nucleation times for the IL suggesting that the differences in behavior of these compounds in these concentration ranges are dominated by nucleation dependent events affecting the soluble form of the protein. The kinetic profile of αS suggests optimal fibrillation conditions (*i.e.*, a combination of minimal nucleation times and maximal growth rates) at 500 mM for both NaCl and IL. These findings are in line with the previously mentioned endpoint intensities for NaCl but not for IL (300 mM) suggesting that the differences in fluorescence intensities are a result of significant off pathway aggregation events that are significantly more pronounced in the presence of IL. These alternative modes of aggregation are responsible for diverting the available pool of αS monomers into the formation of amorphous aggregates. Ac-αS shows a distinct kinetic profile to its non-acetylated counterparts. When in NaCl, Ac-αS displays reduced growth rates as well as considerable nucleation times in moderate to high concentration ranges (300 to 800 mM). Suggesting that the protein is considerably more stable than αS when in the presence of salt. The stability of Ac-αS seems to be considerably affected by the presence of IL. This behavior can be justified by the

diminished nucleation times and the increased growth rates of the protein in moderate to high concentrations (600 to 1000 mM).

CSI mapping provides atomic resolution to the previously discussed aggregation patterns of (Ac-)αS, thus allowing for a detailed characterization of the interactions of the protein through the identification of the preferred interacting residues or regions that are directly involved in protein destabilization.

Low concentrations of NaCl (15 mM) induce considerable chemical shifts to the N-terminal and core of αS **(Figure 27)**. Curiously, the C-terminal is not affected at these concentrations indicating that the destabilization of the protein is initiated at the amino terminal region which is an important distinction from Ac-αS. These findings suggest that acetylation influences the protective properties of the N-terminal. The involvement of the N- and C-terminal becomes apparent at moderate concentrations of salt (300 mM). Residues S42 to K45 also show considerable combined chemical shifts suggesting an important role of these residues in the stabilization of the protein. This central region is also expected to interact with the flexible ends of the protein effectively protecting the NAC region. The transition from moderate to high concentrations of NaCl (500-1000 mM) results in an increase in non-specific electrostatic interactions with the protein interactions suggesting that the protein is particularly exposed to the solvent.

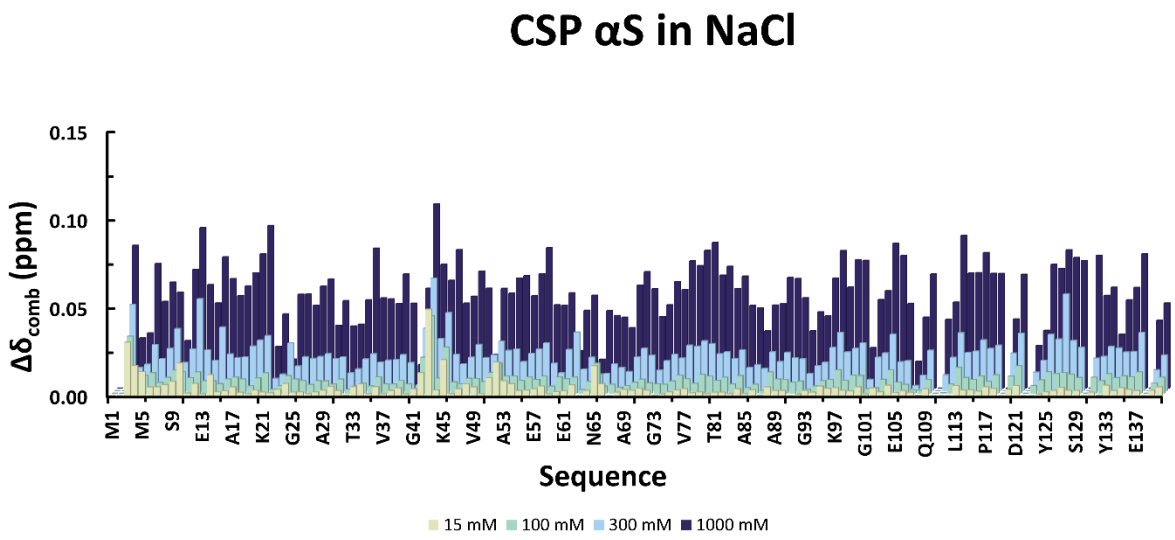

Figure 27 – CSP Overlay of αS in the Presence of NaCl

Combined CSP interactions of αS in the presence of NaCl at representative concentration points (15, 100, 300, and 1000 mM) previously indicated in figure 21. Here the involvement of several residues of the N- and C-terminal are

visible at different stages of the titration of the protein (especially residues S42 to K45). Experiments were acquired at 288 K (15 ºC). Samples (200 µM of protein) were prepared in 105 mM of phosphate buffer (pH 7.2), 0.1% NaN_3, and 100 µM of DSS, ensuring a 9 to 1 H_2O/D_2O ratio.

Low concentrations of NaCl (15 mM) result in a generalized binding to the backbone of Ac-αS, a small involvement of the N- and C-terminal is already visible at these concentrations **(Figure 28)**. These findings are consistent with the electrostatic model of the protein **(Figure 3)** where ions preferably interact with the charged regions of the protein (charge screening effect). It is important to note that fibrillation does not take place at these concentrations, also suggesting that flexible ends of the protein are possibly implicated in the stabilization of the protein. the involvement of the N- and C-terminal becomes more apparent at moderate concentrations of salt (300 mM). Residues S129 and K45 show considerable combined chemical shifts suggesting some degree of interplay between the C-terminal and the core of the protein. Moderate to high concentrations of NaCl (500 to 1000 mM) result in generalized interactions with the protein backbone suggesting that the protein is particularly exposed to the solvent.

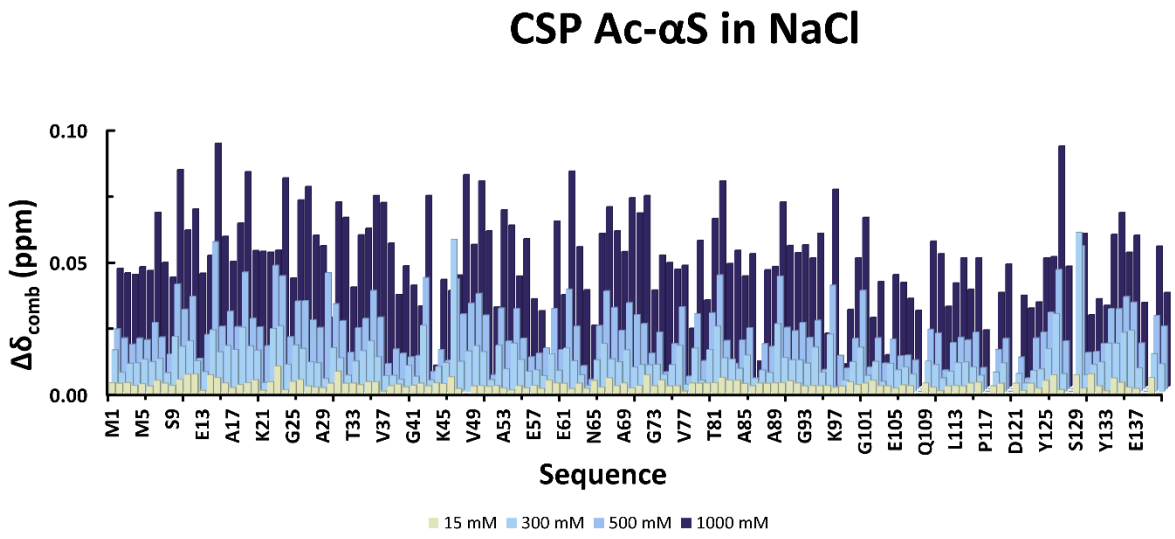

Figure 28 – CSP Overlay of Ac-αS in the Presence of NaCl

Combined CSP interactions of Ac-αS in the presence of NaCl at representative concentration points (15, 300, 500, and 1000 mM) previously indicated in figure 22. Here the involvement of several residues of the N- and C-terminal are visible at different stages of the titration of the protein (especially residues K45 and S129). Experiments were

acquired at 288 K (15 °C). Samples (200 µM of protein) were prepared in 105 mM of phosphate buffer (pH 7.2), 0.1% NaN_3, and 100 µM of DSS, ensuring a 9 to 1 H_2O/D_2O ratio.

The behaviors of αS and Ac-αS are comparable, a pattern consistent with progressive destabilization of the long-range interactions of the protein (N-, C-terminal and core residues) until a critical concentration is reached (approximately 500 mM) which results in a sudden exposure of the protein to the solvent. These findings suggest the formation of the aggregation prone compact conformation of (Ac-)αS.

Low concentrations of [Ch][Glu] (15 mM) show interspersed αS residues with small but significant combined shifts suggesting that the ionic liquid is not particularly disruptive at these concentrations **(Figure 29)**. Moderate concentrations elicit the perturbations of C-terminal and the core of the protein (vicinal to H50). The increase of concentration (500 mM) results in a reduction of the intensities of core residues (vicinal to G41) as well as an increase in perturbations of the C- an N- terminal which are consistent with electrostatic interactions with the flexible terminals of the protein.

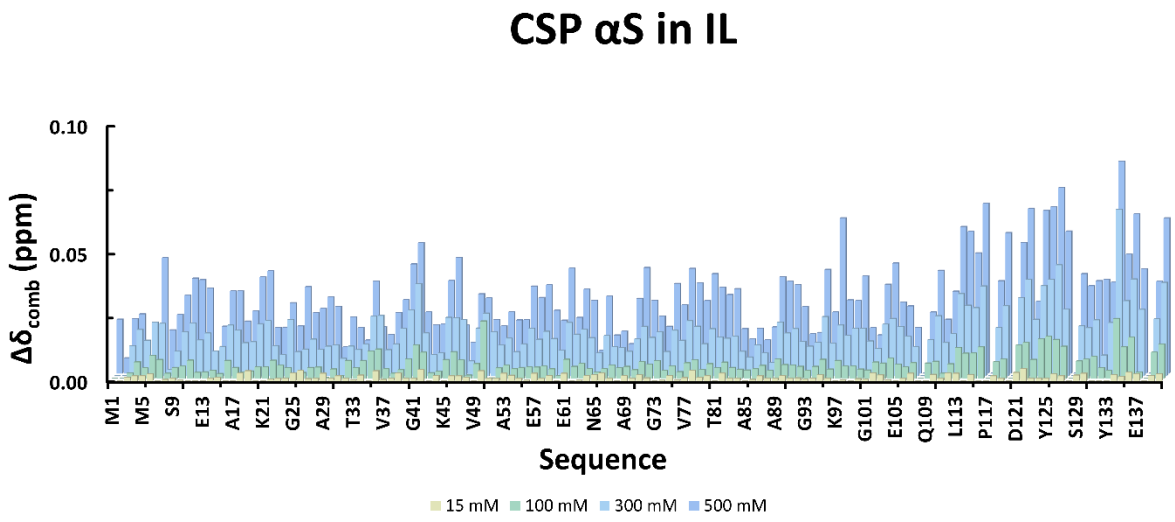

Figure 29 – CSP Overlay of αS in the Presence of [Ch][Glu]

Combined CSP interactions of αS in the presence of IL at representative concentration points (15, 100, 300, and 500 mM) previously indicated in figure 23. Here the involvement of several residues of the N- and C-terminal are visible at different stages of the titration of the protein (especially residues G41 and H50). Experiments were acquired at

288 K (15 ºC). Samples (200 µM of protein) were prepared in 105 mM of phosphate buffer (pH 7.2), 0.1% NaN_3, and 100 µM of DSS, ensuring a 9 to 1 H_2O/D_2O ratio.

Low concentrations of [Ch][Glu] (15 mM) exhibit an involvement of the N- and C-terminal as well as core residues of Ac-αS **(Figure 30).** It is important to note that small amounts of fibrillation occur at these concentrations suggesting that these regions play important roles in the stabilization of the protein and that this ionic liquid is particularly effective at destabilizing the protective interactions of the N-terminal region. Moderate concentrations of the IL (300 mM) display significant chemical shifts at the C-terminal as well as core residues (vicinal to H50). As concentrations progress to 500 mM the involvement of the H50 and vicinal residues becomes less significant, these shifts are progressively substituted by G41 and vicinal residues at higher concentrations (1000 mM). These findings suggest interplay between H50 and G41 as the titration develops and could indicate a two-stage disruption of the interactions between the core of the protein and the C-terminal region. These findings could be representative of the adoption of different conformation in IL. Other important features include the involvement of the N-terminal region, and the shifts at the C-terminal which extend to the center of the protein. These findings are consistent with the electrostatic profile of the protein and suggest that [Ch][Glu] interacts more specifically to (Ac-)αS at high concentrations, which is a distinctive feature from NaCl. These findings could indicate that the compact and aggregation prone conformation found in NaCl can only be partially formed or not formed at all.

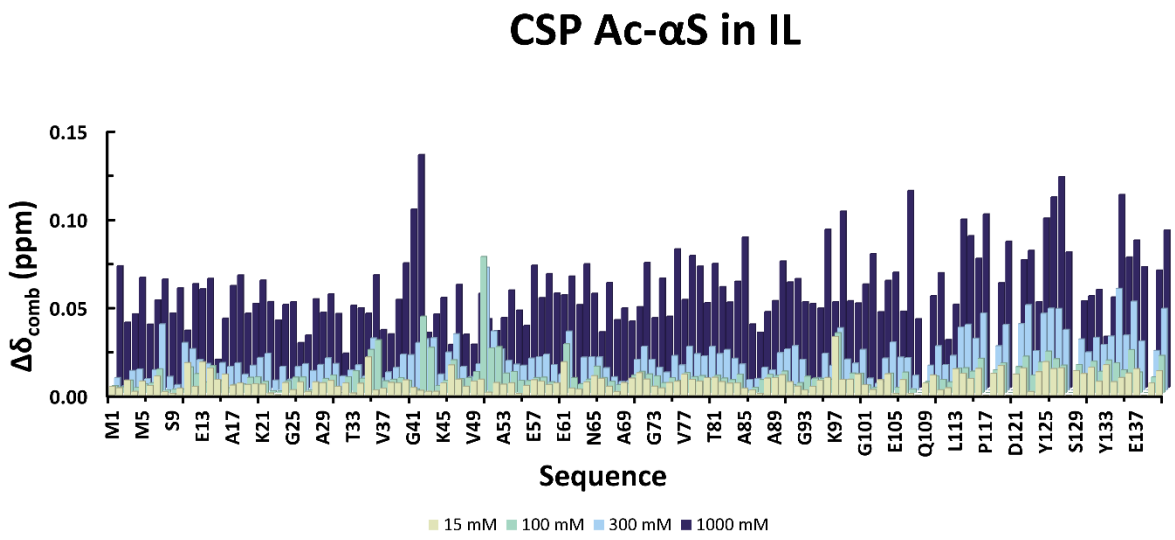

Figure 30 – CSP Overlay of Ac-αS in the Presence of [Ch][Glu]

Combined CSP interactions of Ac-αS in the presence of IL at representative concentration points (15, 100, 300, and 1000 mM) previously indicated in figure 24. Here the involvement of several residues of the N- and C-terminal are visible at different stages of the titration of the protein (especially residues G41 and H50). Experiments were acquired at 288 K (15 ºC). Samples (200 µM of protein) were prepared in 105 mM of phosphate buffer (pH 7.2), 0.1% NaN_3, and 100 µM of DSS, ensuring a 9 to 1 H_2O/D_2O ratio.

The behaviors of αS and Ac-αS are also comparable but show significant differences at the level of the N-terminal, αS only shows significant implications of the amino terminal at moderate to high concentrations (500 mM). In Ac-αS perturbations of the N-terminal are also visible throughout the titration process, suggesting that this residue is implicated in the stabilization of the protein. The core residues implicated in the stabilization of (Ac-)αS are concentration dependent. (Ac-)αS elicits primarily H50 (and vicinal resides) at moderate concentrations and G41 (and vicinal resides) at moderate concentrations suggesting a more complex two-step destabilization of the protein. Another important finding is that [Ch][Glu] interacts more selectively with the backbone of the protein affecting primarily the N- and C-terminal.

When the information integrated holistically the destabilization mechanisms mediated by [Ch][Glu] and NaCl become apparent. NaCl can possibly disrupt the long-range interactions established by the C-terminal and E46 at moderate concentrations of salt. At these concentrations an extended conformation of (Ac-)αS is adopted potentiating fibrillation. As high concentrations are achieved a compacted form of (Ac-)αS is formed (signalized by the generalized electrostatic interactions) with significant propensity to form unstructured aggregates that are

not visible through the fluorescence of ThT. [Ch][Glu] as a moderate to weak kosmotrope, with a richer variety of protein-IL interactions, is capable of not only disrupting the long-range interactions established by the C-terminal and H50 (at moderate concentrations) but also the additional interactions formed by the N-terminal and G41 (at higher concentrations).

Ac-αS appears to be more stable than αS in the presence of NaCl, the reverse tendency can be seen for IL suggesting that [Ch][Glu] is particularly effective at disrupting the N-terminal. [Ch][Glu] possibly promotes the formation of distinct conformers at moderate to high concentrations as evidenced by the two-step disruption of the protein and the prevalence of more specific interactions at moderate to high concentrations.

4.1.4 The Protective role of Histidine 50

Histidine 50 is a critical element for the stabilization of αS. The H50Q point mutation is one of the most aggressive forms of familial Parkinson and is often related to more unfavorable outcomes of PD.[84] Substitutions of H50 with neutral and negative residues (*i.e.*, Asp, Gln, or Ala) result in significant structural changes to the structure of αS, these alterations are associated with a more flexible C-terminal region and therefore a more exposed NAC domain. The substitution of H50 with Arg (positively charged residue) results in a suppression of αS aggregation. These findings could be explained by the presence of long-range interactions between H50 (carries a positive charge at neutral pH) and the C-terminal (negatively charged at physiological pH).[229]

The 15N correlations of histidine's imidazole ring can be used to gain further insights into the role of H50 and neighboring residues. Curiously the side chain correlations of H50 cannot be found in αS (at all concentrations) possibly suggesting an alternative mode of interaction which might be linked long-range interaction. The acetylation state of the protein seems to be particularly important for the presence of side chain correlations, as Ac-αS displays all side chain correlations. The residue H50 of Ac-αS is found in the less common δ-tautomeric state. When in the presence of NaCl or [Ch][Glu] Ac-αS displays a progressive decrease in the 15N chemical shifts of the nδ1-Hε1 correlation suggesting a progressive increase in protonation tendency of the ε2 nitrogen. These findings in turn suggest a promotion of the charged form of Histidine which is more available for binding to the negatively charged C-terminal. Thes findings could be framed in the context of long-range Interactions where H50 and to the C-terminal protect the protein from fibrillation at high concentrations of ionic compound by assuming a more compact conformation.

4.1.5 Ionic Compounds do Not Alter the SSPs of αS

As previously mentioned, the SSP scores of αS variants are minimally affected in the presence of NaCl or IL. These findings share important insights into the pre-fibrillation mechanisms of soluble (Ac-)αS in solution. These findings indicate that the net SSP scores of the (Ac-)αS monomers are unaltered at moderate concentrations of ionic compounds (300 mM). It is important to note that (Ac-)αS suffers the most significant fibrillation at moderate concentrations suggesting that these correspond to the most significant variations of SSPs.

Noteworthy mentions are found in: **(i)** N-terminal domain of the protein (residuesM1 to S9) which present small but significant differences in the SSP score of the first segment. Ac-αS presents higher secondary structure propensities than αS. These findings are in line with the reports of acetylation promoting the alpha helical propensities of the N-terminal (10 initial residues). These changes are caused by the interactions of the added carbonyl group with vicinal amino acids which promotes higher secondary structure propensities.[223] The reference SSP plot of Ac-αS displays the more significant SSP scores followed by NaCl and finally [Ch][Glu], hosting that the IL is more effective at disrupting the alpha helical secondary structure propensities of the N-terminal αS displays comparable SSP's for NaCl and [Ch][Glu] in this region. **(ii)** The second fragment (residues M1 to S9) which presents significant secondary structure propensities only in the presence of salt.

4.2 Orthophosphate may influence the stabilization of αS

The phosphate buffer contains one strong kosmotropic ion; orthophosphate, which may significantly influence aggregation dynamics of (Ac-)αS. Significant promotion of aggregation should only be found at the optimal concentration ranges of 200-325 mM (for 0.1 mg/mL of protein over a 24 h interval).[227] These values are considerably higher than the concentrations of phosphate buffer used in this study (50 to 100 mM) suggesting low interference of this ancillary ion on the fibrillation of αS. Low to moderate concentrations of sodium phosphate (up to 100 mM) are expected stabilize the protein, as αS precipitates in the absence of this IL.[232] Thes findings suggest a possible influence of this ion In the early stages of aggregations. The combined effects of the ions in solution cannot be easily interpreted from available literature. Phosphate may additively contribute to the kosmotropic effects of NaCl while masking the chaotropic effects of [Ch][Glu] in low to moderate concentration ranges.

5
Conclusions

The present work is centered around αS as a high value therapeutic target displaying a strong causative relationship with Parkinson's disease. αS is known to be acetylated in human cells, thus conferring a special interest in the properties of Ac-αS as the physiologically relevant form of the protein. The impact of acetylation on Ac-αS is still unclear under these conditions, prompting the design of an *in vitro* procedure capable of evaluating the structural stability of (Ac-)αS in a chemical environment reminiscent of the crowded presynaptic milieu. In these exceptional environments charged metabolites can reach molar concentrations as well as exhibit, in some cases, remarkable (de)stabilizing properties towards neighboring proteins. High concentrations of charged metabolites is one of the most important prerequisites for the formation of biocompatible ILs, therefore hinting at the formations of endogenous ILs with the capability of positively modulating Ac-αS's stability (main hypotheses). [Ch][Glu] was naturally chosen as the best representative of a putative stabilizing ILs formed in the synaptic area due to the high *in vivo* concentrations and indispensable cellular roles of the constituent ions.

Fluorescence results established [Ch][Glu] and NaCl as destabilizing ionic compounds, capable of interacting with (Ac-)αS in a concentration dependent fashion. The nature of the interacting compounds and the distinct aggregation dynamics of αS variants are early indicators of the divergent aggregation mechanisms of [Ch][Glu] and NaCl. αS variants displayed comparable end point fluorescence's profiles which can be roughly divided into 3 phases: **(i)** stabilizing interactions at low concentrations of salt where aggregation does not take place; **(ii)** destabilizing interactions moderate concentrations where fibrillation is favored; and **(iii)** destabilizing interactions moderate concentrations of salt where aggregation is favored. No conclusions can be drawn when comparing the stability of αS variants in the presence of NaCl as kinetic evidence and end point fluorescence show mixed results. Non acetylated αS displays slower onsets of fibrillation intensities, higher growth rates and nucleation times (in general).

Ac-αS synuclein is considerably less stable than αS in the presence of [Ch][Glu] suggesting that the additional stabilization that is imparted by acetylation is particularly susceptible to being disrupted by the action of the IL. These findings are evidenced by the higher end point fluorescence's, increased growth rates, and reduced nucleation rates of Ac-αS. The aggregation profile of Ac-αS is divided into 3 stages: **(i)** progressive destabilization at low concentrations; and **(ii)** strong destabilization accompanied by fibrillation at moderate concentrations; and **(iii)** progressive destabilization at low concentrations at high concentrations. The aggregation profile of Ac-αS is divided into 2 stages: **(i)** small but progressive destabilization at low concentrations; and **(ii)** stabilization of fluorescence intensities at moderate concentrations.

CSI mapping provided additional insights into the destabilization mechanism of [Ch][Glu] and NaCl by identifying key interacting residues and/or regions. The observed interactions (Ac-)αS with the ionic compound seem to occur at focal points which might be involved in fibril formation. The perturbations of (Ac-)αS are comparable and consistent with the three phases of the NaCl titration. Low concentrations of NaCl stabilize the protein preventing its aggregation. Moderate concentrations disrupt the long-range interactions established by the C-terminal and the proximal residues to E46 exposing the protein to the solvent and promoting fibrillation. High concentrations of NaCl promote unspecific interactions with the protein backbone favoring (Ac-)αS's aggregation.

The perturbations of αS and Ac-αS in the presence of IL are differentiated by the binding to the N-terminal. αS shows delayed perturbations at the amino terminal suggesting that this region is responsible for the drastic differences of IL mediated destabilization of Ac-αS. The disruption of αS variants is made in two stages, primarily recruiting H50 (and vicinal resides) at moderate concentrations and G41 (and vicinal resides) at moderate to high concentrations. When taken together these findings suggest that the stabilizing interactions are acetylation dependent and ionic compound.

The Histidine 50 of Ac-αS shows a progressive protonation of the Imidazole side chain in the presence of both NaCl and [Ch][Glu] promoting a positively charged H50 that can better interact with the C-terminal.

Ac-αS variants do not show significant variations in structure propensities at moderate concentrations of NaCl or IL suggesting the monomers remain mostly disordered in solution and that no significant secondary structure shifts occur in solution.

The work herein presented provided an objective framework for the classification of the interactions of [Ch][Glu] and NaCl with (Ac-)αS while providing key insights into the role of interacting residues and/or protein regions as well as demonstrating the modulating effects of

acetylation in these same interactions. It is important to note that the main conclusions of this study are representative of an *in vitro* model of (Ac-)αS where aggregation of alpha synuclein is mechanically induced under glass beads. Therefore, the biological relevance of these conclusions is still unclear.

This approach resulted in a clear, albeit *in vitro*, demonstration of the potential modulatory effects of osmolytes in the stability of (Ac-)αS; and even though the stabilizing properties of [Ch][Glu] were no confirmed according to the initial hypothesis the possibility of using other combinations of charged metabolites is still valid.

Several important improvements should be made to the current protocol. The role of the phosphate ion could not be completely discarded due to sample variations of said buffer. In the future these problems can be circumvented by simply implementing an additional protein filtration step. The fluorescence assays resulted in inconsistent aggregation patterns which can be explained by the medium binding nature of the microplates. Future assays will require the use of non-binding microplates to prevent this issue. The addition of positive (*i.e.*, seeded) controls can be used to further validate the experiments, controls for viscosity (*i.e.*, glycerol) can be used to discard the effects IL viscosity in the aggregation of the protein, and finally controls for sodium glutamate (NaGlu) and choline chloride (ChoCl) can be used to demonstrate that the effects of [Ch][Glu] on protein stability are a result of the emergent properties of the IL instead of the individual contributions of the base ions. Aggregation assays do not allow the determination of amyloid fibril morphology, which could be made possible through fluorescence microscopy.

6 BIBLIOGRAPHY

[1] V. N. Uversky, *Int. J. Biochem. Cell Biol.* **2011**, *43*, 1090–1103.

[2] V. N. Uversky, J. Li, P. Souillac, I. S. Millett, S. Doniach, R. Jakes, M. Goedert, A. L. Fink, *J. Biol. Chem.* **2002**, *277*, 11970–11978.

[3] J. Burré, M. Sharma, T. C. Südhof, *Cold Spring Harb. Perspect. Med.* **2018**, *8*, 1–28.

[4] K. E. Paleologou, A. Oueslati, G. Shakked, C. C. Rospigliosi, H. Y. Kim, G. R. Lamberto, C. O. Fernandez, A. Schmid, F. Chegini, W. P. Gai, D. Chiappe, M. Moniatte, B. L. Schneider, P. Aebischer, D. Eliezer, M. Zweckstetter, E. Masliah, H. A. Lashuel, *J. Neurosci.* **2010**, *30*, 3184–3198.

[5] B. Fauvet, M. K. Mbefo, M. B. Fares, C. Desobry, S. Michael, M. T. Ardah, E. Tsika, P. Coune, M. Prudent, N. Lion, D. Eliezer, D. J. Moore, B. Schneider, P. Aebischer, O. M. El-Agnaf, E. Masliah, H. A. Lashuel, *J. Biol. Chem.* **2012**, *287*, 15345–15364.

[6] T. Bartels, N. C. Kim, E. S. Luth, D. J. Selkoe, *PLoS One* **2014**, *9*, 1–10.

[7] V. N. Uversky, E. M. Cooper, K. S. Bower, J. Li, A. L. Fink, *FEBS Lett.* **2002**, *515*, 99–103.

[8] V. N. Uversky, *J. Biomol. Struct. Dyn.* **2003**, *21*, 211–234.

[9] A. T. Marvian, D. J. Koss, F. Aliakbari, D. Morshedi, T. F. Outeiro, *J. Neurochem.* **2019**, *150*, 535–565.

[10] R. Guerrero-ferreira, N. M. I. Taylor, D. Mona, P. Ringler, M. E. Lauer, R. Riek, M. Britschgi, H. Stahlberg, *Elife* **2018**, *7*, DOI DOI: https://doi.org/10.7554/eLife.36402.

[11] S. K. Singh, A. W. Savoy, *J. Mol. Liq.* **2020**, *297*, 112038.

[12] E. W. Castner, C. J. Margulis, M. Maroncelli, J. F. Wishart, *Annu. Rev. Phys. Chem.* **2011**, *62*, 85–105.

[13] T. L. Greaves, C. J. Drummond, *Chem. Rev.* **2008**, *108*, 206–237.

[14] Y.-L. Wang, B. Li, S. Sarman, F. Mocci, Z.-Y. Lu, J. Yuan, A. Laaksonen, M. D. Fayer, *Chem. Rev.* **2020**, *120*, 5798–5877.

[15] S. Y. Yang, F. Cicoira, R. Byrne, F. Benito-Lopez, D. Diamond, R. M. Owens, G. G. Malliaras, *Chem. Commun.* **2010**, *46*, 7972.

[16] D. . Bolen, I. V Baskakov, *J. Mol. Biol.* **2001**, *310*, 955–963.

[17] P. H. Yancey, *J. Exp. Biol.* **2005**, *208*, 2819–2830.

[18] M. M. Santoro, Y. Liu, S. M. A. Khan, L. X. Hou, D. W. Bolen, *Biochemistry* **1992**, *31*, 5278–5283.

[19] B. D. Bennett, E. H. Kimball, M. Gao, R. Osterhout, S. J. Van Dien, J. D. Rabinowitz, *Nat. Chem. Biol.* **2009**, *5*, 593–599.

[20] L. Chen, G. E. Mullen, M. Le Roch, C. G. Cassity, N. Gouault, H. Y. Fadamiro, R. E. Barletta,

R. A. O'Brien, R. E. Sykora, A. C. Stenson, K. N. West, H. E. Horne, J. M. Hendrich, K. R. Xiang, J. H. Davis, *Angew. Chemie - Int. Ed.* **2014**, *53*, 11762–11765.
[21] A. Sindhu, R. S. Varma, P. Venkatesu, *ACS Sustain. Chem. Eng.* **2022**, *10*, 9242–9253.
[22] M. S. Silva, {NMR} Investigation of Ion-Pair Modulation of Protein Structure and Dynamics and Their Relation to Protein Stability, **2021**.
[23] M. S. Silva, Design of Bio-Inspired Ionic Liquids for Protein Stabilisation, **2015**.
[24] M. S. Silva, NMR Investigation of Ion-Pair Modulation of Protein Structure and Dynamics and Their Relation to Protein Stability, **2021**.
[25] P. Gracia, J. D. Camino, L. Volpicelli-Daley, N. Cremades, *Int. J. Mol. Sci.* **2020**, *21*, 1–27.
[26] K. K. M. Sweers, M. Stöckl, M. L. Bennink, V. Subramaniam, *Characterizing Nanoscale Morphologic and Mechanical Properties of α-Synuclein Amyloid Fibrils with Atomic Force Microscopy*, Elsevier, **2013**.
[27] E. Dorsey, R. Constantinescu, J. Thompson, K. Biglan, *Neurology* **2007**, *68*, 384–386.
[28] A. M. Gonçalves, Â. Sousa, A. Q. Pedro, M. J. Romão, J. A. Queiroz, E. Gallardo, L. A. Passarinha, *Int. J. Mol. Sci.* **2022**, *23*, 1–14.
[29] J. A. Marsh, V. K. Singh, Z. Jia, J. D. Forman-Kay, *Protein Sci.* **2006**, *15*, 2795–2804.
[30] D. E. Mor, S. E. Ugras, M. J. Daniels, H. Ischiropoulos, *Neurobiol. Dis.* **2016**, *88*, 66–74.
[31] S. Baltic, M. Perovic, A. Mladenovic, N. Raicevic, S. Ruzdijic, L. Rakic, S. Kanazir, *J. Mol. Neurosci.* **2004**, *22*, 199–203.
[32] R. Jakes, M. G. Spillantini, M. Goedert, *FEBS Lett.* **1994**, *345*, 27–32.
[33] N. Gould, D. E. Mor, R. Lightfoot, K. Malkus, B. Giasson, H. Ischiropoulos, *J. Biol. Chem.* **2014**, *289*, 7929–7934.
[34] P. H. Weinreb, W. Zhen, A. W. Poon, K. A. Conway, P. T. Lansbury, *Biochemistry* **1996**, *35*, 13709–13715.
[35] J. Burré, M. Sharma, T. Tsetsenis, V. Buchman, M. R. Etherton, T. C. Südhof, *Science (80-.).* **2010**, *329*, 1663–1667.
[36] J. Diao, J. Burré, S. Vivona, D. J. Cipriano, M. Sharma, M. Kyoung, T. C. Südhof, A. T. Brunger, *Elife* **2013**, *2013*, 1–17.
[37] A. Villar-Piqué, T. Lopes da Fonseca, T. F. Outeiro, *J. Neurochem.* **2016**, *139*, 240–255.
[38] L. Breydo, J. W. Wu, V. N. Uversky, *Biochim. Biophys. Acta - Mol. Basis Dis.* **2012**, *1822*, 261–285.
[39] W. S. Davidson, A. Jonas, D. F. Clayton, J. M. George, *J. Biol. Chem.* **1998**, *273*, 9443–9449.
[40] B. I. Giasson, M. S. Forman, M. Higuchi, L. I. Golbe, C. L. Graves, P. T. Kotzbauer, J. Q. Trojanowski, V. M. Y. Lee, *Science (80-.).* **2003**, *300*, 636–640.
[41] E. Jo, N. Fuller, R. P. Rand, P. St George-Hyslop, P. E. Fraser, *J. Mol. Biol.* **2002**, *315*, 799–807.
[42] S. B. Lokappa, J. E. Suk, A. Balasubramanian, S. Samanta, A. J. Situ, T. S. Ulmer, *J. Mol. Biol.* **2014**, *426*, 2130–2144.
[43] K. Vamvaca, M. J. Volles, P. T. Lansbury, *J. Mol. Biol.* **2009**, *389*, 413–424.
[44] L. A. Munishkina, J. Henriques, V. N. Uversky, A. L. Fink, *Biochemistry* **2004**, *43*, 3289–3300.
[45] K. Uéda, H. Fukushima, E. Masliah, Y. Xia, A. Iwai, M. Yoshimoto, D. A. Otero, J. Kondo, Y. Ihara, T. Saitoh, *Proc. Natl. Acad. Sci.* **1993**, *90*, 11282–11286.
[46] P. Radivojac, L. M. Iakoucheva, C. J. Oldfield, Z. Obradovic, V. N. Uversky, A. K. Dunker, *Biophys. J.* **2007**, *92*, 1439–1456.

[47] K. Pirc, N. P. Ulrih, *Biochim. Biophys. Acta - Biomembr.* **2015**, *1848*, 2002–2012.
[48] E. Jo, N. Fuller, R. P. Rand, P. St George-Hyslop, P. E. Fraser, *J. Mol. Biol.* **2002**, *315*, 799–807.
[49] A. Deleersnijder, M. Gerard, Z. Debyser, V. Baekelandt, *Trends Mol. Med.* **2013**, *19*, 368–377.
[50] J. T. Guo, A. Q. Chen, Q. Kong, H. Zhu, C. M. Ma, C. Qin, *Cell. Mol. Neurobiol.* **2008**, *28*, 35–47.
[51] B. Greten-Harrison, M. Polydoro, M. Morimoto-Tomita, L. Diao, A. M. Williams, E. H. Nie, S. Makani, N. Tian, P. E. Castillo, V. L. Buchman, S. S. Chandra, *Proc. Natl. Acad. Sci. U. S. A.* **2010**, *107*, 19573–19578.
[52] S. Chandra, X. Chen, J. Rizo, R. Jahn, T. C. Südhof, *J. Biol. Chem.* **2003**, *278*, 15313–15318.
[53] D. L. Fortin, V. M. Nemani, S. M. Voglmaier, M. D. Anthony, T. A. Ryan, R. H. Edwards, *J. Neurosci.* **2005**, *25*, 10913–10921.
[54] L. Wang, U. Das, D. A. Scott, Y. Tang, P. J. McLean, S. Roy, *Curr. Biol.* **2014**, *24*, 2319–2326.
[55] J. Burré, M. Sharma, T. C. Südhof, *Proc. Natl. Acad. Sci. U. S. A.* **2014**, *111*, E4274–E4283.
[56] Y. Lai, S. Kim, J. Varkey, X. Lou, J. K. Song, J. Diao, R. Langen, Y. K. Shin, *Biochemistry* **2014**, *53*, 3889–3896.
[57] N. Ostrerova, L. Petrucelli, M. Farrer, N. Mehta, P. Choi, J. Hardy, B. Wolozin, *J. Neurosci.* **1999**, *19*, 5782–5791.
[58] M. Ahn, S. B. Kim, M. Kang, Y. Ryu, T. Doohun Kim, *Biochem. Biophys. Res. Commun.* **2006**, *346*, 1142–1149.
[59] S. Anwar, O. Peters, S. Millership, N. Ninkina, N. Doig, N. Connor-Robson, S. Threlfell, G. Kooner, R. M. Deacon, D. M. Bannerman, J. P. Bolam, S. S. Chandra, S. J. Cragg, R. Wade-Martins, V. L. Buchman, *J. Neurosci.* **2011**, *31*, 7264–7274.
[60] S. Yu, X. Zuo, Y. Li, C. Zhang, M. Zhou, Y. A. Zhang, K. Uéda, P. Chan, *Neurosci. Lett.* **2004**, *367*, 34–39.
[61] Y. Chu, J. H. Kordower, *Neurobiol. Dis.* **2007**, *25*, 134–149.
[62] M. M. Ouberai, J. Wang, M. J. Swann, C. Galvagnion, T. Guilliams, C. M. Dobson, M. E. Welland, *J. Biol. Chem.* **2013**, *288*, 20883–20895.
[63] O. S. Gorbatyuk, S. Li, F. Nha Nguyen, F. P. Manfredsson, G. Kondrikova, L. F. Sullivan, C. Meyers, W. Chen, R. J. Mandel, N. Muzyczka, *Mol. Ther.* **2010**, *18*, 1758–1768.
[64] G. Fusco, A. De Simone, P. Arosio, M. Vendruscolo, G. Veglia, C. M. Dobson, *Sci. Rep.* **2016**, *6*, 1–9.
[65] T. Viennet, M. M. Wördehoff, B. Uluca, C. Poojari, H. Shaykhalishahi, D. Willbold, B. Strodel, H. Heise, A. K. Buell, W. Hoyer, M. Etzkorn, *Commun. Biol.* **2018**, *1*, DOI 10.1038/s42003-018-0049-z.
[66] J. N. Rao, Y. E. Kim, L. S. Park, T. S. Ulmer, *J. Mol. Biol.* **2009**, *390*, 516–529.
[67] E. R. Georgieva, T. F. Ramlall, P. P. Borbat, J. H. Freed, D. Eliezer, *J. Am. Chem. Soc.* **2008**, *130*, 12856–12857.
[68] M. Drescher, F. Godschalk, G. Veldhuis, B. D. van Rooijen, V. Subramaniam, M. Huber, *ChemBioChem* **2008**, *9*, 2411–2416.
[69] J. P. Anderson, D. E. Walker, J. M. Goldstein, R. De Laat, K. Banducci, R. J. Caccavello, R. Barbour, J. Huang, K. Kling, M. Lee, L. Diep, P. S. Keim, X. Shen, T. Chataway, M. G. Schlossmacher, P. Seubert, D. Schenk, S. Sinha, W. P. Gai, T. J. Chilcote, *J. Biol. Chem.* **2006**, *281*, 29739–29752.

[70] G. Muntané, I. Ferrer, M. Martinez-Vicente, *Neuroscience* **2012**, *200*, 106–119.
[71] C. W. Liu, B. I. Giasson, K. A. Lewis, V. M. Lee, G. N. DeMartino, P. J. Thomas, *J. Biol. Chem.* **2005**, *280*, 22670–22678.
[72] E. Gómez-Tortosa, K. Newell, M. C. Irizarry, J. L. Sanders, B. T. Hyman, *Acta Neuropathol.* **2000**, *99*, 352–357.
[73] R. Rott, R. Szargel, J. Haskin, V. Shani, A. Shainskaya, I. Manov, E. Liani, E. Avraham, S. Engelender, *J. Biol. Chem.* **2008**, *283*, 3316–3328.
[74] R. Hodara, E. H. Norris, B. I. Giasson, A. J. Mishizen-Eberz, D. R. Lynch, V. M.-Y. Lee, H. Ischiropoulos, *J. Biol. Chem.* **2004**, *279*, 47746–47753.
[75] H. Takahashi, K. Wakabayashi, *Neuropathology* **2001**, *21*, 315–322.
[76] D. Twohig, H. M. Nielsen, **2019**, 1–19.
[77] E. R. Dorsey, R. Constantinescu, J. P. Thompson, K. M. Biglan, R. G. Holloway, K. Kieburtz, F. J. Marshall, B. M. Ravina, G. Schifitto, A. Siderowf, C. M. Tanner, *Neurology* **2007**, *68*, 384 LP – 386.
[78] E. M. Rocha, B. De Miranda, L. H. Sanders, *Neurobiol. Dis.* **2018**, *109*, 249–257.
[79] C. W. Olanow, P. Brundin, *Mov. Disord.* **2013**, *28*, 31–40.
[80] L. V. Kalia, A. E. Lang, *Lancet* **2015**, *386*, 896–912.
[81] E. P. C. Ramirez, J. P. G. Vonsattel, *Semin. Neurol.* **2014**, *34*, 210–216.
[82] E. M. Garland, W. B. Hooper, D. Robertson, *Pure Autonomic Failure*, Elsevier B.V., **2013**.
[83] Y. Shibasaki, D. Baillie, D. Clair, A. Brookes, *Cytogenet. Genome Res.* **1995**, *71*, 54–55.
[84] M. H. Polymeropoulos, C. Lavedan, E. Leroy, S. E. Ide, A. Dehejia, A. Dutra, B. Pike, H. Root, J. Rubenstein, R. Boyer, E. S. Stenroos, S. Chandrasekharappa, A. Athanassiadou, T. Papapetropoulos, W. G. Johnson, A. M. Lazzarini, R. C. Duvoisin, G. Di Iorio, L. I. Golbe, R. L. Nussbaum, *Science (80-.).* **1997**, *276*, 2045–2047.
[85] J. J. Zarranz, J. Alegre, J. C. Go, E. Lezcano, R. Ros, I. Ampuero, J. Hoenicka, O. Rodriguez, T. Ser, D. G. Mun, *Ann. Neurol.* **2004**, *55*, 164–173.
[86] S. Lesage, M. Anheim, F. Letournel, L. Bousset, A. Honoré, N. Rozas, L. Pieri, K. Madiona, A. Dürr, R. Melki, C. Verny, A. Brice, *Ann. Neurol.* **2013**, *73*, 459–471.
[87] P. Pasanen, L. Myllykangas, M. Siitonen, A. Raunio, S. Kaakkola, J. Lyytinen, P. J. Tienari, M. Pöyhönen, A. Paetau, *Neurobiol. Aging* **2014**, *35*, 2180.e1-2180.e5.
[88] N. J. Rutherford, B. D. Moore, T. E. Golde, B. I. Giasson, *J. Neurochem.* **2014**, *131*, 859–867.
[89] S. Sahay, D. Ghosh, S. Dwivedi, A. Anoop, G. M. Mohite, M. Kombrabail, G. Krishnamoorthy, S. K. Maji, *J. Biol. Chem.* **2015**, *290*, 7804–7822.
[90] J. Li, V. N. Uversky, A. L. Fink, *Biochemistry* **2001**, *40*, 11604–11613.
[91] M. Perni, A. van der Goot, R. Limbocker, T. J. van Ham, F. A. Aprile, C. K. Xu, P. Flagmeier, K. Thijssen, P. Sormanni, G. Fusco, S. W. Chen, P. K. Challa, J. B. Kirkegaard, R. F. Laine, K. Y. Ma, M. B. D. Müller, T. Sinnige, J. R. Kumita, S. I. A. Cohen, R. Seinstra, G. S. Kaminski Schierle, C. F. Kaminski, D. Barbut, A. De Simone, T. P. J. Knowles, M. Zasloff, E. A. A. Nollen, M. Vendruscolo, C. M. Dobson, *Front. Cell Dev. Biol.* **2021**, *9*, DOI 10.3389/fcell.2021.552549.
[92] M. B. Fares, N. Ait-Bouziad, I. Dikiy, M. K. Mbefo, A. Jovičić, A. Kiely, J. L. Holton, S. J. Lee, A. D. Gitler, D. Eliezer, H. A. Lashuel, *Hum. Mol. Genet.* **2014**, *23*, 4491–4509.
[93] R. Ferese, N. Modugno, R. Campopiano, M. Santilli, S. Zampatti, E. Giardina, A. Nardone, D. Postorivo, F. Fornai, G. Novelli, E. Romoli, S. Ruggieri, S. Gambardella, *Parkinsons. Dis.*

2015, *2015*, DOI 10.1155/2015/546462.
[94] H. N. Du, L. Tang, X. Y. Luo, H. T. Li, J. Hu, J. W. Zhou, H. Y. Hu, *Biochemistry* 2003, *42*, 8870–8878.
[95] R. Melki, *Rev. Neurol. (Paris).* 2018, *174*, 644–652.
[96] Y. Li, C. Zhao, F. Luo, Z. Liu, X. Gui, Z. Luo, X. Zhang, D. Li, C. Liu, X. Li, *Cell Res.* 2018, *28*, 897–903.
[97] R. L. Nussbaum, C. E. Ellis, *N. Engl. J. Med.* 2003, *348*, 1356–64.
[98] S. B. Zimmerman, S. O. Trach, *J. Mol. Biol.* 1991, *222*, 599–620.
[99] M. Sarkar, C. Li, G. J. Pielak, *Biophys. Rev.* 2013, *5*, 187–194.
[100] D. K. Eggers, J. S. Valentine, *J. Mol. Biol.* 2001, *314*, 911–922.
[101] A. P. Minton, *J. Biol. Chem.* 2001, *276*, 10577–10580.
[102] K. S. Egorova, E. G. Gordeev, V. P. Ananikov, *Chem. Rev.* 2017, *117*, 7132–7189.
[103] K. S. Egorova, V. P. Ananikov, *J. Mol. Liq.* 2018, *272*, 271–300.
[104] A. A. M. Elgharbawy, M. Moniruzzaman, M. Goto, *Biochem. Eng. J.* 2020, *154*, DOI 10.1016/j.bej.2019.107426.
[105] P. Kumari, V. V. S. Pillai, A. Benedetto, *Biophys. Rev.* 2020, *12*, 1187–1215.
[106] N. Wood, G. Stephens, *Phys. Chem. Chem. Phys.* 2010, *12*, 1670.
[107] Y. Marcus, *Ionic Liquid Properties*, Springer International Publishing, Cham, 2016.
[108] M. Vert, Y. Doi, K.-H. Hellwich, M. Hess, P. Hodge, P. Kubisa, M. Rinaudo, F. Schué, *Pure Appl. Chem.* 2012, *84*, 377–410.
[109] P. G. Jessop, *Faraday Discuss.* 2018, *206*, 587–601.
[110] S. S. de Jesus, R. Maciel Filho, *Renew. Sustain. Energy Rev.* 2022, *157*, 112039.
[111] V. G. Maciel, D. J. Wales, M. Seferin, C. M. L. Ugaya, V. Sans, *J. Clean. Prod.* 2019, *217*, 844–858.
[112] A. Hospido, H. Rodríguez, in *Encycl. Ion. Liq.*, Springer Singapore, Singapore, 2019.
[113] F. van Rantwijk, *Angew. Chemie Int. Ed.* 2013, *52*, 3065–3066.
[114] D. R. MacFarlane, M. Kar, J. M. Pringle, *Fundamentals of Ionic Liquids*, Wiley-VCH Verlag GmbH & Co. KGaA, Weinheim, Germany, 2017.
[115] K. Fumino, P. Stange, V. Fossog, R. Hempelmann, R. Ludwig, *Angew. Chemie Int. Ed.* 2013, *52*, 12439–12442.
[116] P. A. Hunt, C. R. Ashworth, R. P. Matthews, *Chem. Soc. Rev.* 2015, *44*, 1257–1288.
[117] R. Hayes, G. G. Warr, R. Atkin, *Chem. Rev.* 2015, *115*, 6357–6426.
[118] R. Matsumoto, M. W. Thompson, P. T. Cummings, *J. Phys. Chem. B* 2019, DOI 10.1021/acs.jpcb.9b08509.
[119] A. Sirjoosingh, S. Alavi, T. K. Woo, *J. Phys. Chem. B* 2009, *113*, 8103–8113.
[120] R. Giernoth, *Angew. Chemie Int. Ed.* 2010, *49*, 2834–2839.
[121] X. Sun, H. Luo, S. Dai, *Chem. Rev.* 2012, *112*, 2100–2128.
[122] C. Maton, N. De Vos, C. V. Stevens, *Chem. Soc. Rev.* 2013, *42*, 5963–5977.
[123] D. M. Vriezema, M. C. Aragonès, J. A. A. W. Elemans, J. J. L. M. Cornelissen, A. E. Rowan, R. J. M. Nolte, *Chem. Rev.* 2005, *105*, 1445–1489.
[124] A. S. Kashin, K. I. Galkin, E. A. Khokhlova, V. P. Ananikov, *Angew. Chemie* 2016, *128*, 2201–2206.
[125] S. Magina, A. Barros-Timmons, S. P. M. Ventura, D. V. Evtuguin, *J. Hazard. Mater.* 2021, *412*, 125215.
[126] W. Silva, M. Zanatta, A. S. Ferreira, M. C. Corvo, E. J. Cabrita, *Int. J. Mol. Sci.* 2020, *21*, 1–

37.
[127] E. Rodríguez-Cárdenas, J. Cardoso-Martínez, A. Nieto-Camacho, B. A. Frontana-Uribe, *J. Mol. Liq.* **2017**, *236*, 435–444.
[128] C. Thomazeau, H. Olivier-Bourbigou, L. Magna, S. Luts, B. Gilbert, *J. Am. Chem. Soc.* **2003**, *125*, 5264–5265.
[129] C. Yue, D. Fang, L. Liu, T. F. Yi, *J. Mol. Liq.* **2011**, *163*, 99–121.
[130] J. J. Tindale, K. D. Hartlen, A. Alizadeh, M. S. Workentin, P. J. Ragogna, *Chem. – A Eur. J.* **2010**, *16*, 9068–9075.
[131] A. Beiraghi, M. Shokri, *Talanta* **2018**, *178*, 616–621.
[132] M. Matzke, S. Stolte, K. Thiele, T. Juffernholz, J. Arning, J. Ranke, U. Welz-Biermann, B. Jastorff, *Green Chem.* **2007**, *9*, 1198–1207.
[133] K. A. Kurnia, T. E. Sintra, C. M. S. S. Neves, K. Shimizu, J. N. Canongia Lopes, F. Gonçalves, S. P. M. Ventura, M. G. Freire, L. M. N. B. F. Santos, J. A. P. Coutinho, *Phys. Chem. Chem. Phys.* **2014**, *16*, 19952–19963.
[134] C. Zhang, S. V. Malhotra, A. J. Francis, *J. Hazard. Mater.* **2014**, *264*, 246–253.
[135] V. Z. Bergamo, R. K. Donato, D. F. Dalla Lana, K. J. Z. Donato, G. G. Ortega, H. S. Schrekker, A. M. Fuentefria, *Lett. Appl. Microbiol.* **2015**, *60*, 66–71.
[136] Q. Ye, T. Gao, F. Wan, B. Yu, X. Pei, F. Zhou, Q. Xue, *J. Mater. Chem.* **2012**, *22*, 13123–13131.
[137] R. Ferraz, L. C. Branco, C. Prudêncio, J. P. Noronha, Ž. Petrovski, *ChemMedChem* **2011**, *6*, 975–985.
[138] M. McLaughlin, M. J. Earle, M. A. Gîlea, B. F. Gilmore, S. P. Gorman, K. R. Seddon, *Green Chem.* **2011**, *13*, 2794–2800.
[139] K. S. Egorova, V. P. Ananikov, *ChemSusChem* **2014**, *7*, 336–360.
[140] N. Jain, A. Kumar, S. M. S. Chauhan, *Tetrahedron Lett.* **2005**, *46*, 2599–2602.
[141] A. D. dos Santos, A. R. C. Morais, C. Melo, R. Bogel-Łukasik, E. Bogel-Łukasik, *Fluid Phase Equilib.* **2013**, *356*, 18–29.
[142] I. Noshadi, B. W. Walker, R. Portillo-Lara, E. S. Sani, N. Gomes, M. R. Aziziyan, N. Annabi, *Sci. Rep.* **2017**, *7*, 1–18.
[143] V. P. Priyanka, R. L. Gardas, *Sep. Purif. Technol.* **2020**, *234*, 116048.
[144] A. Idris, R. Vijayaraghavan, U. A. Rana, D. Fredericks, A. F. Patti, D. R. MacFarlane, *Green Chem.* **2013**, *15*, 525–534.
[145] P. Moriel, E. J. García-Suárez, M. Martínez, A. B. García, M. A. Montes-Morán, V. Calvino-Casilda, M. A. Bañares, *Tetrahedron Lett.* **2010**, *51*, 4877–4881.
[146] Q. Zhang, M. Benoit, K. De Oliveira Vigier, F. JØrôme, Q. Zhang, M. Benoit, K. De Oliveira Vigier, J. Barrault, F. JØrôme, *Chem. – A Eur. J.* **2012**, *18*, 1043–1046.
[147] X. Cao, X. Ye, Y. Lu, Y. Yu, W. Mo, *Anal. Chim. Acta* **2009**, *640*, 47–51.
[148] T. Welton, *Biophys. Rev.* **2018**, *10*, 691–706.
[149] T. Welton, *Chem. Rev.* **1999**, *99*, 2071–2084.
[150] G. Kaur, H. Kumar, M. Singla, *J. Mol. Liq.* **2022**, *351*, DOI 10.1016/j.molliq.2022.118556.
[151] S. Rahali, R. Zarrougui, M. Marzouki, O. Ghodbane, *J. Electroanal. Chem.* **2020**, *871*, 114289.
[152] M. Opallo, A. Lesniewski, *J. Electroanal. Chem.* **2011**, *656*, 2–16.
[153] C. Li, B. Knierim, C. Manisseri, R. Arora, H. V Scheller, M. Auer, K. P. Vogel, B. A. Simmons, S. Singh, **2009**, DOI 10.1016/j.biortech.2009.10.066.

[154] D. K. Magnuson, J. W. Bodley, D. F. Evans, *J. Solution Chem.* **1984**, *13*, 583–587.
[155] R. M. Vrikkis, K. J. Fraser, K. Fujita, D. R. MacFarlane, G. D. Elliott, *J. Biomech. Eng.* **2009**, *131*, DOI 10.1115/1.3156810/400864.
[156] V. V. S. Pillai, A. Benedetto, *Biophys. Rev.* **2018**, *10*, 847–852.
[157] L. Gianfreda, M. R. Scarfi, *Mol. Cell. Biochem.* **1991**, *100*, 97–128.
[158] H. Weingärtner, C. Cabrele, C. Herrmann, *Phys. Chem. Chem. Phys.* **2012**, *14*, 415–426.
[159] T. A. Page, N. D. Kraut, P. M. Page, G. A. Baker, F. V. Bright, *J. Phys. Chem. B* **2009**, *113*, 12825–12830.
[160] R. Buchfink, A. Tischer, G. Patil, R. Rudolph, C. Lange, *J. Biotechnol.* **2010**, *150*, 64–72.
[161] N. Byrne, L. M. Wang, J. P. Belieres, C. A. Angell, *Chem. Commun.* **2007**, *0*, 2714–2716.
[162] X. Chen, T. Yang, S. Kataoka, P. S. Cremer, *J. Am. Chem. Soc.* **2007**, *129*, 12272–12279.
[163] S. K. Shukla, J. P. Mikkola, *Front. Chem.* **2020**, *8*, DOI 10.3389/fchem.2020.598662.
[164] H. Zhao, O. Olubajo, Z. Song, A. L. Sims, T. E. Person, R. A. Lawal, L. D. A. Holley, *Bioorg. Chem.* **2006**, *34*, 15–25.
[165] R. Patel, M. Kumari, A. B. Khan, *Appl. Biochem. Biotechnol.* **2014**, *172*, 3701–3720.
[166] Y. Zhang, S. Furyk, D. E. Bergbreiter, P. S. Cremer, *J. Am. Chem. Soc.* **2005**, *127*, 14505–14510.
[167] Y. Zhang, P. S. Cremer, *Curr. Opin. Chem. Biol.* **2006**, *10*, 658–663.
[168] T. Takekiyo, Y. Yoshimura, *Biophys. Rev.* **2018**, *10*, 853–860.
[169] H. R. Kalhor, M. Kamizi, J. Akbari, A. Heydari, *Biomacromolecules* **2009**, *10*, 2468–2475.
[170] H. Hwang, H. Choi, H. kyung Kim, D. H. Jo, T. D. Kim, *Anal. Biochem.* **2009**, *386*, 293–295.
[171] S. Y. Bae, S. Kim, H. Hwang, H. K. Kim, H. C. Yoon, J. H. Kim, S. Y. Lee, T. D. Kim, *Biochem. Biophys. Res. Commun.* **2010**, *400*, 531–536.
[172] O. Robert, J. Sabatier, D. Desoubzdanne, J. Lalande, S. Balayssac, V. Gilard, R. Martino, M. Malet-Martino, *Anal. Bioanal. Chem.* **2011**, *399*, 987–999.
[173] V. W. Jaeger, J. Pfaendtner, *J. Phys. Chem. B* **2016**, *120*, 12079–12087.
[174] P. I. Larsen, L. K. Sydnes, B. Landfald, A. R. Strøm, *Arch. Microbiol.* **1987**, *147*, 1–7.
[175] Y. Zhang, P. S. Cremer, *Annu. Rev. Phys. Chem.* **2010**, *61*, 63–83.
[176] P. Bharmoria, A. Kumar, *Biochim. Biophys. Acta - Gen. Subj.* **2016**, *1860*, 1017–1025.
[177] W. Neuhofer, F. X. Beck, *Physiology* **2006**, *21*, 171–180.
[178] T. Arakawa, S. N. Timasheff, *Biophys. J.* **1985**, *47*, 411–414.
[179] Z. Ignatova, L. M. Gierasch, *Methods Enzymol.* **2007**, *428*, 355–372.
[180] F.-X. Theillet, A. Binolfi, T. Frembgen-Kesner, K. Hingorani, M. Sarkar, C. Kyne, C. Li, P. B. Crowley, L. Gierasch, G. J. Pielak, A. H. Elcock, A. Gershenson, P. Selenko, **2014**, DOI 10.1021/cr400695p.
[181] D. R. MacFarlane, R. Vijayaraghavan, H. N. Ha, A. Izgorodin, K. D. Weaver, G. D. Elliott, *Chem. Commun.* **2010**, *46*, 7703–7705.
[182] D. S. Wishart, Y. D. Feunang, A. Marcu, A. C. Guo, K. Liang, R. Vázquez-Fresno, T. Sajed, D. Johnson, C. Li, N. Karu, Z. Sayeeda, E. Lo, N. Assempour, M. Berjanskii, S. Singhal, D. Arndt, Y. Liang, H. Badran, J. Grant, A. Serra-Cayuela, Y. Liu, R. Mandal, V. Neveu, A. Pon, C. Knox, M. Wilson, C. Manach, A. Scalbert, *Nucleic Acids Res.* **2018**, *46*, D608–D617.
[183] P. B. Barker, B. J. Soher, S. J. Blackband, J. C. Chatham, V. P. Mathews, R. Nick Bryan, *Quantitation of Proton NMR Spectra of the Human Brain Using Tissue Water as an Internal Concentration Reference*, **1993**.
[184] E. Lamy, L. Pilyser, C. Paquet, E. Bouaziz-Amar, S. Grassin-Delyle, *Talanta* **2021**, *224*,

121881.
[185] S. H. Zeisel, K. Da Costa, P. D. Franklin, E. A. Alexander, J. T. Lamont, N. F. Sheard, A. Beiser, *FASEB J.* **1991**, *5*, 2093–2098.
[186] S. H. Zeisel, J. K. Blusztajn, *Annu. Rev. Nutr.* **1994**, *14*, 269–296.
[187] J. K. Blusztajn, *Science (80-.).* **1998**, *281*, 794–795.
[188] A. Kumar, K. Bhakuni, P. Venkatesu, *Phys. Chem. Chem. Phys.* **2019**, *21*, 23269–23282.
[189] A. Scimemi, M. Beato, *Mol. Neurobiol. 2009 403* **2009**, *40*, 289–306.
[190] M. Erecińska, I. A. Silver, *Prog. Neurobiol.* **1990**, *35*, 245–296.
[191] L. Gontrani, *Biophys. Rev.* **2018**, *10*, 873–880.
[192] S. Miao, R. Atkin, G. Warr, *Green Chem.* **2022**, DOI 10.1039/d2gc02282f.
[193] K. E. Paleologou, A. W. Schmid, C. C. Rospigliosi, H. Y. Kim, G. R. Lamberto, R. A. Fredenburg, P. T. Lansbury, C. O. Fernandez, D. Eliezer, M. Zweckstetter, H. A. Lashuel, *J. Biol. Chem.* **2008**, *283*, 16895–16905.
[194] M. Johnson, A. T. Coulton, M. A. Geeves, D. P. Mulvihill, *PLoS One* **2010**, *5*, 1–5.
[195] E. Gasteiger, M. R. Wilkins, A. Bairoch, J. C. Sanchez, K. L. Williams, R. D. Appel, D. F. Hochstrasser, *Methods Mol. Biol.* **1999**, *112*, 531–552.
[196] W. Hoyer, T. Antony, D. Cherny, G. Heim, T. M. Jovin, V. Subramaniam, *J. Mol. Biol.* **2002**, *322*, 383–393.
[197] M. M. Wördehoff, H. Shaykhalishahi, L. Groß, L. Gremer, M. Stoldt, A. K. Buell, D. Willbold, W. Hoyer, *J. Mol. Biol.* **2017**, *429*, 3018–3030.
[198] P. Wingfield, *Curr. Protoc. Protein Sci.* **1998**, A.3F.1-A.3F.8.
[199] A. D. Stephens, N. Nespovitaya, M. Zacharopoulou, C. F. Kaminski, J. J. Phillips, G. S. Kaminski Schierle, *Anal. Chem.* **2018**, *90*, 6975–6983.
[200] H. Schägger, *Nat. Protoc.* **2006**, *1*, 16–22.
[201] E. Alcalde, I. Dinarès, A. Ibáñez, N. Mesquida, *Chem. Commun.* **2011**, *47*, 3266–3268.
[202] E. Alcalde, I. Dinarès, A. Ibáñez, N. Mesquida, *Molecules* **2012**, *17*, 4007–4027.
[203] S. De Santis, G. Masci, F. Casciotta, R. Caminiti, E. Scarpellini, M. Campetella, L. Gontrani, *Phys. Chem. Chem. Phys.* **2015**, *17*, 20687–20698.
[204] M. Wördehoff, W. Hoyer, *Bio-Protocol* **2018**, *8*, 1–11.
[205] Y. D. Álvarez, J. A. Fauerbach, J. V. Pellegrotti, T. M. Jovin, E. A. Jares-Erijman, F. D. Stefani, *Nano Lett.* **2013**, *13*, 6156–6163.
[206] D. S. Wishart, C. G. Bigam, J. Yao, F. Abildgaard, H. J. Dyson, E. Oldfield, J. L. Markley, B. D. Sykes, *J. Biomol. NMR* **1995**, *6*, 135–140.
[207] R. L. J. Keller, **2004**.
[208] L. Kang, M. K. Janowska, G. M. Moriarty, J. Baum, *PLoS One* **2013**, *8*, 1–10.
[209] L. Mariño, R. Ramis, R. Casasnovas, J. Ortega-Castro, B. Vilanova, J. Frau, M. Adrover, *Unravelling the Effect of N(ε)-(Carboxyethyl)Lysine on the Conformation, Dynamics and Aggregation Propensity of α-Synuclein*, **2020**.
[210] M. P. Williamson, *Prog. Nucl. Magn. Reson. Spectrosc.* **2013**, *73*, 1–16.
[211] F. H. Schumann, H. Riepl, T. Maurer, W. Gronwald, K. P. Neidig, H. R. Kalbitzer, *J. Biomol. NMR* **2007**, *39*, 275–289.
[212] J. G. Pelton, D. A. Torchia, N. D. Meadow, S. Roseman, *Protein Sci.* **1993**, *2*, 543–558.
[213] H. Zhang, S. Neal, D. S. Wishart, *J. Biomol. NMR* **2003**, *25*, 173–195.
[214] H. LeVine, *Methods Enzymol.* **1999**, *309*, 274–284.
[215] V. I. Stsiapura, A. A. Maskevich, V. A. Kuzmitsky, K. K. Turoverov, I. M. Kuznetsova, *J. Phys.*

Chem. A **2007**, *111*, 4829–4835.
[216] L. S. Wolfe, M. F. Calabrese, A. Nath, D. V. Blaho, A. D. Miranker, Y. Xiong, *Proc. Natl. Acad. Sci. U. S. A.* **2010**, *107*, 16863–16868.
[217] H. Kaufmann, K. Nahm, D. Purohit, D. Wolfe, *Neurology* **2004**, *63*, 1093–1095.
[218] V. N. Uversky, J. Li, P. Souillac, I. S. Millett, S. Doniach, R. Jakes, M. Goedert, A. L. Fink, *J. Biol. Chem.* **2002**, *277*, 11970–11978.
[219] Z. Sárkány, F. Rocha, A. M. Damas, S. Macedo-Ribeiro, P. M. Martins, *Chem. - An Asian J.* **2019**, *14*, 500–508.
[220] L. Giehm, D. E. Otzen, *Anal. Biochem.* **2010**, *400*, 270–281.
[221] A. L. Carvalho, T. Santos-Silva, M. J. Romao, E. J. Cabrita, F. Marcelo, *Structural Elucidation of Macromolecules*, **2018**.
[222] R. Porcari, C. Proukakis, C. A. Waudby, B. Bolognesi, P. P. Mangione, J. F. S. Paton, S. Mullin, L. D. Cabrita, A. Penco, A. Relini, G. Verona, M. Vendruscolo, M. Stoppini, G. G. Tartaglia, C. Camilloni, J. Christodoulou, A. H. V. Schapira, V. Bellott, *J. Biol. Chem.* **2015**, *290*, 2395–2404.
[223] A. Iyer, A. Sidhu, V. Subramaniam, *Front. Neurosci.* **2022**, *16*, DOI 10.3389/FNINS.2022.1003997.
[224] M. C. Tettamanzi, C. Keeler, S. Meshack, M. E. Hodsdon, **n.d.**, DOI 10.1021/bi800444t.
[225] K. Tamiola, F. A. A. Mulder, *Biochem. Soc. Trans.* **2012**, *40*, 1014–1020.
[226] C. Xue, T. Y. Lin, D. Chang, Z. Guo, *R. Soc. Open Sci.* **2017**, *4*, DOI 10.1098/rsos.160696.
[227] K. Yamaguchi, M. So, C. Aguirre, K. Ikenaka, H. Mochizuki, Y. Kawata, Y. Goto, *J. Biol. Chem.* **2021**, *296*, 100510.
[228] C. W. Bertoncini, Y. S. Jung, C. O. Fernandez, W. Hoyer, C. Griesinger, T. M. Jovin, M. Zweckstetter, *Proc. Natl. Acad. Sci. U. S. A.* **2005**, *102*, 1430–1435.
[229] Y. C. Chi, G. S. Armstrong, D. N. M. Jones, E. Z. Eisenmesser, C. W. Liu, *J. Biol. Chem.* **2014**, *289*, 15474–15481.
[230] L. Kang, G. M. Moriarty, L. A. Woods, A. E. Ashcroft, S. E. Radford, J. Baum, *Protein Sci.* **2012**, *21*, 911–917.
[231] R. Ramis, J. Ortega-Castro, B. Vilanova, M. Adrover, J. Frau, *Biomacromolecules* **2020**, *21*, 5200–5212.
[232] K. Furukawa, C. Aguirre, M. So, K. Sasahara, Y. Miyanoiri, K. Sakurai, K. Yamaguchi, K. Ikenaka, H. Mochizuki, J. Kardos, Y. Kawata, Y. Goto, *Curr. Res. Struct. Biol.* **2020**, *2*, 35–44.

A

APPENDIX

A. Appendix

List of Figures

LIST OF TABLES

6.A. SDS-PAGE

Table SM1 – Composition for Tris-Tricine-SDS-Page
Discontinuous gel consisting of a separating gel (R, 12%) and stacking gel (St, 4%). Quantities for 1, 2 and 4 units are described.

Reagents		x1		x2		x4		
		R	St	R	St	R	St	
1	Water	2.1	1.95	4.2	3.9	8.4	7.8	mL
2	Gel Buffer	2.5	0.775	5	1.55	10	3.1	
3	30% Acrylamide	3	0.4	6	0.8	12	1.6	
4	100% Glycerol	0.75	-	1.5	-	3	-	
5	10% APS	21	21	42	42	84	84	µL
6	TEMED	7	7	14	14	28	28	

Notes: 1) BD water **2)** Gel Buffer- 3 M Tris/HCl, 0.3% SDS pH 8,45. It is important to in first place adjust Tris-Base with HCl, only then add SDS. Tris-Base (≥99,9% NZYTech); HCl 37% (Carlo Erba); SDS- Sodium dodecyl sulphate (≥99% Panreac) **3)** Use gloves as Acrylamide is neurotoxic. Solution tends to crystallize, to avoid this problem keep stock solution stored at 7 to 10 ºC. Acrylamide (99,9% Fluka) **4)** Glycerol (99,5% Scharlau) **5)** Stock solutions should be freshly prepared. Should be the last component to be added (responsible for gel polymerization). APS- Ammonium persulphate (≥98% NZYTech) **6)** Should be the last component to be added as it is responsible for gel polymerization. TEMED- Tetramethyl-ethylenediamine (99% Riedel-de-Haën).

Table SM2 – Electrode buffer composition in Tris-Tricine–SDS-PAGE. Cathode (C) and anode (A) buffers composition for 500 mL, 1 and 2 L batches

Reagents		$C^{\#6}$	$A^{\#5}$	$C^{\#6}$	$A^{\#5}$	$C^{\#6}$	$A^{\#5}$	
1	Tris-Base	60.55	121	121.1	242	242.2	484	g
2	Triscine	89.6	-	179.2	-	358.4	-	
3	20% SDS	25	-	50	-	100	-	mL
4	Water	Add to:		Add to:		Add to:		
		500	500	1000	1000	2000	2000	

Notes: 1) Tris-Base (≥ 99,8% NZYTech) **2)** Triscine (≥98% Amresco) **3)** SDS- Sodium duodecil sulphate (99% Panreac) **4)** BD water **5)** 10X concentration, dilute before using **6)** Cathode buffer pH should be ~8.25.

Table SM3 – Sample buffer (SB) composition (25 and 50 mL batches)

	Reagents	SB	SB	
1	1 M Tris/HCl pH 7	5	10	mL
2	100% Glycerol	12	24	
3	SDS	4	8	g
4	DTT	1,55	3,1	
5	Coomassie Blue R-250	10	20	mg
6	Water	Add up to: 25	Add up to: 50	mL

Notes: 1) Buffer composition available in Table SM11 **2)** Glycerol (99,5% Scharlau) **3)** SDS-Sodium duodecil sulphate (99% Panreac) **4)** DTT- 1,4-Dithiothreitol (≥ 99% NZYTech) **5)** Coomassie Brilliant Blue R-250 (Panreac) **6)** BD water.

Table SM4 – Composition for staining and destaining solutions. Compositions for 500 mL, 1 and 2 L batches

	Reagents	S	D	S	D	S	D	
1	Coomassie Blue R250	0.5	-	1	-	2	-	g
2	Methanol	250	200	500	400	1000	800	
3	Glacial Acetic acid	50	50	100	100	200	200	mL
4	Water	Add to:		Add to:		Add to:		
		500	500	1000	1000	2000	2000	

Notes: 1) Coomassie Brilliant Blue R250 (Panreac) **2)** Methanol (Sigma-Aldrich) **3)** Glacial Acetic acid (Panreac) **4)** BD water.

6.B. Expression and Purification of αS

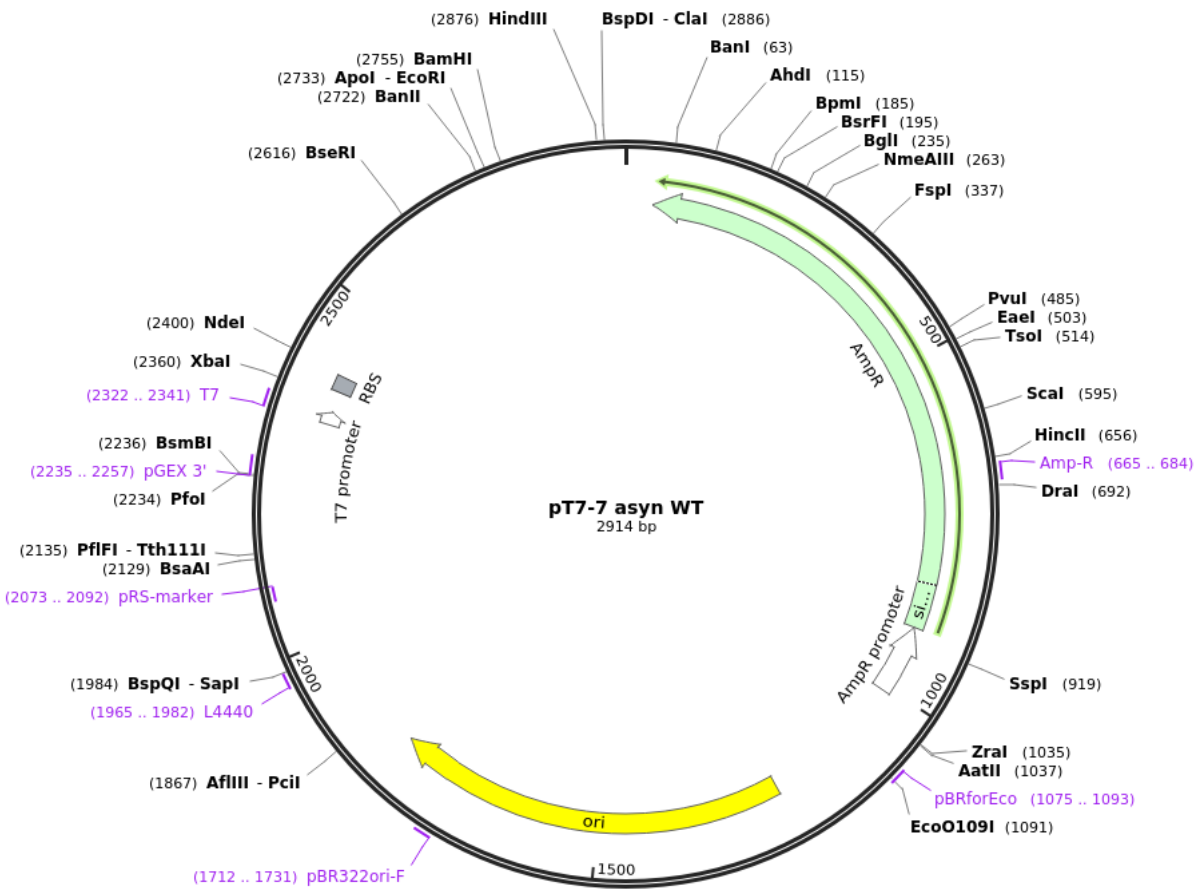

Figure SM1 – pT7-7 Plasmid map

pT7-7 plasmid encodes for human wild type alpha synuclein (wt-αS) and includes several important features: (i) a selection mark (AmpR gene) that encodes for β-lactamase, confers resistance ampicillin, carbenicillin and related antibiotics, (ii) the respective promoter (AmpR promoter); (iii) an origin of replication (ori), making this a high copy number plasmid; (iv) a T7 promoter for T7 bacteriophage RNA polymerase, and respective (v) binding site (RBS); (vi) multiple cloning sites.

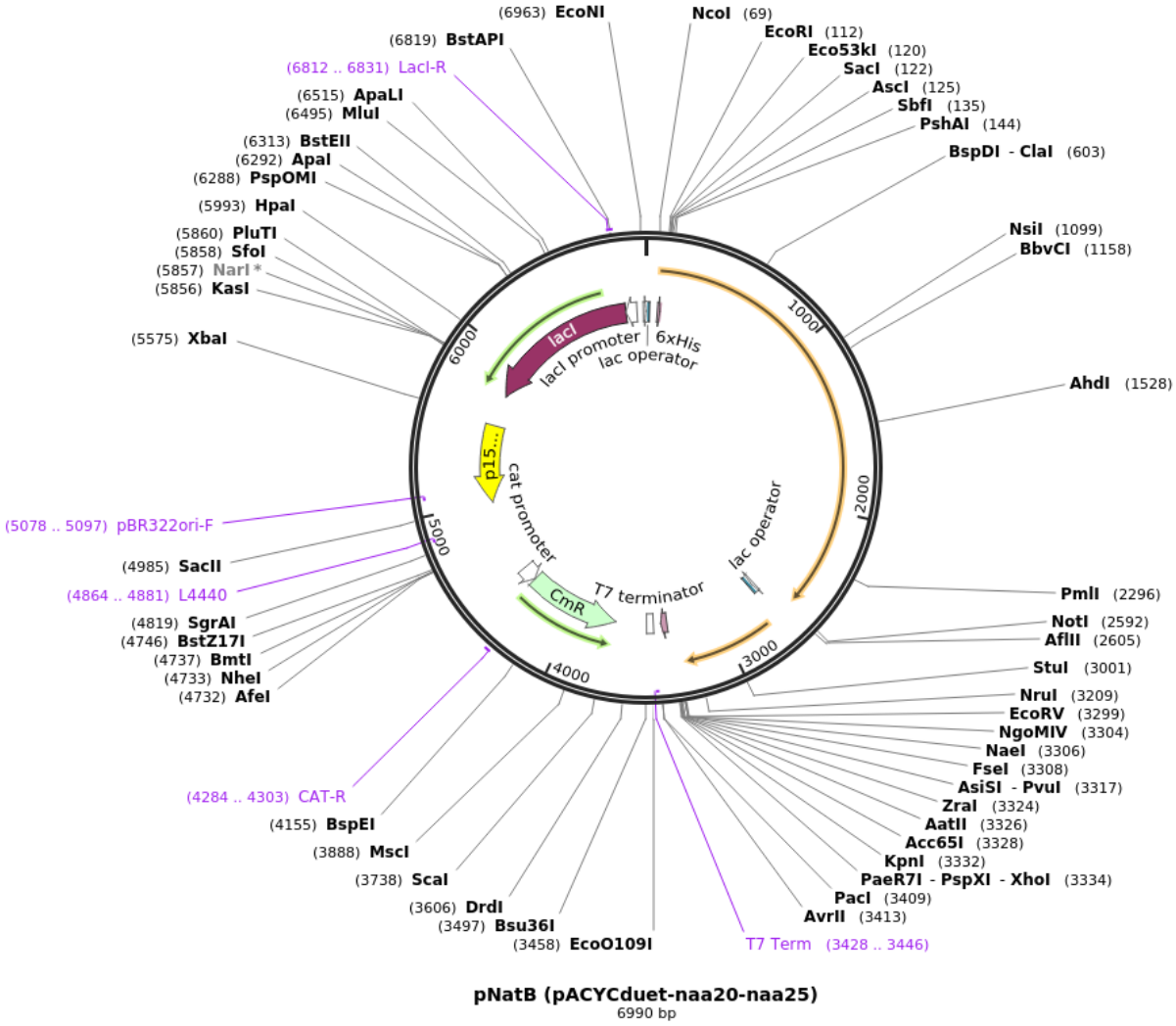

Figure SM2 – pACYCduet-naa20-naa25 plasmid map

pACYCduet-naa20-naa25 plasmid encodes for N-terminal acetyl transferase (NAT) subunits naa 20 (auxiliary subunit) and naa 25 (catalytic subunit), the plasmid includes several important features: (i) a selection mark (CmR gene) that encodes for chloramphenicol-methyl-transferase, confers resistance to chloramphenicol; (ii) the respective promoter (CAT promoter); (iii) a origin of replication (p15A ori), making this also a high copy number plasmid; (iv) a T7 promoter for RNA polymerase of T7 bacteriophage, (v) and finally multiple cloning sites.

Table SM5 – E. coli Genotypes (for strains B21-DE3 and DH5α)

E. Coli strain		Genotype
1	DH5α	F- φ80lacZΔM15 Δ(lacZYA-argF)U169 recA1 endA1 hsdR17(rk -, mk +) phoA supE44 thi-1 gyrA96 relA1 λ-
2	BL21(DE3)	F- ompT hsdSB (rB-mB-) gal dcm (DE3)

Notes: Raleigh, E. A., Elbing, K., & Brent, R. (2002). Selected topics from classical bacterial genetics. Current protocols in molecular biology, 59(1), 1-4.

Table SM6 – Molecular weight and molar extinction coefficients for non-labeled αS and double labeled (15N13C) αS

	Protein Variant	MW (Da)	ε ($M^{-1}cm^{-1}$)
1	αS	14460	5960
2	Ac-αS	14502	5960
3	αS ($^{15}N^{13}C$)	15245	5960
4	Ac-αS ($^{15}N^{13}C$)	15289	5960

Notes: 1) Molecular weight of αS labeled variants was estimated with: http://sopnmr.ucsd.edu/biomol-tools.htm. **2)** Molar extinction coefficient was estimated with Expasy Protparam: Gasteiger, E., Hoogland, C., Gattiker, A., Wilkins, M. R., Appel, R. D., & Bairoch, A. (2005). Protein identification and analysis tools on the ExPASy server. In The proteomics protocols handbook (pp. 571-607). Humana press.

Table SM7 – Expression yields for αS Variants

	Protein Variants	Yield	
1	αS	29.04	**mg/L**
2	Ac-αS	16.35	
3	αS ($^{15}N^{13}C$)	12.79	
4	Ac-αS ($^{15}N^{13}C$)	11.62	

6.C. Culture Media

Table SM8 – LB culture medium composition (250 mL, 1 and 2 L batches)

	Reagentes	LB	LB	LB	
1	NaCl	2,5	10	20	**g**
2	Triptone	2,5	10	20	
3	Yeast extract	1,25	5	10	
4	water	Add to: 250	Add to: 1	Add to: 2	**L**

Notes: 1) NaCl (≥ 99% Panreac). **2)** Triptone (NZYTech). **3)** Yeast extract (Cultimed). **4)** BD water.

Table SM9 – LA culture medium composition (batches of 100, 250, and 500 mL)

	Reagentes	LA[#3]	LA[#3]	LA[#3]	
1	LB medium	100	250	500	**mL**
2	Bacteriological agar	1,5	3,75	7,5	**g**

Notes: 1) LB composition available in Table SM7. **2)** Bacteriological agar (NZYTech). **3)** Autoclave before using. BD water. When making selective plates, cool to ~40ºC to avoid antibiotic degradation. Dispense ~20 ml per plate.

Table SM10 – Composition for M9 salts (batches of 500 mL, 1 and 2 L)

	Reagentes	S-10X[#4]	S-10X[#4]	S-10X[#4]	
1	Na2HPO4	30	60	120	**g**
2	KH2PO4	15	30	60	
3	NaCl	2,5	5	10	
4	water	Add to: 500	Add to: 1000	Add to: 2000	**mL**

Notes: 1) Na2HPO4 (≥ 99%Sigma-Aldrich). **2)** KH2PO4 (≥ 99% Panreac). **3)** NaCl (≥ 99% Panreac) **4)** Autoclave before using, BD water.

Table SM11 – M9 minimal medium composition (batches of 100, 250, and 500 mL)

	Reagentes	M9	M9	M9	
1	M9 salts (10X)	25	50	100	mL
2	2 M $MgSO_4$	0,25	0,5	1	
3	100 mM $CaCl_2$	0,25	0,5	1	
4	100 mM $FeSO_4$	0,25	0,5	1	
5	Thiamine-HCl	2,5	5	10	mg
6	$^{13}C_6H_{12}O_6$	0,75	1,5	3	g
7	$^{15}NH_4Cl$	0,38	0,76	1,52	
8	MEM vitamins (100X)	2,5	10	20	mL
9	water	Add to: 250	Add to: 500	Add to: 1000	

Notes: 1) Composition available in Table SM11. **2)** Filter before using, MgSO4 (≥ 96% Panreac). **3)** Filter before using, CaCl2 (≥ 99% Panreac). **4)** FeSO4 (≥ 99% Panreac). **5)** Thiamine-HCl (≥ 99,1% Fagron). **6)** 13C6H12O6 (≥ 99% Cambridge Isotope Laboratories). **7)** 15NH4Cl (≥ 99% Cambridge Isotope Laboratories). **8)** MEM vitamin solution (Sigma-Aldrich). **9)** Autoclaved BD water. **10)** Adjust glucose and ammonium chloride depending on the protein being expressed, non-labeled protein requires 2 g of glucose and 2,5 g of ammonium sulphate instead of the indicted 0,75 g and 0,38 g for the labeled variants (for 250 mL culture medium).

6.D. Buffer and Solution composition

Table SM12 – 1 M Tris/HCl Buffer composition for pH=7 (TH7) and pH=8 (TH8); batches of 500 mL, 1 and 2 L

	Reagentes	TH#4 (pH 8,0)		TH#4 (pH 8,0)		TH#4 (pH 8,0)	
1	Tris-Base	60.57	g	121.14	g	242.28	g
2	37% HCl	Add until pH 8	NA	Add until pH 8	NA	Add until pH 8	NA
3	Water	Add up to: 500	mL	Add up to: 1000	mL	Add up to: 2000	mL

	Reagentes	TH#4 (pH 7,0)		TH#4 (pH 7,0)		TH#4 (pH 7,0)	
1	Tris-Base	60.57	g	121.14	g	242.28	g
2	37% HCl	Add until pH 7	NA	Add until pH 7	NA	Add until pH 7	NA
3	Water	Add up to: 500	mL	Add up to: 1000	mL	Add up to: 2000	mL

Notes: 1) Tris-Base (> 99,9% NZYTech). **2)** HCl 37% (Carlo Erba). **3)** BD water. **4)** Dissolve Tris-base in ~70% of the available water, add HCl until pH 8 is reached, and add up to the total volume.

Tabela 13 – Phosphate Buffer composition (PB; 0.5 M, batches of 500 mL, 1 and 2 L)

	Reagentes	PB (pH 7,0)		PB (pH 7)		PB (pH 7)	
1	Na2HPO4	23.62	g	47.24	g	94.48	g
2	NaH2PO4	10.03		20.06		40.12	
3	Water	Add up to: 500	mL	Add up to: 1000	mL	Add up to: 2000	mL

Notes: 1) Na2HPO4 (≥ 99% Sigma-Aldrich). **2)** NaH2PO4 (≥ 99% Panreac). **3)** BD water.

Table SM14 – Lysis Buffer composition (LyL; 30 mL batch) and respective stock solution

	Reagentes	Stock	
1	EDTA (250 mM)	5	g
2	Water	Add to: 50 mL	mL

	Reagentes	LyB	
1	Protease inhibitor (Pill)	1	Pill
2	EDTA (1mM)	0,119	mL
3	Tris-HCl Buffer (10 mM, pH 8)	0,3	
4	Water	Add to: 30 mL	

Notes: 1) EDTA - Ethylenediamine tetra acetic acid (≥ 99% Sigma-Aldrich). **2)** BD water. **3)** Protease inhibitor cocktail (cOmplete Mini EDTA-free Protease Inhibitor Cocktail, Roche). **4)** EDTA stock solution. **5)** Buffer composition available in Table SM11, dilute accordingly (100X dilution). **6)** BD water.

Table SM15 – Saturated ammonium sulphate solution (AS; batches of 100, 250, and 500 mL)

	Reagentes	AS	AS	AS	
1	Ammonium sulfate (3,9 M)	68,17	136,34	272,68	g
4	Water	Add to: 100 mL	Add to: 250 mL	Add to: 500 mL	mL

Notes: 1) Saturated at 0ºC; Ammonium sulphate (≥ 99% M&B) **2)** BD water **3)** Solution can be stored at room temperature but must be refrigerated to 0ºC before usage.

Table SM16 – IEC Buffer composition (Batches of 500 mL, 1 and 2 L)

	Reagentes	IEC	IEC	IEC	
1	Tris/HCl Buffer (10 mM, pH 8)	5	10	20	mL
4	Water	Add to: 500 mL	Add to: 1 L	Add to: 2 L	

Notes: 1) Buffer composition available in table D1, dilute accordingly (100X dilution). **2)** BD water.

Table SM17 – A Buffer composition (AB, Batches of 500 mL, 1 and 5 L)

	Reagentes	AB	AB	AB	
1	Tris/HCl Buffer (20 mM, pH 8)	10	20	40	**mL**
4	Water	Add to: 500 mL	Add to: 1 L	Add to: 5 L	

Notes: 1) Buffer composition available in table D1, dilute accordingly (50X dilution) (≥ 99% M&B). **2)** BD water.

Table SM18 – B Buffer composition (BB; Batches of 500 mL, 1 and 2 L)

	Reagentes	BB	BB	BB	
1	Tris/HCl Buffer (20 mM, pH 8)	10	20	40	**mL**
2	NaCl (1 M)	29,22	58,44	116,88	**g**
4	Water	Add up to: 500 mL	Add up to: 1 L	Add up to: 2 L	**mL**

Notes: 1) Buffer composition available in table D1, dilute accordingly (50X dilution) **2)** NaCl (≥ 99,5% Panreac) **3)** BD water.

Table SM19 – Analysis Buffer composition (An; batches of 100, 250 mL, and 5 L)

	Reagentes	An	An	An	
1	Phosphate Buffer (20 mM, pH 7)	20	40	80	**mL**
2	Water	Add to: 100 mL	Add to: 250 mL	Add to: 5 L	

Notes: 1) Buffer composition available in table D1, dilute accordingly (25X dilution). **2)** BD water.

Table SM 20 – Organization of the 96 well microplate used in ThT fluorescence assay for αS and Ac-αS in the presence of NaCl
A black, medium-binding, full bottom 96 well microplate was used for the assay non-binding, preheated to 37°C. The procedure lasted for 140 h.

	1	2	3	4	5	6	7	8	9	10	11	12
A	50 μM α-S N/A 10 μM ThT	50 μM α-S N/A 10 μM ThT	50 μM α-S N/A 10 μM ThT	N/A 0.005% NaN3 10 μM ThT	N/A 0.01% NaN3 10 μM ThT	N/A 0.02% NaN3 10 μM ThT	N/A 0.04% NaN3 10 μM ThT	N/A 0.06% NaN3 10 μM ThT	N/A 0.08% NaN3 10 μM ThT	N/A 0.1% NaN3 10 μM ThT	N/A 0.15% NaN3 10 μM ThT	N/A 0.2% NaN3 10 μM ThT
B	ThT & Buffer	N/A 10 mM NaCl 10 μM ThT	N/A 25 mM NaCl 10 μM ThT	N/A 50 mM NaCl 10 μM ThT	N/A 100 mM NaCl 10 μM ThT	N/A 200 mM NaCl 10 μM ThT	N/A 300 mM NaCl 10 μM ThT	N/A 500 mM NaCl 10 μM ThT	N/A 600 mM NaCl 10 μM ThT	N/A 800 mM NaCl 10 μM ThT	N/A 1000 mM NaCl 10 μM ThT	Buffer
C	ThT & Water	N/A 10 mM LI 10 μM ThT	N/A 25 mM LI 10 μM ThT	N/A 50 mM LI 10 μM ThT	N/A 100 mM LI 10 μM ThT	N/A 200 m LI 10 μM ThT	N/A 300 mM LI 10 μM ThT	N/A 500 mM LI 10 μM ThT	N/A 600 mM LI 10 μM ThT	N/A 800 mM LI 10 μM ThT	N/A 1000 mM LI 10 μM ThT	Water
D	50 μM α-S 10 mM LI 10 μM ThT	50 μM α-S 10 mM LI 10 μM ThT	50 μM α-S 10 mM LI 10 μM ThT	50 μM α-S 25 mM LI 10 μM ThT	50 μM α-S 25 mM LI 10 μM ThT	50 μM α-S 25 mM LI 10 μM ThT	50 μM α-S 50 mM LI 10 μM ThT	50 μM α-S 50 mM LI 10 μM ThT	50 μM α-S 50 mM LI 10 μM ThT	50 μM α-S 100 mM LI 10 μM ThT	50 μM α-S 100 mM LI 10 μM ThT	50 μM α-S 100 mM LI 10 μM ThT
E	50 μM α-S 200 mM LI 10 μM ThT	50 μM α-S 200 mM LI 10 μM ThT	50 μM α-S 200 mM LI 10 μM ThT	50 μM α-S 300 mM LI 10 μM ThT	50 μM α-S 300 mM LI 10 μM ThT	50 μM α-S 300 mM LI 10 μM ThT	50 μM α-S 500 mM LI 10 μM ThT	50 μM α-S 500 mM LI 10 μM ThT	50 μM α-S 500 mM LI 10 μM ThT	50 μM α-S 600 mM LI 10 μM ThT	50 μM α-S 600 mM LI 10 μM ThT	50 μM α-S 600 mM LI 10 μM ThT
F	50 μM α-S 800 mM LI 10 μM ThT	50 μM α-S 800 mM LI 10 μM ThT	50 μM α-S 800 mM LI 10 μM ThT	50 μM α-S 1000 mM LI 10 μM ThT	50 μM α-S 1000 mM LI 10 μM ThT	50 μM α-S 1000 mM LI 10 μM ThT	50 μM α-S 1000 mM NaCl 10 μM ThT	50 μM α-S 1000 mM NaCl 10 μM ThT	50 μM α-S 1000 mM NaCl 10 μM ThT	50 μM α-S 800 mM NaCl 10 μM ThT	50 μM α-S 800 mM NaCl 10 μM ThT	50 μM α-S 800 mM NaCl 10 μM ThT
G	50 μM α-S 600 mM NaCl 10 μM ThT	50 μM α-S 600 mM NaCl 10 μM ThT	50 μM α-S 600 mM NaCl 10 μM ThT	50 μM α-S 500 mM NaCl 10 μM ThT	50 μM α-S 500 mM NaCl 10 μM ThT	50 μM α-S 500 mM NaCl 10 μM ThT	50 μM α-S 300 mM NaCl 10 μM ThT	50 μM α-S 300 mM NaCl 10 μM ThT	50 μM α-S 300 mM NaCl 10 μM ThT	50 μM α-S 200 mM NaCl 10 μM ThT	50 μM α-S 200 mM NaCl 10 μM ThT	50 μM α-S 200 mM NaCl 10 μM ThT
H	50 μM α-S 100 mM NaCl 10 μM ThT	50 μM α-S 100 mM NaCl 10 μM ThT	50 μM α-S 100 mM NaCl 10 μM ThT	50 μM α-S 50 mM NaCl 10 μM ThT	50 μM α-S 50 mM NaCl 10 μM ThT	50 μM α-S 50 mM NaCl 10 μM ThT	50 μM α-S 25 mM NaCl 10 μM ThT	50 μM α-S 25 mM NaCl 10 μM ThT	50 μM α-S 25 mM NaCl 10 μM ThT	50 μM α-S 10 mM NaCl 10 μM ThT	50 μM α-S 10 mM NaCl 10 μM ThT	50 μM α-S 10 mM NaCl 10 μM ThT

6.E. Additional Data

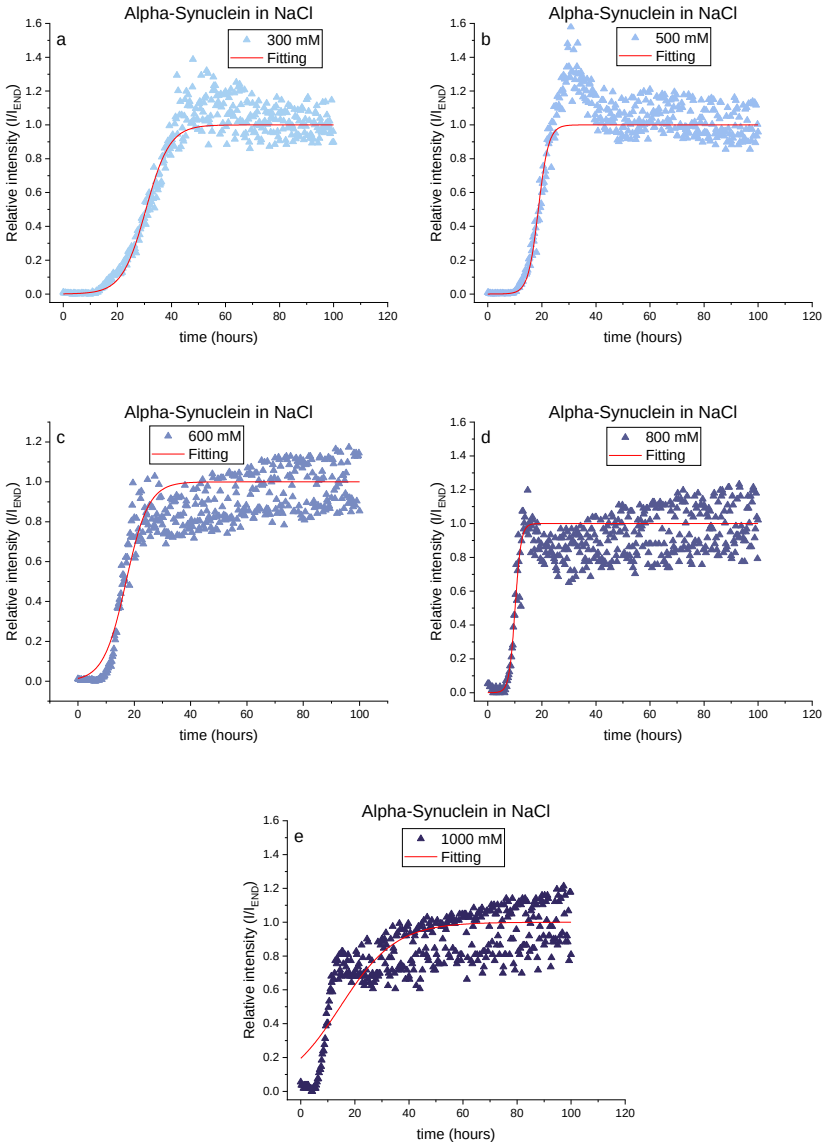

Figure SM3 – Fitting of the fibrillation curves of αS (NaCl)

Experimental curves were fitted (using Origin 2021) to the simplified F-W model for the estimation of independent kinetic parameters (TN and v). The error bars associated with each concentration curve were determined according to the fitting error. The fitting was made to concentration points where extensive fibrillation was reached (i.e., a plateau is present) and correspond to the concentrations of 300, 500, 600, 800, and 1000 mM. The selection of the aggregation curves amongst triplicates was made according to the morphology and variation of the stationary phase. The selected aggregation curves found in this figure are also present in figure 16A. The kinetic values estimated from the fitting are presented in table SM 21. Experiments were monitored over 100 hours at 37 ºC, fibril formation is monitored by the fluorescence of Tht. Samples (200 µM of protein) were prepared in 77 mM of phosphate buffer (pH 7.2), 200 µM of ThT, and 0.02% NaN_3.

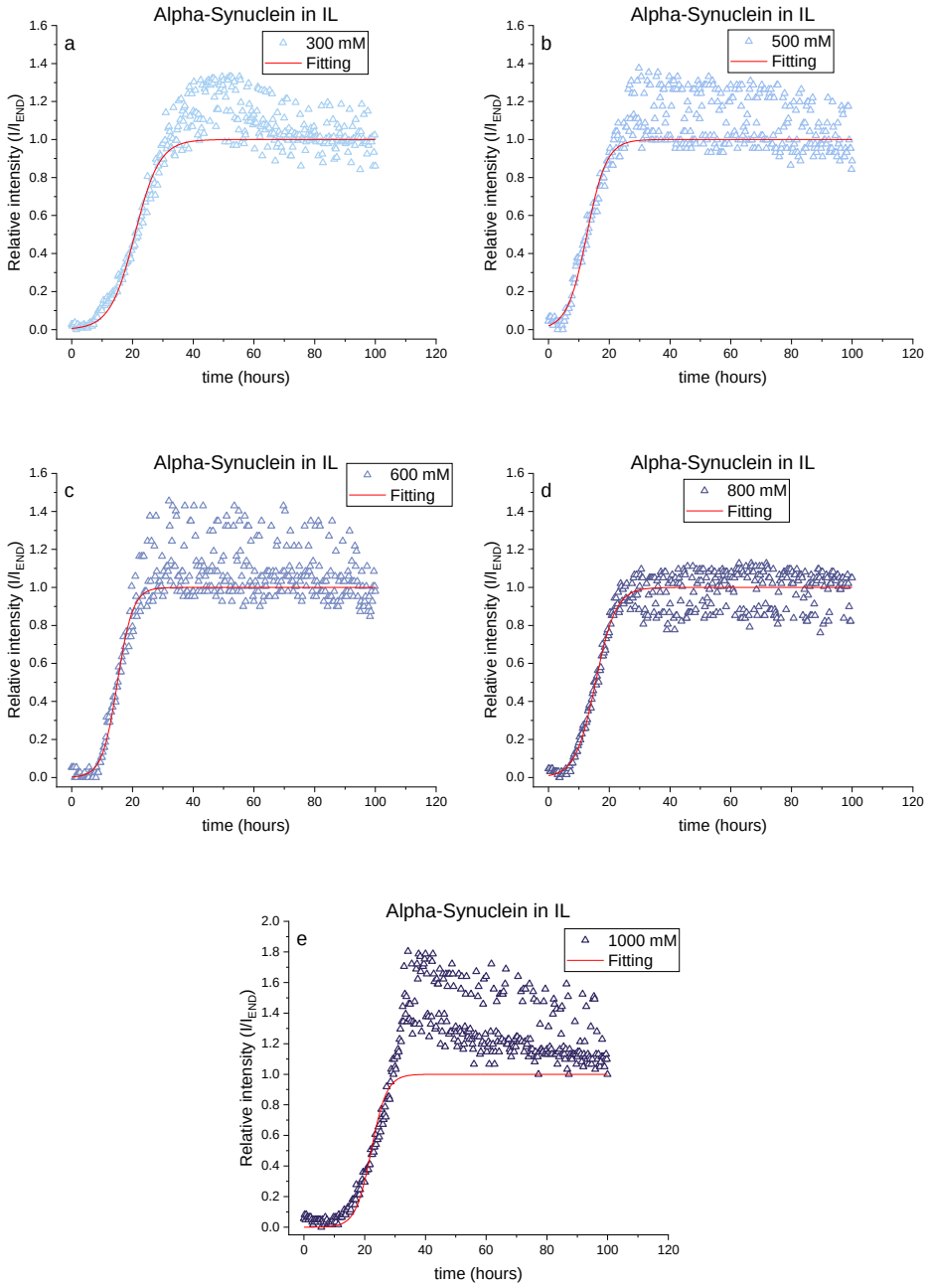

Figure SM4 – Fitting of the fibrillation curves of αS (IL)

The fitting was made to concentration points where extensive fibrillation was reached (i.e., a plateau is present) and correspond to the concentrations of 300, 500, 600, 800, and 1000 mM. The selected aggregation curves found in this figure are also present in figure 16C. The kinetic values estimated from the fitting are presented in table SM 22. Experiments were monitored over 100 hours at 37 ºC, fibril formation is monitored by the fluorescence of Tht. Samples (200 µM of protein) were prepared in 77 mM of phosphate buffer (pH 7.2), 200 µM of ThT, and 0.02% NaN_3.

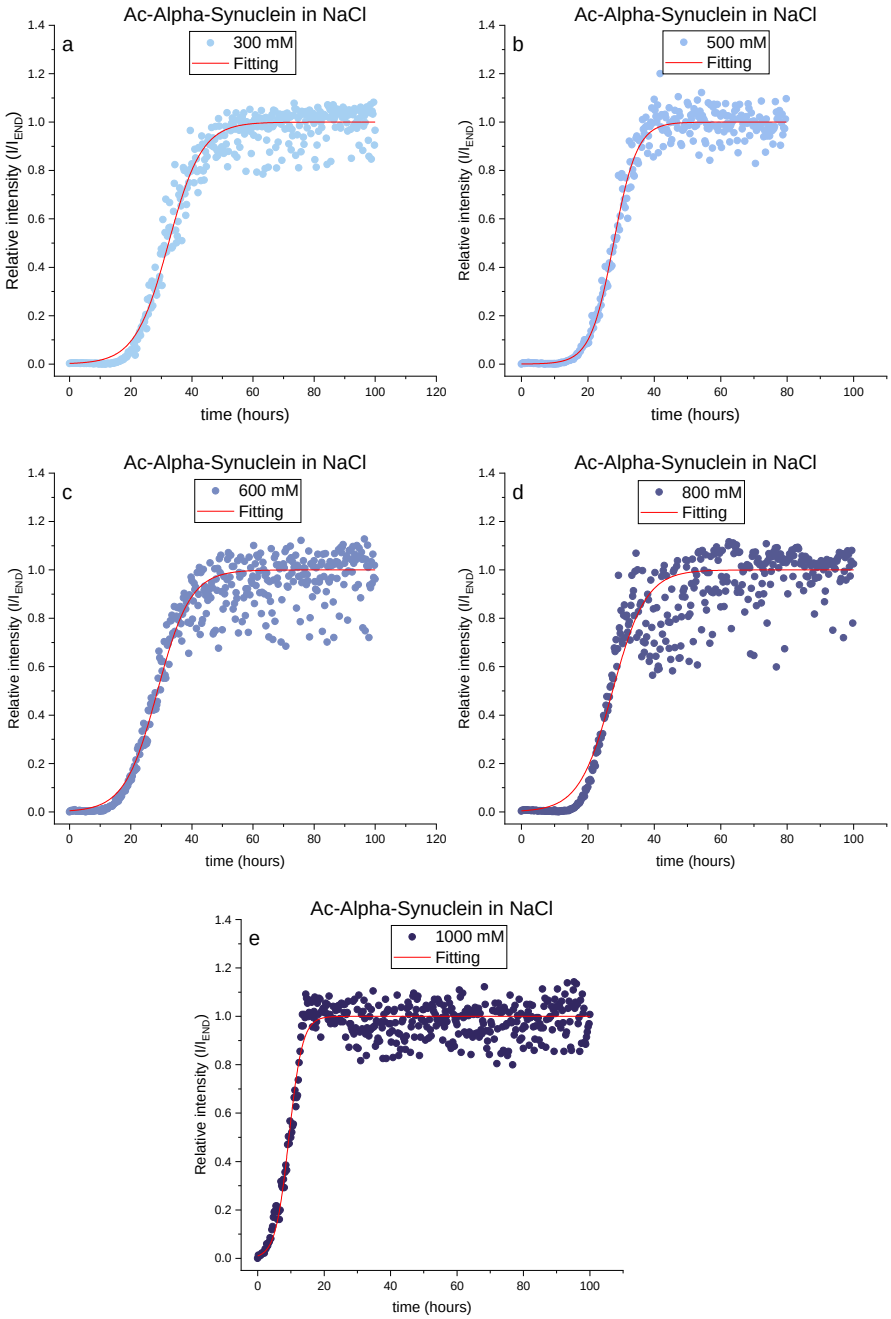

Figure SM5 – Fitting of the fibrillation curves of Ac-αS (NaCl)

The fitting was made to concentration points where extensive fibrillation was reached (i.e., a plateau is present) and correspond to the concentrations of 300, 500, 600, 800, and 1000 mM. The selected aggregation curves found in this figure are also present in figure 16B. The kinetic values estimated from the fitting are presented in table SM 23. Experiments were monitored over 100 hours at 37 ºC, fibril formation is monitored by the fluorescence of Tht. Samples (200 µM of protein) were prepared in 77 mM of phosphate buffer (pH 7.2), 200 µM of ThT, and 0.02% NaN_3.

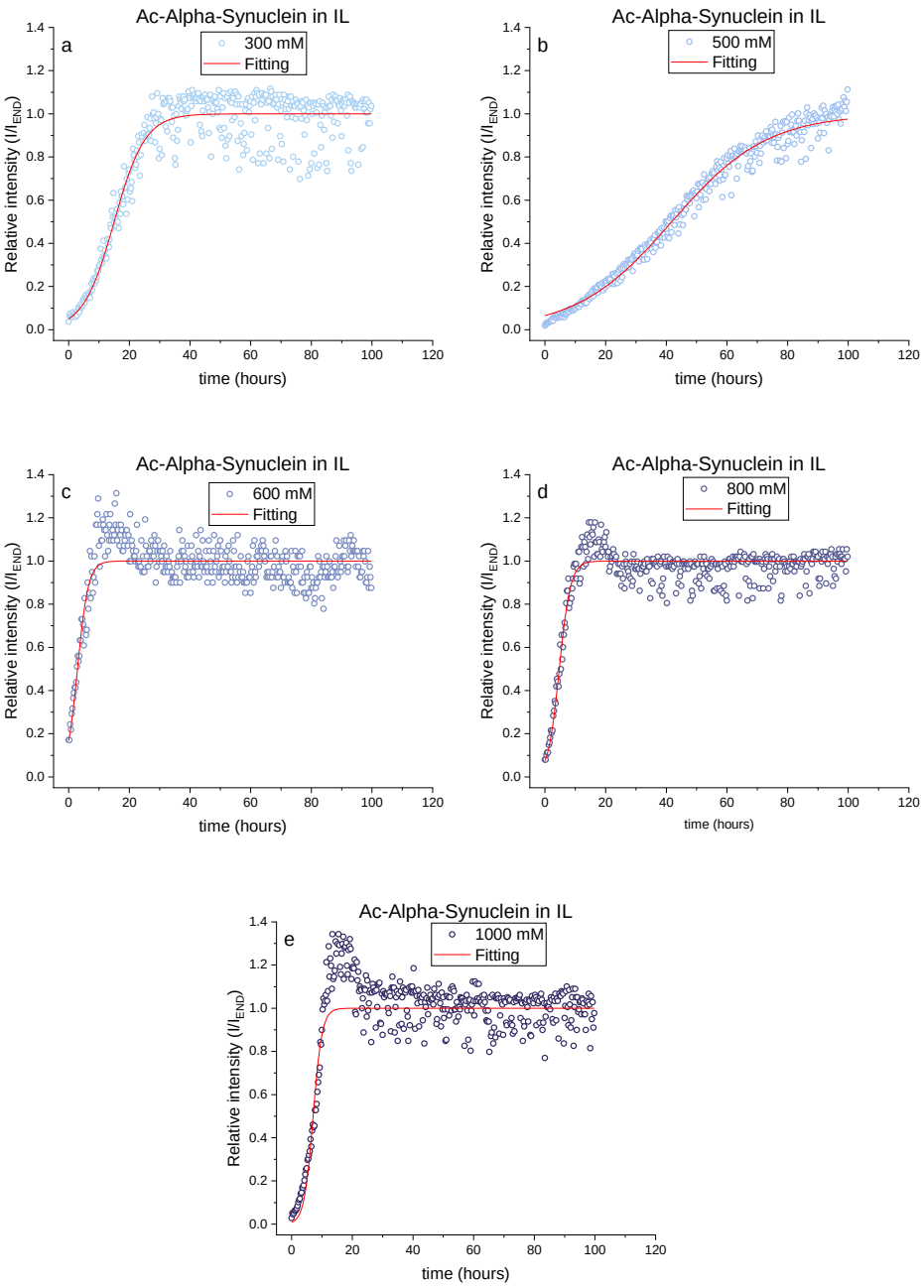

Figure SM6 – Fitting of the fibrillation curves of Ac-αS (IL)

The fitting was made to concentration points where extensive fibrillation was reached (i.e., a plateau is present) and correspond to the concentrations of 300, 500, 600, 800, and 1000 mM. The selected aggregation curves found in this figure are also present in figure 16D. The kinetic values estimated from the fitting are presented in table SM 24. Experiments were monitored over 100 hours at 37 ºC, fibril formation is monitored by the fluorescence of Tht. Samples (200 µM of protein) were prepared in 77 mM of phosphate buffer (pH 7.2), 200 µM of ThT, and 0.02% NaN_3.

Table SM21 – Fitting parameter for αS in NaCl

αS							
NaCl	**v (h-1)**	**E (v)**	**$t_{1/2}$ (h)**	**E ($t_{1/2}$)**	**TN (h)**	**E (T_N)**	**R^2**
300 mM	0.054	0.02	30.6	0.2	21.3	3.4	0.972
500 mM	0.1300	0.01	18.70	0.2	14.9	0.4	0.901
600 mM	0.06	0.004	17.1	0.3	9.0	0.6	0.847
800 mM	0.220	0.03	10.1	0.2	7.8	0.4	0.767
1000 mM	0.024	0.002	14.6	0.6	-6.2	1.8	0.71

Table SM22 – Fitting parameter for αS in [Ch][Glu]

αS							
[Cho][Glu]	**v (h-1)**	**E (v)**	**$t_{1/2}$ (h)**	**E ($t_{1/2}$)**	**TN (h)**	**E (T_N)**	**R^2**
300 mM	0.062	0.003	20.8	0.3	12.7	0.5	0.9
500 mM	0.0770	0.007	12.60	0.3	6.1	0.7	0.818
600 mM	0.10	0.009	15.0	0.3	9.9	0.6	0.858
800 mM	0.075	0.004	15.5	0.2	8.8	0.4	0.932
1000 mM	0.1	0.02	22.1	0.6	17.1	1.2	0.641

Table SM23 – Fitting parameter for Ac-αS in NaCl

Ac-αS							
NaCl	**v (h-1)**	**E (v)**	**$t_{1/2}$ (h)**	**E ($t_{1/2}$)**	**TN (h)**	**E (T_N)**	**R^2**
300 mM	0.046	0.001	32.4	0.2	21.5	0.3	0.977
500 mM	0.0710	0.002	27.80	0.2	20.8	0.3	0.987
600 mM	0.05	0.002	28.7	0.2	17.8	0.5	0.95
800 mM	0.050	0.003	27.4	0.3	17.4	0.7	0.915
1000 mM	0.123	0.007	9.4	0.1	5.3	0.3	0.925

Table SM24 – Fitting parameter for Ac-αS in [Ch][Glu]

Ac-αS							
[Cho][Glu]	**v (h-1)**	**E (v)**	**$t_{1/2}$ (h)**	**E ($t_{1/2}$)**	**TN (h)**	**E (T_N)**	**R^2**
300 mM	0.049	0.002	15.0	0.2	4.8	0.5	0.963
500 mM	0.0159	0.0002	41.80	0.2	10.4	0.4	0.984
600 mM	0.14	0.01	2.9	0.2	-0.7	0.3	0.691
800 mM	0.134	0.007	4.7	0.1	1.0	0.2	0.874
1000 mM	0.17	0.02	7.1	0.2	4.2	0.4	0.819